THESIS FOR THE DEGREE OF DOCTOR OF PHILOSOPHY

Beyond Perturbation: Modeling Anharmonicity in Materials

Fredrik Eriksson

Department of Physics
CHALMERS UNIVERSITY OF TECHNOLOGY
Göteborg, Sweden 2024

Beyond Perturbation: Modeling Anharmonicity in Materials
Fredrik Eriksson

isbn 978-91-8103-041-9
Doktorsavhandlingar vid Chalmers tekniska högskola. Ny serie nr 5499
issn 0346-718X

Department of Physics
Chalmers University of Technology
se-412 96 Göteborg, Sweden
Telephone +46 (0)31 772 10 00

Cover: This thesis should at least be somewhat useful.

Typeset in XeLaTeX using the Memoir class. Template by M. Petisme and J. M. Rahm.

Chalmers digitaltryck
Göteborg, Sweden 2024

Beyond Perturbation: Modeling Anharmonicity in Materials

Fredrik Eriksson
Department of Physics
Chalmers University of Technology

Abstract

The vibrational motion of atoms is essential for understanding condensed matter systems. It directly influences numerous thermodynamic properties with significant technological implications. Additionally, these atomic movements indirectly contribute to a variety of electronic and optical properties, making the study of vibrations both challenging and rewarding.

Today, we conceptualize these collective vibrational excitations as phonons. The study of phonons bridges theoretical and experimental approaches through computer simulations. Typically, phonons are studied at the lowest harmonic order and occasionally to the first order using perturbation theory. However, in many systems of interest, anharmonic motion, which represents interactions among phonons, is critical. Modeling this anharmonicity beyond perturbation theory is computationally intensive. Fortunately, recent advancements in various fields, both within and outside condensed matter physics, have made these simulations more feasible.

In this thesis, the primary computational tools for studying phonons are outlined and applied to a diverse range of materials. Emphasis is placed on understanding the underlying dynamics through microscopic correlation functions and their link to experimental observables via spectral functions. Additionally, some practical details, often overlooked in the literature, are discussed. Specifically, the framework of lattice dynamics and the characterization of the potential energy surface through force constants are described. For complex systems that extend beyond perturbation theory, the complementary approach of molecular dynamics is explored, with a focus on phonon dynamics.

These techniques are applied to two sets of materials currently of interest. First, anisotropic thermal conduction in rotationally disordered 2D van der Waals structures is examined using the Green-Kubo method. The findings align well with experimental results, demonstrating a substantial anisotropy that could be advantageous for managing thermal waste in integrated circuits. Moreover, the chemistry-independent suppression of through-plane thermal conductivity in these materials is shown. Additionally, through-plane thermal conduction as a function of the moiré twist angle is analyzed and correlated with an entropy measure. Lastly, the limitations of the quasi-particle picture of phonons are investigated in an inorganic halide perovskite. It is found that the soft phonons are overdamped over a wide temperature range above the phase transition but remain consistent with the model of independent damped harmonic oscillators.

Keywords: Force Constants, Molecular Dynamics, Lattice dynamics, Peierls-Boltzmann Transport Equation, Green-Kubo, Lattice Thermal Conductivity, Anharmonicity, Phonons

LIST OF APPENDED PAPERS

This thesis is partly based on the author's licentiate thesis (F. Eriksson, *Development and application of techniques for predicting and analysing phonon-derived materials properties* (2022)). It consists of a background to the field and the following papers:

I **The Hiphive Package for the Extraction of High-Order Force Constants by Machine Learning.**
Fredrik Eriksson, Erik Fransson and Paul Erhart
Advanced Theory and Simulations **2**, 1800184 (2019)
doi: 10.1002/adts.201800184

II **Efficient construction of linear models in materials modeling and applications to force constant expansions.**
Erik Fransson, Fredrik Eriksson and Paul Erhart
npj Computational Materials **6**, 135 (2020)
doi: 10.1038/s41524-020-00404-5

III **Extremely anisotropic van der Waals thermal conductors.**
Shi En Kim, Fauzia Mujid, Akash Rai, Fredrik Eriksson, Joonki Suh, Preeti Poddar, Ariana Ray, Chibeom Park, Erik Fransson, Yu Zhong, David A. Muller, Paul Erhart, David G. Cahill and Jiwoong Park
Nature **597**, 660–665 (2021)
doi: 10.1038/s41586-021-03867-8

IV **Tuning the through-plane lattice thermal conductivity in van der Waals structures through rotational (dis)ordering.**
Fredrik Eriksson, Erik Fransson, Christopher Linderälv, Zheyong Fan and Paul Erhart
ACS Nano **17**, 25565–25574 (2023)
doi: 10.1021/acsnano.3c09717

V **Limits of the phonon quasi-particle picture at the cubic-to-tetragonal phase transition in halide perovskites.**
Erik Fransson, Petter Rosander, Fredrik Eriksson, J. Magnus Rahm, Terumasa Tadano and Paul Erhart
Communications Physics **6**, 173 (2023)
doi: 10.1038/s42005-023-01297-8

The author's contribution to the papers:

I Main developer of the code, performed the majority of the simulations and wrote most of the paper.

II Discussed the work and implemented some of the functionality needed. Performed the thermal conductivity calculations for the clathrate and proof-read the paper.

III Constructed the atomic structures and performed the Green-Kubo simulations. Leading role in writing the corresponding theory section of the paper and the discussion of the computational results.

IV Constructed the atomic structures and performed the Green-Kubo simulations. Wrote most of the manuscript.

V Discussed and double-checked the oscillator model. Assisted the work on the mode projection analysis. Proof-read the paper.

PUBLICATIONS NOT INCLUDED IN THIS THESIS

Efficient Calculation of the Lattice Thermal Conductivity by Atomistic Simulations with Ab Initio Accuracy.
Joakim Brorsson, Arsalan Hashemi, Zheyong Fan, Erik Fransson, Fredrik Eriksson, Tapio Ala-Nissila, Arkady V. Krasheninnikov, Hannu-Pekka Komsa and Paul Erhart
Advanced Theory and Simulation **5**, 2100217 (2022)
doi: 10.1002/adts.202100217

Thermal conductivity in intermetallic clathrates: A first-principles perspective.
Daniel O. Lindroth, Joakim Brorsson, Erik Fransson, Fredrik Eriksson, Anders Palmqvist and Paul Erhart
Physical Review B **100**, 045206 (2019)
doi: 10.1103/PhysRevB.100.045206

Contents

List of abbreviations

ACF auto-correlation function. 45, 47–49, 51
AIC Akaike information criterion. 66, 72
AIMD ab initio molecular dynamics. 36, 39, 44, 57
ARDR automatic relevance determination regression. 66, 71

BCC body-centered cubic. 34
BIC Bayesian information criterion. 66, 72

CS compressive sensing. 66, 69

DFPT density functional perturbation theory. 18, 27
DFT density functional theory. 2, 4, 11, 15, 19, 24, 28, 39, 40, 62–64, 66

EAM embedded atom method. 41
EHM effective harmonic model. 36, 63
EMD equilibrium molecular dynamics. 54, 56, 59

FC force constant. 17–24, 26–28, 31, 33–37, 54, 62, 63, 65, 66, 69
FCP force constant potential. 36, 64, 65

GK Green-Kubo. 53, 56, 57, 63, 64, 67
GP Gaussian process. 42, 43
GPU graphical processing unit. 21, 61

HNEMD homogeneous non-equilibrium molecular dynamics. 58, 60, 67, 68

INS inelastic neutron scattering. 9, 13, 14
IXS inelastic x-ray scattering. 9

LASSO least absolute shrinkage and selection operator. 66, 69, 70, 73
LJ Lennard-Jones. 40
LO-TO longitudinal optic–transverse optic. 27, 28
LTC lattice thermal conductivity. 53, 56

MC Monte Carlo. 36, 44, 47
MD molecular dynamics. 17, 21, 24, 35, 36, 39, 40, 43, 44, 47, 50, 51, 53, 56, 62, 64, 65, 67, 68

ML machine learning. 39, 40, 42–44, 61–64, 67
MSE mean squared error. 72

NEMD non-equilibrium molecular dynamics. 53, 56
NN neural network. 42, 43, 63
NPT isothermal-isobaric. 45
NVE microcanonical. 44, 45, 53, 56
NVT canonical. 45

OLS ordinary least squares. 19, 34, 66, 69
OMP orthogonal matching pursuit. 70

PBTE Peierls-Boltzmann transport equation. 25, 53–56, 64, 67, 68
PES potential energy surface. 17, 19–21, 25, 34, 36, 39, 42, 54, 63–65, 70

RFE recursive feature elimination. 66, 70, 71
RMSE root mean squared error. 66, 72
RTA relaxation time approximation. 55

SCHA self-consistent harmonic approximation. 35
SCP self consistent phonons. 35, 63
SMRTA single-mode relaxation time approximation. 56
SSCHA stochastic self-consistent harmonic approximation. 35

TDEP temperature-dependent effective potential. 36

vdW van der Waals. vii, 6, 11, 17, 40, 41, 64, 67

1 Introduction

Why look it up if you can make it up?

E. B.

1.1 Modeling materials dynamics

This thesis concerns the computer aided modeling of atomic [1] vibrational dynamics in condensed matter systems with a focus on the solid state. Atomic vibrations are important for many structural and thermodynamic properties but also influence, e.g., electronic and optical properties of materials [1, 2]. The plethora of different materials with different macroscopic properties is a key part of technology and thus it is of great interest to understand the underlying microscopic mechanisms [3, 4]. One of the goals in materials science is to understand how these properties emerge from the constituent atoms. One approach is to predict and interpret experiments using only quantum mechanics and constants of nature. This is called *ab initio* modeling and today much of this modeling is aided by computer simulations [5, 6]. Many modern simulation methodologies can provide excellent quantitative agreement with experiments — ideally for the right reasons. Today, there are many computer codes which are available for performing simulations of condensed matter systems. Especially during the last decade

[1] In this thesis the terms ions, nuclei and atoms will often be used interchangeably

open source software has had a large impact on the workflow of computational materials scientists as many codes are now easily accessible. By a hierarchy of methods it is in principle possible to go all the way from the microscopic description of matter via coarse grained models to the macroscopic world.

The two main ingredients needed to study atomic vibrations are (1) a means to calculate the forces acting between atoms by solving the Schrödinger equation of the electrons and ions, and (2) a method for integrating the resulting equations of motions to predict the vibrational dynamics. The most common technique for task (1) is density functional theory (DFT), an electronic structure method, which enables the calculation of energy and forces, along with a wide array of derived properties. One can also use interatomic potentials including machine-learned ones, which are often parametrized using data from DFT calculations. With regard to (2) depending on the system at hand, one usually uses either lattice dynamics (Chapter 2) or molecular dynamics (Chapter 3) to solve the equations of motion. In short, lattice dynamics, as the name suggests, is limited to more or less crystalline systems but allows one to more naturally handle quantum effects. Molecular dynamics on the other hand is a mostly classical method that can, however, also be applied to model disordered solids and even liquids. However, it is possible in both frameworks to overcome each respective limitation to some degree which can be useful in cases where observables of interest are more natural to calculate in one framework compared to the other. In the two main chapters, Chapter 2 and Chapter 3, we shall take a brief look at both of the principal techniques used to study atomic vibrations. In the rest of this introduction we shall take a more pedestrian approach to vibrational properties of solids. The particular type of properties we will be concerned with are those directly connected to atomic vibrations.

How to model the atomic vibrations is intimately connected to the microscopic structure of the material and the interactions among the constituent atoms. Let us consider some different types of systems from simple molecules to complex liquids. For instance, in a diatomic gas (like nitrogen N_2 or carbon monoxide CO) the vibrations of each molecule are largely decoupled from the vibrations of all other molecules, apart from occasional collisions. In other words, the diffusive motion of the molecules is largely independent of the intramolecular vibrations. This allows us to study the vibrations in a single individual molecule in detail while being able to describe related properties of the macroscopic molecular gas. As we shall see later this makes it possible to predict infrared absorption spectra.

It is also possible to study the vibrations of large molecules in solutions. In this case the dynamics of the solvent and the interaction with the solute can often be coarse grained. The vibrations of the large molecule can be modeled as the vibrations of the isolated molecule under the influence of some stochastic external interaction. This is different from the previous example where the interactions where instead rare. We will see an explicit example of how to model this at the end of Chapter 3 where we discuss the damped harmonic oscillator.

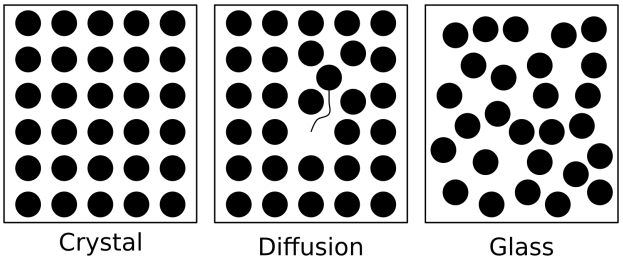

Figure 1.1: The difference between (1) a crystal where the atoms are perfectly aligned, (2) a crystal where atoms can diffuse around, and (3) a disordered glass. A liquid is like a glass where the atoms can diffuse around freely, i.e. a combination of (2) and (3).

There is also the possibility to model vibrations in liquids. Although liquids are qualitatively very different from solids many concepts are common. In liquids the problem is that the vibrational dynamics can not be decoupled from the diffusive motion. However, the stochastic nature of atomic motion in liquids makes the dynamics somewhat less sensitive on the details of the description of the atomic interactions. For instance many models of water will replicate the macroscopic behavior of the liquid but fail at describing the different phases of ice [7].

The main systems studied in this thesis are bonded solids such that no or very little diffusion is observed. They will furthermore be either ordered/crystalline or disordered/amorphous (sometimes called glassy). Amorphous systems share many similarities with liquids in that there is no long-range order. Most solid materials we encounter are either disordered like glasses or poly-crystalline. In polycrystalline materials, grains of randomly oriented crystals are surrounded by less ordered or disordered regions called grain boundaries. Even materials that we might assume to be made up of perfect crystals contain different types of defects. These can be point defects such as missing atoms ("vacancies") and interstitials or higher dimensional defects such as stacking faults. The study of defects is a large and important area but in this thesis we shall mainly deal with vibrations of perfect crystalline materials. Our hope is that by understanding the crystalline case we can transfer the knowledge to more complex systems. An illustration of the difference between the systems is provided in Fig. 1.1. A large part of the challenge of simulating vibrations in solids is that many interesting materials are somewhere between perfect order and total disorder.

However, as mentioned, the simplest systems to start the analysis are crystalline solids. The study of atomic vibrations in crystalline solids is an old topic called lattice dynamics. Atoms in the crystal vibrate back and forth under the influence of the motion of neighboring atoms. Even in liquid systems where the atoms are subject to diffusion there are characteristic frequency components of the motion. Much of the modern theory of lattice vibrations was formulated by Max Born and Theodore von Kármán in 1912–1913. In this theory the atomic motion is coupled and correlated and

the individual atomic vibrations (or excitations) are replaced by collective excitations called phonons where the atoms move together in a wavelike manner. To understand the properties of the material with respect to the atomic motion is then to understand the dynamics of the phonons. The energies and vibrational frequencies of different types of phonons of different wavelengths are a key properties to understand. A classical analogy of a phonon are elastic waves such as sound waves ("phono" means sound) or vibrations on strings. The basic framework of the dynamics and interaction among phonons and their role in, e.g., heat transport was to large extent already understood by the end of the 1950s and early 1960s. In the subsequent years we saw the advent of molecular dynamics and DFT and it appears the modern approach has not changed much from at least the late 1980s.

We appreciate that once we can calculate the interaction among atoms we can in principle understand in detail how the atoms vibrate in terms collective excitations called phonons. The details of how to go from a model of the interaction between atoms to the properties of the phonons is the topic of Chapter 2. Although indirectly important for other properties as well, there are then several macroscopic materials properties directly related to atomic vibrations which we can observe directly and try to predict. Some everyday examples are thermal expansion, heat capacity and elasticity. The contribution to these quantities from the atomic vibrations can today be computed relatively easily.

A more challenging property is for example the free energy which controls the stability of different phases of a material with important implications for applications. Many, in principle significant, materials for crucial applications such as thermoelectrics and photovoltaics fall short due to kinetic free energy barriers in synthesis and structural instability at ambient temperature variations. The reason is that a large proportion of the free energy of a material can originate from the vibrational entropy. Because materials synthesis is difficult and expensive it is convenient to have a computational approach to try to predict the stability of a material. The methods described later in the thesis can be used to calculate phase diagrams for different materials ranging from simple ordered crystals to disordered liquids. This can also be useful before synthesis in order to guide the experimental setup and subsequent analysis of experimental data.

A further macroscopic property of interest is the thermal conductivity which is slightly different from the structural and equilibrium properties mentioned above. It is a non-equilibrium property that is remarkably hard to both measure and simulate [8, 9]. The thermal conductivity is an important property for technical applications in, e.g., electronics, aerospace and automotive engineering as well as energy production and storage. Experimentally, it can be measured using, e.g., the 3ω-method [10]. In Paper III the thermal conductivity of disordered MoS_2 was measured using the time domain thermoreflectance method instead, as discussed in reference [11]. While the free energy needed for phase transitions in principle can be accessed from Monte Carlo simulations the thermal conductivity is intimately related to the materials dynamics [12] and

is thus a different probe of the accuracy of the underlying model of the atomic interactions. Both properties are, however, challenging to simulate and there are still open questions related to thermal conduction in disordered systems [13] and the need for exact microscopic definitions of heat currents [14].

With the above discussion as motivation we will now go a bit deeper into how to model phonons. In the simplest models the phonons act as independent excitations, or in the language of quantum mechanics, they are exact energy eigenstates. Thus a particular type of phonon (called polarization) with some wavelength will oscillate with some fixed frequency corresponding to the energy of the excitation. This mode of oscillation will act as an independent harmonic oscillator and thus its spectrum can be described as a delta-function centered at this frequency. If there are several phonons of different wavelengths we hope to see those frequencies also in some spectra if we can probe the material in such a way to detect the phonons. We shall take a look at some of this type of experiments and see how the picture of harmonic oscillations fails. In particular we shall see that the peaks in the spectrum are not delta-functions but rather have some finite width. With a finite width in frequency and the relation between energy and time we understand that a width in frequency means an uncertainty in energy. This means that the phonons are not exact eigenstates but will in general decay into other phonons after some time. In this case the harmonic picture must be abandoned and we must treat the anharmonicity of atomic vibrations. To understand this anharmonicity is the topic of the thesis and how to analyze anharmonicity using perturbative and fully anharmonic methods. Now, let us take a look at some of the primary experiments motivating and guiding us.

1.2 Experimental probes

Bulk properties are interesting from the perspective of applications as well as for testing theories and computational methodologies. However, they do not provide much insight into the microscopic dynamics needed for further understanding. For example, both the free energy and lattice thermal conductivity are obtained through integration and therefore errors can cancel out. In order to gain a deeper understanding of the different types of motion in a material we need to interact with the modes directly. To this end we can employ diffraction and scattering techniques using thermal neutrons, x-rays or infrared photons, and even electrons. In diffraction experiments the structure of the material is probed and is also sensitive to some thermal averaged properties. This is sometimes used in pump-probe experiments where the material is pumped with, e.g., a laser and then, some (short) time later, probed with, e.g., x-rays. In Fig. 1.8 an electron diffraction pattern can be seen which is typically used to map out the structure of the material of interest. While there are many types of techniques for diffraction and scattering experiments we shall take a brief look at three common ones. First we will

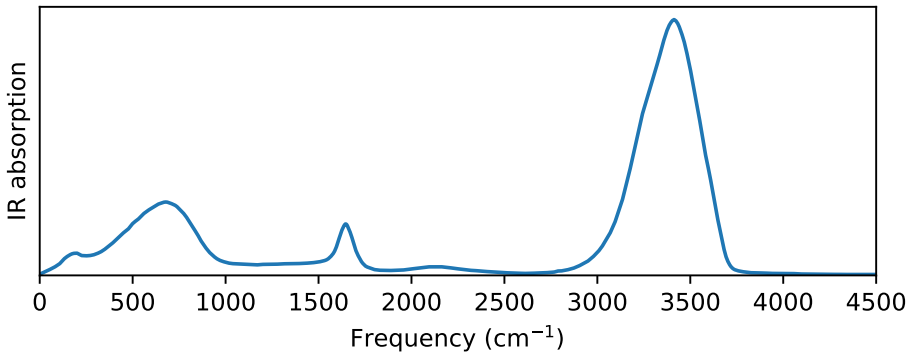

Figure 1.2: Infrared absorption of water. Notice the broadening of the peaks. Data from reference [15].

consider infrared absorption where an incoming photon interacts with and excites a single phonon by being absorbed. Next up is Raman spectroscopy where the incoming photon is of too high energy (not in resonance) to be absorbed but rather scatters inelastically. Finally we take a brief look at inelastic neutron scattering which is similar to Raman scattering but using neutrons instead of photons. The change in energy and direction observed in inelastic scattering experiments can be measured and (in first order, directly) related to the frequencies of phonons with different wavelengths.

1.2.1 Infrared absorption

Infrared absorption is a technique where photons in the infrared range are absorbed by the material under study. The infrared spectra stretches from wavelengths of 700 nm to 1 mm which corresponds to frequencies of 300 GHz to 430 THz. Sometimes the spectrum is divided into near, mid and far-infrared with respect to the vicinity to the visible spectrum. Typical phonon frequencies range from around 100 THz for very strong covalent bonds to less than 1 THz for weak vdW bonds and long wavelength acoustic phonons. This match in frequency is the reason why infrared photons are well suited for studying vibrations. On the other hand we know that typical atomic radii are around 1 Å and the typical spacings between atoms in solids are around 1–10 Å. So although the photon frequencies match the typical phonon frequencies the momentum will typically not be matched except for phonons of very long wavelength. This is one of the main problems of probing bulk materials using photons while for molecules this is less of an issue. Another issue are the selection rules for transitions between different vibrational states while absorbing a photon. For infrared absorption the first order process requires a total change in dipole moment which limits which phonons can be excited in the material.

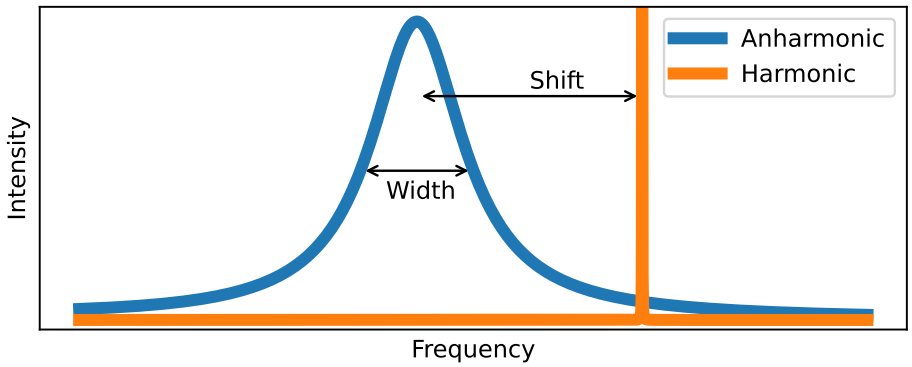

Figure 1.3: Schematic illustration of the difference in the spectral function between a harmonic and an anharmonic oscillator.

So what do we expect to see in a typical infrared absorption spectra? From the Einstein model where each atom in the sample acts as an independent 3D oscillator of the same frequency we would expect to see the spectrum of a quantum harmonic oscillator, which is indeed the spectrum we observe in diatomic gases. However since we know that the atomic vibrations are not independent a general spectrum would consist of sharp peaks at the frequencies of the different types of phonon frequencies. In Fig. 1.2 the infrared absorption spectrum for water is displayed and as expected we see roughly three intense peaks at discrete frequencies. We can however also observe that the peaks have a finite width. More so, if we were to increase the temperature in general we can observe a broadening and shift of the peaks and to explain this will be one of our goals. The difference is schematically illustrated in Fig. 1.3. For an example of how infrared spectroscopy and computer simulation can be combined see, e.g., reference [16].

1.2.2 Raman spectroscopy

Now let us look at Raman spectroscopy where laser light is used as the probe. Traditional Raman is typically off-resonance and it is the inelastic scattered light which is measured. The typical setup uses polarization filters for filtering the incoming light as well as the scattered light. Often, due to the small momentum, only the back-scattered light is used but in principle Raman can be momentum resolved. Raman is a complementary technique to, e.g., infrared absorption. For example the selection rules are different as the states only need to differ in polarizability. In principle Raman can be used for any material except metals due to the strong screening. As with infrared absorption one of the main limitations of Raman is the small momentum of the photons which makes it hard to probe motions far from the Γ-point at the center of the Brillouin

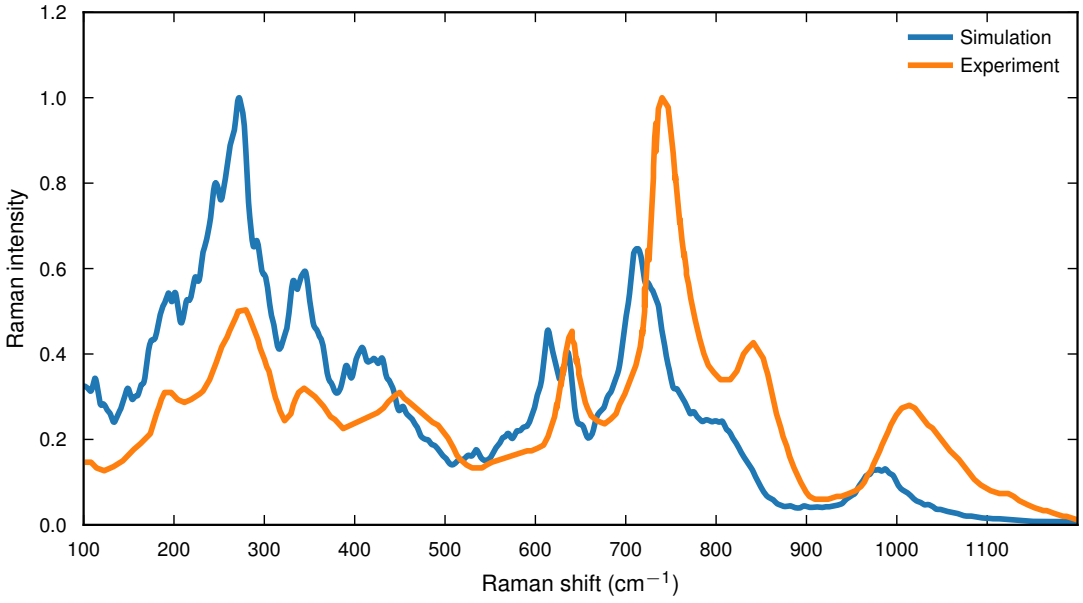

Figure 1.4: Raman spectrum for $BaZrO_3$. Data from [17].

zone (i.e., phonons with long wavelengths). This can partially be overcome by studying higher-order effects in which two or more phonons are excited by the incoming photon. By carefully using the polarization and orientation of the crystal together with atomistic simulations it is possible to untangle the convoluted spectra of such experiments.

Raman spectra are typically reported as intensity as a function of the so called Raman shift. The Raman shift is the amount of energy that the scattered photon gains or loses. If the photon loses energy, it is called Stokes scattering and if it gains energy it is called anti-Stokes scattering. If no change in energy is observed the scattering is elastic and is denoted Rayleigh scattering. Typically the Stokes process is reported as negative shifts (to the left) and anti-Stokes as positive shifts (to the right) but conventions may vary depending on whether frequency or wavelength are used. At any temperature, but especially noticeable at lower temperatures, the intensity of Stokes scattering is higher (at zero Kelvin there are no excited phonons from which the photon can gain energy). In Fig. 1.4 the Raman spectrum of the perovskite $BaZrO_3$ is presented. Inverse centimeters is the typical unit used to report Raman shifts, where $1\,\mathrm{cm}^{-1} = 0.03\,\mathrm{THz} = 0.124\,\mathrm{meV}$. As we can see in the figure the peaks are far from sharp delta-functions but, as the simulations elude to, it is possible to explain the shapes of the peaks using the methods described in this thesis.

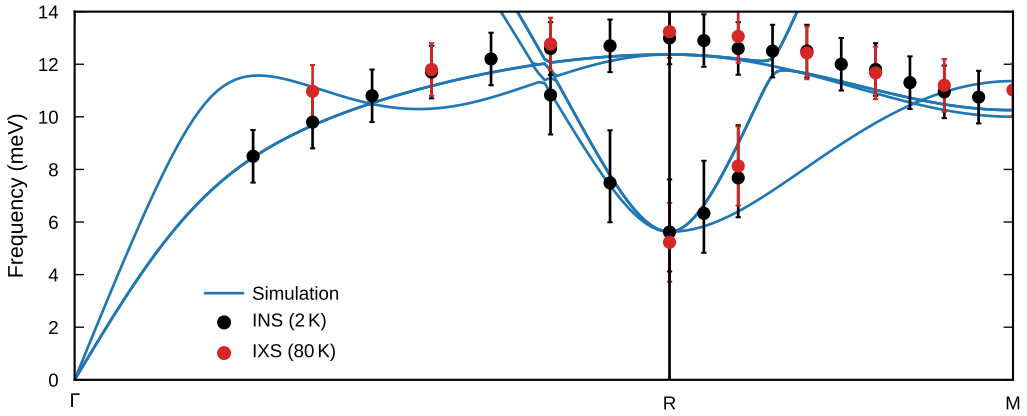

Figure 1.5: The theoretical and simulated dispersion relation for $BaZrO_3$. For the inelastic neutron scattering (INS) the bars indicate the linewidth while for inelastic x-ray scattering (IXS) the instrument resolution is indicated. Data from Ref. [20].

1.2.3 Neutron scattering

The final technique we shall take a look at is neutron scattering. While infrared absorption and inelastic Raman scattering work with photons inelastic neutron scattering (INS) works with neutrons. INS is very similar to inelastic x-ray scattering (IXS) where the incoming photons scatter of the core electrons. Neutrons, however, have a nice advantage over photons in that the energy of a thermal neutron ($k_B T$ at room temperature is around 25 meV) is around 2 Å which matches typical interatomic distances in crystals. As 25 meV is around 6 THz we see that also the energies match typical phonon energies. This makes neutrons an excellent probe for measuring phonons in solids, although it is limited by the accessibility to the expensive facilities needed for such experiments.

The main difference between Raman and INS is that we now have access directly to frequencies of vibrations occurring at different wavelengths. The intensity of the scattered particles at different angles and energies is typically communicated using either the static or the dynamical structure factor sometimes called the spectral function. The dynamic structure factor as measured by INS or IXS experiments is one of the most direct measures of the dispersion relation (i.e., energy/frequency as a function of wavelength) of the material as it measures the pair correlation between the motion of atomic nuclei. In Fig. 1.5 the dispersion relation for the perovskite $BaZrO_3$ can be observed. Just as in Raman spectroscopy the shape of the spectrum can be probed and lineshapes can be constructed. In our case only the peak position of the simulations are reported while the line width is reported for INS and the instrument resolution for IXS, respectively. For an application of elastic neutron scattering see, e.g., [18] and for INS see, e.g., reference [19].

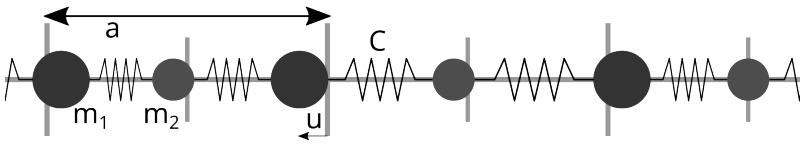

Figure 1.6: Diatomic linear chain of atoms with mass m_1 and m_2, respectively, with lattice parameter a and interatomic force constant of strength C. The displacement u of a selected atom is indicated.

With that we conclude this section about the experimental motivation for going beyond the simple harmonic models typically used. In this thesis we want to understand the actually observed peaks (their shape, width and positions) as well as how they change with temperature or when the material is close to a phase transition for example. We shall look at both the case when the modes can be described by harmonic oscillators affected by a weak perturbation and when the modes are far from harmonic. In the following section we will describe a simple model for phonons in solid materials and some elaboration on the concepts mentioned in this section.

1.3 Modeling atomic vibrations

To introduce the concepts for the later chapters we will go through a simple example found in many textbooks. Consider a simple 1D crystal with a basis containing two atoms of different mass. Each atom in the basis vibrates around some equilibrium position and the restoring force is supplied by springs connected to each of its two neighbors. The setup is depicted in Fig. 1.6. The solutions to the equation of motion for this system can be found in terms of lattice waves. Since there are two atoms in the basis and they are restricted to move in only one dimension there will be two types of waves. These are called acoustic (the two atoms in the basis move together) and optical (the two atoms move against each other) modes. If the atoms could move perpendicular to the chain there would also be a transverse mode (the atoms moving perpendicular to the propagation of the wave). In our case we will only have longitudinal motion (movement along the chain). The relation between the wavelength (or wave number k) and the frequency ω is called the dispersion relation. The analytical expression for the dispersion relation is

$$\omega^2 = \frac{C}{m_1 m_2/(m_1+m_2)}\left(1 \pm \sqrt{1 - \frac{2m_1 m_2}{(m_1+m_2)^2}(1-\cos 2\pi k a)}\right) \tag{1.1}$$

where C is the force constant, m_1 and m_2 are the masses of the two atoms, and a is the lattice spacing. The function is plotted in Fig. 1.7. Note that the frequencies of the modes are functions of the interaction strength between atoms, the masses of the

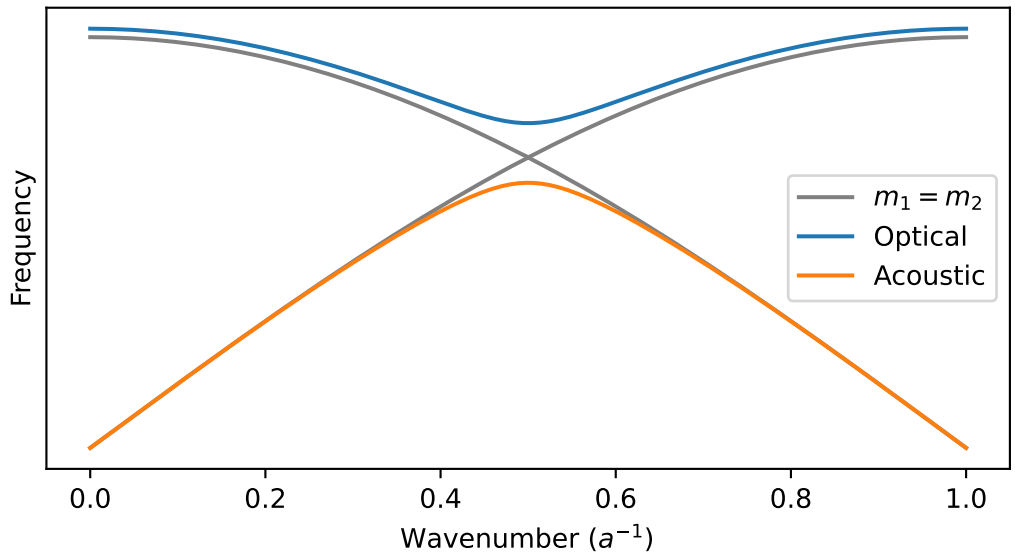

Figure 1.7: Dispersion relation for the diatomic linear chain over from the center of the first to the center of the second Brillouin zone. The dispersion relates the frequency (energy) to the wavenumber (quantum state). The mass difference splits the dispersion into an optical and acoustic branch. Notice how the dispersion is folded back in the case of equal masses.

atoms and the geometry of the crystal. The theory of lattice dynamics is essentially the generalization of these concepts and is outlined in Chapter 2. For a long time the force constants were calculated using simple models of electronic structure theory for simple systems or fitted to a few macroscopic observables. Today the force constants can be calculated with the help of approximate electronic structure methods based on DFT or exact approaches based on Hartree-Fock.

1.4 Materials

Although the emphasis of this thesis is on the methods they are motivated by challenges in modeling interesting materials. The first class of materials are disordered, layered vdW materials which are challenging to model due to the combination of order and disorder. The second class is perovskites which exhibit a strongly anharmonic potential energy landscape which can be hard to model using standard methods.

1.4.1 Layered vdW materials

In Paper III and Paper IV we studied disorder effects in a class of materials known as 2D vdW structures. These structures are composed of 2D layers stacked on top of

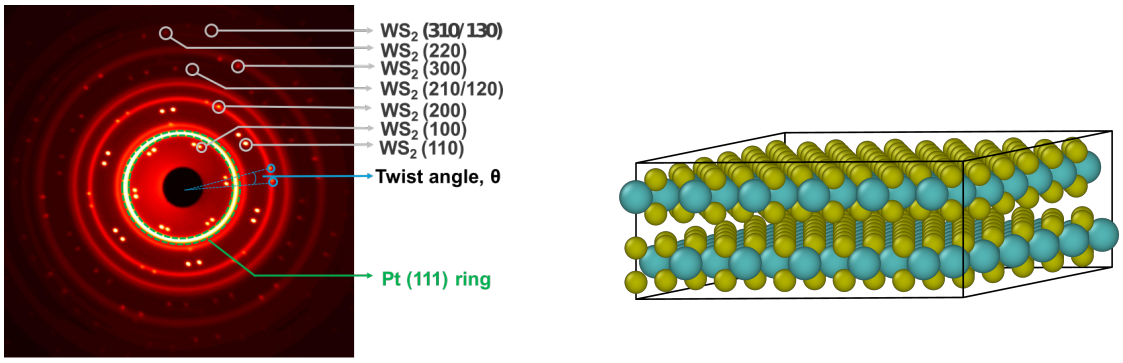

Figure 1.8: Electron diffraction pattern of WS_2 moire bilayer. Twist angle $\theta = 8^\circ$. The diffraction pattern represents the inverse cell of the material. Each peak is doubled due to the moire twist angle. Figure courtesy Prof. Aditya Sood, Princeton University (unpublished). Measured at the MeV-UED facility at SLAC National Accelerator Laboratory. For the atomic structure yellow atoms corresponds to sulfur and teal to molybdenum.

each other forming highly anisotropic crystals. Common examples of these structures include common graphite, which is composed of graphene layers stacked in a AB stacking sequence. Here, the designation indicates the stacking sequence where each letter represents a distinct translation and/or rotation relative to a reference layer. Other examples also studied in the aforementioned papers include hexagonal boron nitride and molybdenum disulfide. These materials inherit some of the interesting and sometimes exotic features of the constituent 2D monolayers. These structures are also highly tunable, through, e.g., doping and mixing but also the way in which the materials are stacked. In the context of this thesis, heat conduction across interfaces of these structures is of particular interest [21–23]. For an overview of heat conduction in graphene in particular see, e.g., [24, 25].

Two important classes include 2D hetero-structures, where different materials are stacked on top of each other in alignment and moiré structures where the monolayers are rotated relative to each other. In the latter types of structures the mismatch between the layers leads to an effective increase in the unit cell. This can give rise to surprising effects such as the widely cited superconductivity in magic angle bilayer graphene. More mundane effects are the extremely low through-plane thermal conductivity of these materials which has been linked to disorder. Typically disorder is challenging to model as the typical framework using quasi-particles becomes questionable in addition to the problem of measuring low conductivities [26–28].

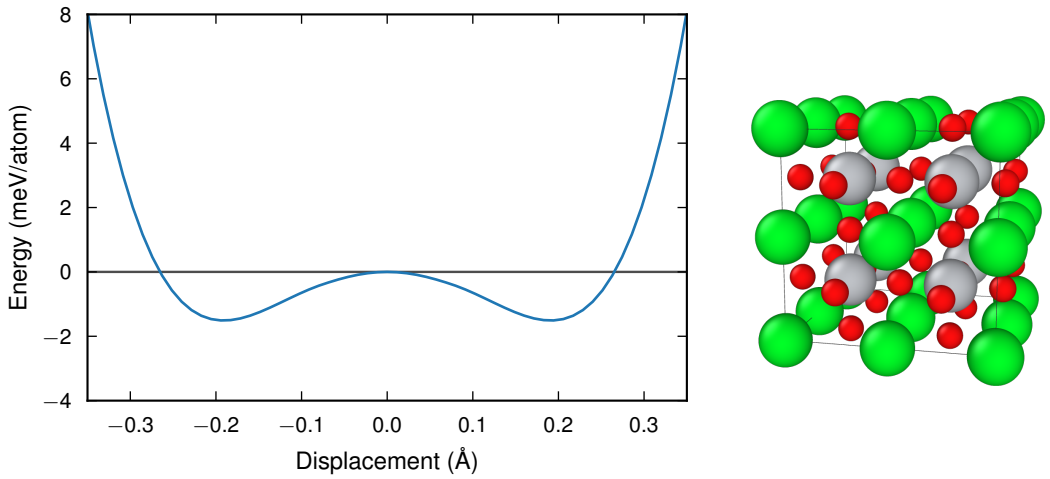

Figure 1.9: The anharmonic energy landscape of a tilting mode in a perovskite along with the crystal structure of the perovskite $SrTiO_3$ (STO) in its cubic phase. Green atoms corresponds to strontium, gray to titanium and red to oxygen.

1.4.2 Perovskites

Perovskite is the name for the mineral $CaTiO_3$ but is also the name of a class of materials with a similar structure. This has been a very popular class of materials for many decades thanks to the large configurational flexibility and interesting electronic and optical properties. Perovskites are used in various applications including sensors, actuators, fuel cells, photovoltaics and lighting. Some examples of common perovskites are$BaZrO_3$ (BZO), $SrTiO_3$ (STO) and $CsPbBr_3$. There are even organic-inorganic ("hybrid") perovskites in which one of the cations is exchanged for a molecule such as in $CH_3NH_3PbI_3$ (MAPI) [29].

One of the more interesting features of perovskites from a dynamical point of view is the tilting motion of the octahedra. These tilting motions are associated with phase transitions in the perovskite and often they exhibit octahedral, tetragonal or cubic symmetry in order of increasing symmetry. The potential energy landscape of these tilting modes can be very anharmonic. This makes the analysis of the vibrations difficult but interesting. Some perovskites also exhibit special dynamics due to quantum mechanics. For an example of a combined INS and theoretical study of the popular perovskite STO see, e.g., [30].

1.5 Outline

As has been demonstrated in the previous sections there are many materials properties that we wish to predict accurately yet computationally efficiently using simulations. In addition there are experimental techniques, such as INS, which can help us understand the microscopic vibrations via spectral functions. In a very abstract sense we want to understand the shape and dynamics of the phase space distribution function $\rho(x(t), p(t); H(t))$, which depends on the coordinates and momenta of the constituent atoms for some system described by a Hamiltonian. For example how will the system evolve (or propagate) from $(x(t_1), p(t_1))$ to $(x(t_2), p(t_2))$ on average or what is the probability to observe the system in state (x, p). Just like any static distribution can be decomposed and understood in terms of its moments (the mean, variance and so on) the dynamics of the phase space distribution function can be understood in terms of correlation functions of increasing orders between quantities at different times. For example the second order correlation functions can answer question of the sort: What is the probability or correlation of an observation A at time t given that we did an observation B at time 0. The spectral functions of a scattering experiment can be directly related to certain correlation functions. The spectral function is thus one of the key quantities we want to be able to calculate as it relates directly to experiments and to the microscopic motions in the material.

In quantum mechanics these correlation functions can be thought of as bare and dressed propagators relating the wave function at one point in space and time to another. In many body theory they appear instead as Green's functions for higher orders while in classical mechanics they are typically just called higher-order correlation functions. There are distinctions between propagators, correlation functions and Green's functions but for our purposes they can conceptually mostly be considered to be the same. Just as the partition function in statistical mechanics is enough to calculate system properties the one and two-point Green's functions can be used to calculate all single particle properties. To first order the spectral function captures two important effects namely the frequency shifts and broadening of the atomic motion. Going even further, by decomposing the spectral functions we can gain insight into contributions from different types of motion and effects to properties of interest. Ultimately we want to obtain a coherent picture of the dynamics where we can make statements of how the material can be modified in order to, e.g., optimize it for some specific property.

Hopefully the following chapters will make this discussion less opaque. In Chapter 2 the analysis of atomic vibrations in crystalline materials will be discussed. We will see how the interaction among atoms can be described using a Taylor expansion of the potential energy surface, which is also the topic of Paper I and Paper II. The connection to observables and the concepts of phonon frequencies and lifetimes will (hopefully) be made clear. The correlation functions of interest will be computed using perturbation theory. This is the oldest approach and mostly useful for relatively simple

systems. When the electronic structure theory calculations are expensive this is the only practical approach.

Next in Chapter 3 we will consider the more general technique of molecular dynamics which is useful for the complex systems analyzed in Paper III, Paper IV and Paper V. This technique has previously been limited due to the cumbersome process of constructing interatomic potentials in combination with the expensive evaluation of the system phase space. Today, however using modern machine learning potentials, the energy landscape obtained from DFT calculations can be accurately described and cheaply predicted, which makes the use of molecular dynamics for complex systems more accessible.

Finally, in Chapter 4 we will see how our correlation functions can be used to calculate the thermal conductivity using two different methods connected to lattice and molecular dynamics respectively.

2

Lattice dynamics

In this chapter, an overview of the framework of lattice dynamics is presented. Lattice dynamics concerns the vibrations of atoms around equilibrium positions in solids. The framework naturally handles small vibrations of atoms in crystals. Disordered solids such as glasses and single molecules can be analyzed also, albeit with some limitations. For liquids and systems where diffusion is important lattice dynamics is not suitable. In those cases other techniques such as molecular dynamics (MD) and generalized vdW theory are more appropriate. Nevertheless, the general ideas and concepts from lattice dynamics are still applicable in those systems.

This chapter will proceed as follows: First, a qualitative description of the potential energy surface (PES) of the atoms in the crystal, in terms of a Taylor expansion in small displacements called the force constant (FC) expansion, is described. Some general features of this expansion are discussed including anharmonic terms, symmetries and long-range corrections. This is followed by an introduction to phonons, which are the solutions to the equations of motion for the FC expansion truncated at the harmonic level. Features of the dispersion relation in crystals are discussed together with some thermodynamic properties. Next, anharmonic properties are introduced including spectral broadening and the connection to lifetimes, frequency shifts and spectral functions. Lastly, some techniques for handling strong anharmonicity are1 discussed.

Excellent general introduction to the topic of lattice dynamics are the works by Born and Huang [31], Ziman [32], Choquard [33], Wallace [34], Srivastava [35], Cowley [36], Callaway[37] and Dove [38].

2.1 Force constants

In order to analyze vibrations in a crystal we need a model Hamiltonian describing the interactions between the atoms. These interactions are described by the poten-

tial energy function, or simply "the potential". The first step is to apply the Born-Oppenheimer approximation in which the atomic nuclei move in the potential created by the electrons in the electronic ground state of the given instantaneous configuration of the nuclei. We can then write the lattice contribution to the potential energy of the crystal as a Taylor expansion in displacements u around some reference positions $\boldsymbol{R}$,

$$H = K + V = K + E_0 + \Phi_i u_i + \frac{1}{2!}\Phi_{ij} u_i u_j + \frac{1}{3!}\Phi_{ijk} u_i u_j u_k + \dots , \tag{2.1}$$

where $\boldsymbol{K}$ is the kinetic energy of the atoms and Φ are the FCs which relate the energy to the displacements. The indices here are in general compound indices $i = \{\mu, \alpha, \boldsymbol{n}\}$ where μ enumerates the basis of the crystal, α denotes the (Cartesian) direction of the displacement and $\boldsymbol{n} \in \mathbb{Z}$ enumerates the primitive cells in the crystal. The first coefficient E_0 is the cohesive energy of the crystal, which is not important when describing the vibrations. This constant term is, however, important as it enters into the free energy of the crystal which is important when assessing the relative stability of different phases. The second term Φ_i is exactly zero if the crystal is in a local energy minimum at zero temperature where all forces are zero. This first-order linear term is often assumed zero and we shall also make this assumption. The second-order term is the basis for the harmonic analysis of crystals to be discussed later in this chapter. Third and higher-order terms are referred to as anharmonic terms and play an important role in, e.g., phase transitions and thermal transport. This expansion is schematically illustrated in Fig. 2.1.

2.1.1 The displacement method

The first hurdle of describing vibrations in the framework of lattice dynamics is to calculate the FCs which enter as parameters in our theory. Once specified we can use the methods described in later sections to determine properties or microscopic mechanisms of interest. Notice that the FC expansion is an interatomic potential, which given the positions of the atoms can provide us with the forces. Thus if we can find the coefficients, this description of the interaction among atoms can be systematically improved by increasing the order of the expansion. However, being a Taylor expansion, we know it will not in general be able to describe displacements far from equilibrium positions.

A common method to extract interatomic FCs is to use the displacement method where we calculate the Hellmann-Feynman forces acting on the nuclei for some displaced structure using, e.g., density functional perturbation theory (DFPT). The force is simply the gradient of the above expansion with respect to the atomic positions

$$F_i = -\frac{\partial V}{\partial u_i} = -\Phi_i - \Phi_{ij} u_j - \frac{1}{2!}\Phi_{ijk} u_j u_k - \dots \tag{2.2}$$

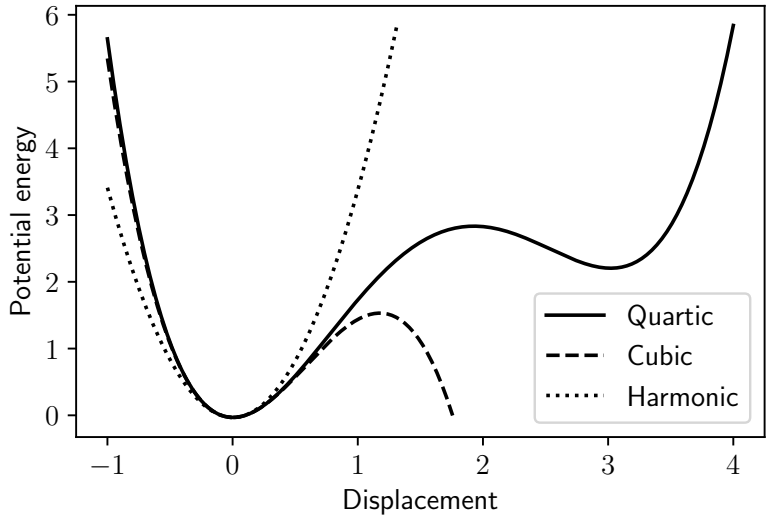

Figure 2.1: Illustration of the PES of a system described by a fourth-order polynomial. The harmonic approximation (only second-order polynomial) is only good for low energies (low temperatures). The cubic correction (third-order polynomial) would improve the description of the landscape close to the origin but makes the potential unstable after about 1 distance unit. To fully describe the fourth-order potential energy landscape the quartic term must be added. A quartic term is typically necessary when describing dynamically stabilized phases.

and is still linear in the free parameters (the FCs). Thus, for a fixed set of configurations (displacements) this can be written in matrix form as

$$F_i = U_{ia}\Phi_a, \tag{2.3}$$

where U_{ia} is a matrix mapping for all the displacements and Φ_a is the collection of FCs flattened to an array

$$\Phi_a = [\Phi_0, \Phi_1, \dots, \Phi_N, \Phi_{00}, \Phi_{01}, \dots, \Phi_{NN}, \Phi_{000}, \dots]. \tag{2.4}$$

Thus to find the coefficients we can use ordinary least squares (OLS) to fit the expansion to reference forces calculated using, e.g., DFT.

In order to generate forces from DFT calculations we need atomic configurations in order to generate the fit data (consisting displacements and forces). Systematic enumeration is the most straightforward (albeit not the most efficient) way to generate this data. By displacing only one or a few atoms in a supercell the FCs can be read off directly from the forces or extracted via a simple OLS fit. This procedure has been used extensively in the past with very good results for second-order FCs in many systems. Systematic enumeration generates the exact amount of data needed in order to

correctly identify all FCs and each configuration contains minimal noise. Many software packages implement this method, which is often called the small displacement method, introduced by Parlinski, Li, and Kawazoe [39]. Examples include PHONOPY [40] for second-order FCs and THIRDORDER.PY [41], PHONO3PY [42], and ALAMODE [43] for third-order FCs. one can in principle also use this method to calculate higher order FCs but this quickly becomes prohibitively expensive for disordered systems or high orders.

The fundamental issue with the systematic enumeration is the low information content per configuration. This can be counteracted by randomly displacing all the atoms and solving the corresponding regression problem that arises. This method is sometimes called the regression method and was introduced by Esfarjani and Stokes [44]. They also argued that the noise in the data is effectively canceled due to the random nature of the displacements adding to the benefits of the increased information content. Many methods exist for generating suitable configurations and the most simple one is the rattle method where random displacements drawn from a zero mean normal distribution are applied to the atoms. The distribution of displacements would correspond to that of an Einstein crystal, which is typically a poor approximation of most solids. It is a simple method but can lead to unphysical configurations probing unwanted anharmonicity in the crystal. At the end of this chapter we shall take a look at some better ways for generating the displacements.

2.1.2 Truncation of the expansion

Even though the regression method can be used to increase the amount of information gained from each structure there are still too many FCs to be independently determined. Thus the FC expansion must be truncated in some way in order to keep the number of unknown coefficients manageable. First and foremost we cut off the expansion after some order. For harmonic models only second-order terms are kept. If we want to study heat transport at least third-order terms must be included while dynamically stabilized materials might need fourth-order terms to adequately describe the PES. It is also possible to incorporate our physical intuition that atoms far away from each other only interact weakly. Thus we can view the above expansion as a cluster expansion where each FC coefficient $\Phi_{ijk\ldots}$ represents a cluster of atoms $(ijk\ldots)$. For example a cluster $(ijkk)$ would be a three-body, fourth-order cluster; see Fig. 2.2 for an illustration of clusters and crystal symmetries. Now we postulate that if two atoms i and j are further away from each other than some cutoff c all FCs where these two atoms are present must be zero, i.e., $\Phi_{\ldots i\ldots j} = 0$. In addition, we posit that in general n-body clusters are more important than $n+1$-body clusters and higher orders are typically less important than lower orders for most applications.

The FC expansion has advantages and disadvantages compared to other ways of describing the interatomic interactions. It is mathematically well studied and forms the

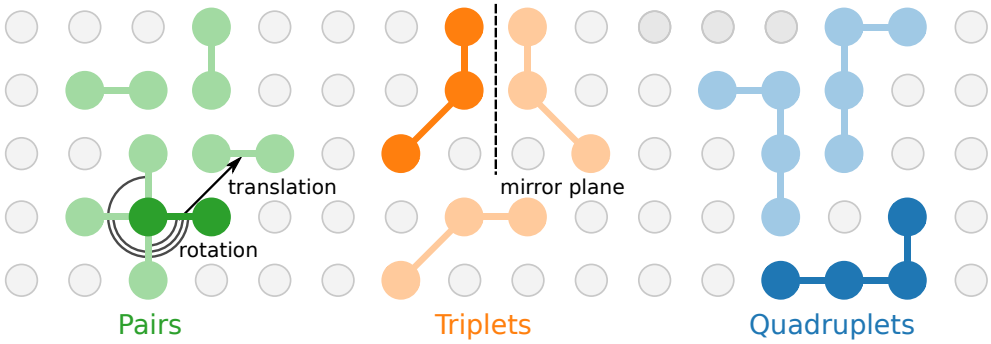

Figure 2.2: Illustration of possible clusters in a lattice. To each cluster belongs a set of FCs which must obey the lattice symmetries.

basis of the standard theory of lattice dynamics as we shall see later. Thus, it makes it straightforward to combine and compare (computer aided) theoretical techniques with direct computer simulations such as MD. The functional form is also simple to implement on, e.g., graphical processing units (GPUs) which makes it fast to evaluate for, e.g., MD [45]. There is no limit (other than computer memory and speed) to including larger clusters and higher order thus making the model scalable and tunable. The FC expansion is also linear in the unknown coefficients (the FCs) which makes it easier to analyze and fit compared to some other interatomic potentials.

On the other hand, the number of free parameters to determine grows rapidly with increasing anharmonicity (order), range (cutoff) and disorder (number of atoms in the primitive cell). Since the number of parameters dictates the amount of training data needed from usually computationally demanding reference calculations this makes it difficult to use for, e.g., glasses. The expansion is also firmly rooted in the notion of a lattice and (small) displacements around fixed lattice points. Thus when the PES is shallow and the atoms move far from the lattice points the expansion can quickly become unstable and lead to nonsensical predictions. This can for example happen near a phase transition or when the defect formation energy is low.

Next, the main symmetries of the FC expansion will be presented and what must be taken into account in order to make the extraction of the coefficients feasible in practice.

2.1.3 Crystal symmetries

The crystal lattice imposes certain symmetries on the FCs. These symmetries can be used to reduce the number of free parameters needed to determine the FCs. These symmetries originate from the functional form, the spatial symmetries of the crystal and physical symmetries in general.

For example the equality of mixed partials enforces

$$\Phi_{ij\dots} = \Phi_{P(ij\dots)}, \tag{2.5}$$

where P is any permutation of a list of indices $[ij\dots]$ of length n. In the harmonic case (second order) this simply means that the FCs are described by a symmetric matrix. An explicit example for third order would be

$$\Phi_{i=2,j=5,k=4} = \Phi_{i=4,j=2,k=5}. \tag{2.6}$$

The crystal/molecular symmetries impose further conditions on the FCs. Consider the symmetry of a 180 degree clockwise rotation of a diatomic molecule oriented along the horizontal axis in two dimensions. The symmetry operation which takes the original displacements u and transforms them to the symmetrically equivalent displacements $\tilde{u}$ looks like

$$\tilde{u} = \begin{bmatrix} \tilde{u}^x_{\text{left}} \\ \tilde{u}^y_{\text{left}} \\ \tilde{u}^x_{\text{right}} \\ \tilde{u}^y_{\text{right}} \end{bmatrix} = \begin{bmatrix} 0 & 0 & -1 & 0 \\ 0 & 0 & 0 & -1 \\ -1 & 0 & 0 & 0 \\ 0 & -1 & 0 & 0 \end{bmatrix} \begin{bmatrix} u^x_{\text{left}} \\ u^y_{\text{left}} \\ u^x_{\text{right}} \\ u^y_{\text{right}} \end{bmatrix} = Su. \tag{2.7}$$

But since the total energy of this configuration must be the same we have

$$\frac{1}{2}\phi_{ij}u_iu_j = \frac{1}{2}\phi_{ij}\tilde{u}_i\tilde{u}_j \tag{2.8}$$

$$\phi_{ij}u_iu_j = \phi_{ij}S_{ii'}u_{i'}S_{jj'}u_{j'}. \tag{2.9}$$

Since this must hold for all displacements u we get

$$\phi_{ij} = \phi_{i'j'}S_{i'i}S_{j'j}. \tag{2.10}$$

By flattening the indices $ij \to a$ we can write this relation as an eigenvalue equation

$$\phi_a = M_{aa'}\phi_{a'}, \tag{2.11}$$

where M is now a 16×16 matrix. In scaled coordinates this matrix will always be an integer matrix. The set of possible FCs is now described by the set of eigenvectors of M with eigenvalue 1. Or in other words, the FCs are spanned by the kernel of $1 - M$. Using this technique the set of independent parameters for the FCs can be reduced using the crystal symmetries. Note that the interatomic potential is of course independent of *any* rotation of the molecule and will lead to the so-called rotational sum rules described later.

Another important symmetry for crystals is the translational invariance of the lattice

$$\Phi(n, n', \dots) = \Phi(n + N, n' + N, \dots), \tag{2.12}$$

where n and N index the primitive cells. Note that they are all expressed as linear constraints and thus relatively easy to handle computationally. All these symmetries are used in HIPHIVE which is the code developed in Paper I via SPGLIB [46] in order to reduce the number of free parameters. More information can be found in Paper I. Next we consider the effect of two global symmetries in the form of continuous translations and rotations of the complete crystal.

2.1.4 Global symmetries

Apart from the local symmetries the FC expansion must obey some global symmetries, namely translational and rotational invariance. These symmetries define so-called sum rules, For the translational invariance, e.g., one obtains

$$\sum_{\mu n} \Phi^{\alpha}_{\mu\ldots}(n, \ldots) = 0. \tag{2.13}$$

The translational sum rule ensures that no force acts on the atoms as the result of a translation of the lattice. Note that the Cartesian component has been moved out of the compound index i as the sum has to be fulfilled for all three Cartesian directions independently. The translational sum rule is important for the behavior of the dispersion relation near the Γ point (i.e., at zero momentum) where it should tend to zero for acoustic phonons, see Fig. 2.3.

For the rotational symmetry there are two kinds of sum rules [31, 34]. The (second-order) Born-Huang sum rule reads

$$\sum_{j} \Phi^{\alpha\beta}_{ij} r^{\gamma}_{j} = \sum_{j} \Phi^{\alpha\gamma}_{ij} r^{\beta}_{j} \tag{2.14}$$

and embodies that no torque is induced as the result of a rotation of the lattice. In general, these sum rules will couple different orders of the expansion to each other but only considering second-order sum rules is sufficient to enforce the quadratic behavior of out-of-plane (ZA) modes in 2D materials [47]. This effect can be seen in Fig. 2.3

Additionally, there are the Huang constraints enforcing the correct behavior of the elasticity tensor

$$\sum_{ij} \Phi^{\alpha\beta}_{ij} r^{\gamma}_{i} r^{\delta}_{j} = \sum_{ij} \Phi^{\gamma\delta}_{ij} r^{\alpha}_{i} r^{\beta}_{j}, \tag{2.15}$$

which are important for the elastic constants to exhibit the correct symmetries. The rotational sum rules are especially important in two-dimensional materials, where they are needed to enforce the correct quadratic behavior of the transverse acoustic modes near the Γ-point, see Fig. 2.3.

The two sets of symmetries (crystal and global) define a set of irreducible FCs ϕ where any set of FCs obeying the above symmetries can be written as a linear combination of

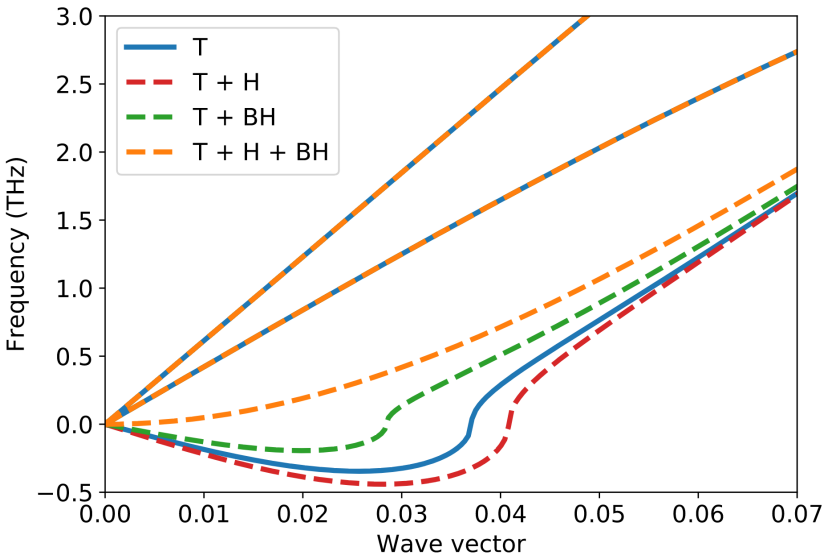

Figure 2.3: Dispersion relation of MoS_2 near the Γ-point (i.e., zero momentum) along the ⟨100⟩ direction. The translational (T) sum rules (2.13) are fulfilled as the dispersion goes to zero at Γ. The Born-Huang (BH) sum rules (2.14) and Huang (H) constraints (2.15) are needed to enforce the correct quadratic behavior of the lowest transverse acoustic mode.

the irreducible ones, i.e.,

$$\Phi = \sum_k a_k \phi^k. \tag{2.16}$$

This can be either combined with the crystal symmetries to reduce the number of free parameters in the fitting procedure or enforced as a post-processing step.

In summary the FCs are a linear basis in which we can relate the forces with the displacements in the system. To determine the FCs we calculate forces using, e.g., DFT for some supercells with displacements and solve the system of linear equations. Symmetry relations can be used to reduce the number of free parameters and thus reduce the computational cost of computing the FCs using electronic structure theory calculations. The FCs can for instance then be used to run MD simulations as described in Chapter 3 and [45] to calculate various properties of interest. They can also be used in analytical methods to calculate properties directly using, e.g., Green's functions methods. The basics of this approach will be outlined in the following sections.

2.2 Harmonic phonons

The basi(c)s for understanding the thermodynamics of vibrations in crystals is the phonon picture. In the harmonic approximation only the second-order FCs are kept

and the Hamiltonian is exactly solvable. The solutions to this system in the framework of quantum mechanics are called phonons (in classical mechanics they are sometimes called normal modes). These solutions are typically regarded as quasi-particles but can be equally categorized as collective excitations. Nevertheless, the particle picture is especially useful in the context of the Peierls-Boltzmann transport equation (PBTE) which we will come across later in Chapter 4. In addition, the exactly solvable model serves as a starting point for Green's function methods to calculate higher-order corrections to physical observables due to the anharmonicity. The theory is covered in many text books (see the introduction to this chapter) and starts with the real space representation of the PES leading to the following Hamiltonian

$$H = \sum_{n\mu\alpha} \frac{\left|p_\mu^\alpha(n)\right|^2}{2m_\mu} + \frac{1}{2} \sum_{\substack{n,n' \\ \mu\nu \\ \alpha\beta}} \Phi_{\mu\nu}^{\alpha\beta}(n,n') u_\mu^\alpha(n) u_\nu^\beta(n'), \tag{2.17}$$

where n indexes the unit cells in the lattice, μ and ν index the atoms in the basis, while α and β index the Cartesian directions. p is the momentum, u the displacement and m_μ the mass of the atoms.

The solution to this Hamiltonian proceeds in two steps. First the lattice translation symmetry is diagonalized by a discrete Fourier transform which introduces the momentum coordinate k (this is the wave part). Second, the resulting dynamical matrix is diagonalized which introduces the band index s and corresponding frequencies ω and polarization vectors W.

We simply state the solution here without details. The dynamical matrix is a central object as its spectrum provides the frequencies and polarizations

$$D_{\mu\nu}^{\alpha\beta}(k) = \sum_n \frac{\Phi_{\mu\nu}^{\alpha\beta}(0,n)}{\sqrt{m_\mu m_\nu}} e^{-ik(R_\mu - R_\nu(n))} = \sum_s W_{\mu s}^\alpha(k) \omega_s^2(k) W_{\nu s}^\beta(k). \tag{2.18}$$

The new coordinates are in the form of lattice waves

$$q_s(k) = \sum_{\mu\alpha n} \sqrt{m_\mu} u_\mu^\alpha(n) W_{\mu s}^\alpha(k) \mathrm{e}^{ik\cdot R_\mu(n)} \qquad u_\mu^\alpha(n) = \frac{1}{\sqrt{m_\mu}} \sum_{ks} q_s(k) W_{\mu s}^\alpha(k) \mathrm{e}^{ik\cdot R_\mu(n)} \tag{2.19}$$

with polarization vectors W and frequencies ω. The polarizations describe orthogonal displacement patterns in the unit cell which are modulated by plane waves of wave vector k and frequency ω. One needs to be careful with respect to the the phase factor since it is a matter of convention whether it is taken to be the position of the origin of each primitive cell or the equilibrium position of the atom.

From the above expressions it is apparent that the central objects of interest are the dispersion relation $\omega_s(k)$ and the corresponding polarization vectors $W_{s\mu}^\alpha(k)$. The

dispersion relation relates the quantum states of the system indexed by the wave vector k and the band index s to the frequencies (energies) $\omega_s(k)$ of the modes. The dispersion relation is sometimes just called the spectrum. It is important to note that the modes produced by the harmonic approximation do not interact. The energy eigenvalues are thus exact and the states have "infinite" lifetimes.

2.2.1 The dispersion relation

k can in principle be any vector in the Brillouin zone (the central primitive cell in the inverse lattice) and is typically communicated by taking a path between high symmetry points in the inverse lattice and plotting the corresponding frequencies for the different bands indexed by s. Such a dispersion is illustrated in Fig. 2.4.

Let us go over some of the main features of the dispersion in Fig. 2.4. The y-axis denotes the frequency (energy) of the mode and is typically reported in THz (meV or cm^{-1}). Typical phonon frequencies are on the order of 1 to 100 THz (1 THz = 4.136 meV = 33.36 cm^{-1}). A very high frequency mode occurs in the stretch bond of the H_2 molecule at around 125 THz or 500 meV. Long wavelength modes and soft modes near phase transitions modes can have almost zero frequency.

Along the x-axis is the k-point under consideration. The labels indicate certain high symmetry points in the Brillouin zone such as zone edges, faces or corners. Γ is the zone center and represents waves of infinite wavelength in which all atoms in the different unit cells move in the same way.

From the Γ-point emerge two lines in each direction from zero frequency. These are the two (in this case degenerate) TA modes and the single LA mode. The LA mode is typically higher in energy as most materials resist compression better than shear strain. The A stands for acoustic and originates from the fact that the slope of the dispersion curve correspond to the group velocity of a traveling wave. In other words the speed of sound and the elastic constants of the material can be read off from the slope of the acoustic modes close to the zone center.

At higher frequencies at the Γ-point we can find the optical modes. Their name originate from the fact that they typically correspond to out of phase motion of neighboring atoms which in certain crystals induce a polarization. This polarization allows a coupling to electromagnetic radiation, typically in the infrared regime and hence the modes can be optically excited. This effect is used in, e.g., infrared and Raman spectroscopy.

One very important thing to note is that while the real space sum in Eq. 2.17 in principle extends to infinity, the fact that the interatomic FCs do not, implies that we can limit the sum to neighboring cells in which the FCs are finite. This means that if we can calculate the FCs for a small supercell in which the FCs go to zero before atoms start to interact with their own mirror images, we can calculate the dynamical matrix for any k-point we want – even those not supported by the supercell. This also implies that once in reciprocal space the dynamical matrices can be exactly interpolated

without the need to go back to real space.

On the other hand if the FCs do not decay to zero within the supercell we will end up with aliasing where long-range FCs fold back and appear like short-range FCs. This can be a big problem in systems with electrostatic interactions and weak screening as in polar insulators. The remedy is to create a model for how the long-range interactions should look like, partition the FCs into a long-range and short-range contribution, calculate each separately and then stitch them together again. This is described in the seminal papers by Gonze and Lee [48] and partly described in the next section.

On the bright side, for certain choices of k in Eq. 2.17 the sum is exact, even if the atoms interact with their own images. These k correspond to the inverse lattice points of the supercell and thus the dispersion at those points is exact by construction. This effect is illustrated for NaCl, which has very long ranged FCs, in Fig. 2.4. The dispersion is compared using FCs in supercells of increasing size. The black line is effectively the dispersion for an infinitely large system. The supported inverse lattice points are indicated with circles. As we can see, even if the dispersions do not align with that of the infinite systems they do agree at the supported points. This is, however, only true if *all* FCs in the supercell are used. The blue lines indicate what happens if the FCs are truncated using a spherical cutoff which roughly corresponds to a $2 \times 2 \times 2$ supercell.

2.2.2 Long range corrections

We shall now discuss how the correct dispersion (the black line) was constructed in Fig. 2.4. As mentioned above, as long as the cutoffs are longer than the expected interactions in the material, the above approach, using cutoffs to limit the number of free parameters, works well. In some cases though there are long-range forces present. This can for example happen in two-dimensional materials where the screening is weak in the out-of-plane direction or in polar materials with large dynamic (Born effective) charges such as in NaCl. In these materials the displacements induce long-ranged electrostatic dipole-dipole interactions [49], which in theory have infinite range. This effect is the reason behind the so-called LO-TO splitting where the longitudinal optical (LO) and transverse optic (TO) modes exhibit a seemingly non-analytical behavior near the Γ-point [50], see Fig. 2.4.

This can be effectively remedied using the technique introduced by Gonze and Lee [48, 51] and the dispersion can be corrected around the Γ-point. It is important to remember that if the FCs are constructed in a finite periodic supercell and all FCs are included, the corresponding dispersion is correct at supported inverse lattice points [39] as discussed in the previous section. If the FCs are long-ranged the Fourier interpolation near the Γ-point at large wave lengths will fail. In practice the fix is to use the Born effective charges calculated from DFPT to construct a long-ranged dynamical matrix via Ewald techniques for the supercell in question and calculate the long-ranged real space FCs Φ_{LR} due to the interacting Born-charges (dipoles). The short-ranged FCs Φ_{SR}

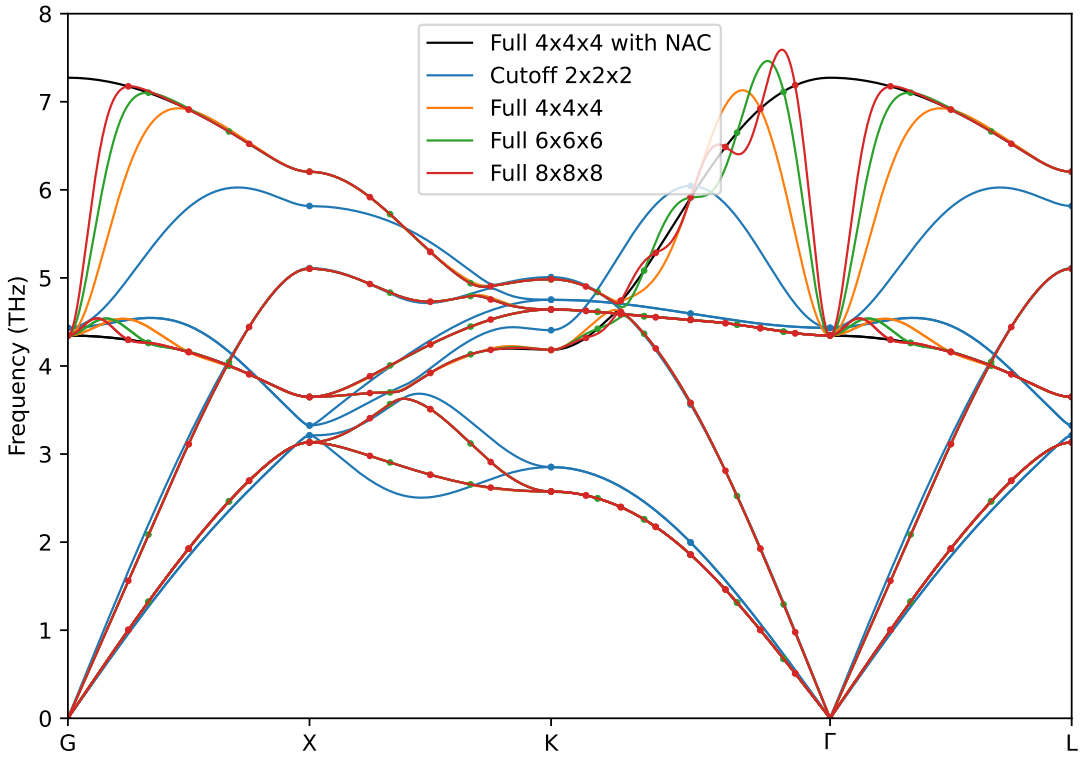

Figure 2.4: Dispersion relation of NaCl. Demonstration of how the choice of supercell size and method affects the phonon dispersion. Solid blue: A spherical cutoff corresponding to a $2 \times 2 \times 2$ supercell cannot replicate the correct dispersion (black solid line) even at supported reciprocal points. Solid orange/green/red: Exact FCs without any cutoff imposed in increasing supercell sizes give an exact dispersion relation at supported reciprocal points. Solid black: Full dispersion for the long-ranged interaction obtained from a $4 \times 4 \times 4$ supercell and corrected using the method by Gonze and Lee. The splitting at the Γ-point is called longitudinal optic–transverse optic (LO-TO) splitting.

are fitted to the remainder of the DFT forces

$$F_{\text{DFT}} - (-\Phi_{LR} u) = -\Phi_{SR} u. \tag{2.20}$$

Now the FCs are separated in a long-ranged analytical part and a short-ranged fitted part and the analysis can continue as usual for any intermediate points.

2.2.3 Thermodynamics of phonons

We will now see how the phonons can be used in order to calculate various properties of interest. A useful way of representing the phonons is in the language of second

quantization. Remember that the original harmonic Hamiltonian (Eq. 2.17) reduces to a set of independent waves described by the wave number k and band index s.

$$H = \frac{1}{2} \sum_{ks} \left(\left| p_s(k) \right|^2 + \omega_s^2(k) \left| q_s(k) \right|^2 \right) \tag{2.21}$$

or in the framework of second quantization in terms of creation and annihilation operators

$$H = \sum_{ks} \left(\frac{1}{2} + a_s^\dagger(k) a_s(k) \right) \hbar \omega_s(k) \tag{2.22}$$

following the standard procedure.

We are now in the position to take a look at some equilibrium properties of phonons. In theory the harmonic approximation is limited to thermodynamic equilibrium properties at zero Kelvin. In practice the anharmonic effects are often small and thermodynamic properties are calculated for higher temperatures. Take for instance the expected number of phonons in a mode λ given by the Bose-Einstein distribution

$$n = \left\langle a^\dagger a \right\rangle = \frac{1}{\mathrm{e}^{\hbar\omega/k_\mathrm{B}T} - 1}. \tag{2.23}$$

Another interesting case can be seen in the probability distribution of finding the oscillator at position q at some temperature T. The distribution is, just as in the classical case, given by a normal distribution but with a different variance

$$\sigma^2_{\text{quantum}} = \frac{\hbar}{2\omega} \coth \frac{\hbar\omega}{2k_\mathrm{B}T} \tag{2.24}$$

compared to the classical case $\sigma^2_{\text{classical}} = k_\mathrm{B}T/\omega^2$. This is straightforward to show using the Mehler kernel and the real space solutions to the quantum harmonic oscillator, see, e.g., [52]. This is useful if we want to generate configurations based on quantum statistics.

Other equilibrium thermodynamics quantities can be derived from the Helmholtz free energy

$$F = \sum_{ks} \frac{1}{2} \hbar\omega_s(k) + k_\mathrm{B}T \log\left(1 - \mathrm{e}^{-\beta\omega_s(k)/k_\mathrm{B}T}\right). \tag{2.25}$$

Two other important equilibrium thermodynamic properties are the constant volume heat capacity C_V and density of states $\rho(\omega)$. The heat capacity is given by

$$C_V = \sum_\lambda \left(\frac{\hbar\omega_\lambda}{k_\mathrm{B}T} \right) \frac{\mathrm{e}^{\hbar\omega/k_\mathrm{B}T}}{\left(\mathrm{e}^{\hbar\omega/k_\mathrm{B}T} - 1\right)^2} \tag{2.26}$$

and the density of states is defined as

$$\rho(\omega) = \sum_\lambda \delta(\hbar\omega - \hbar\omega_\lambda). \tag{2.27}$$

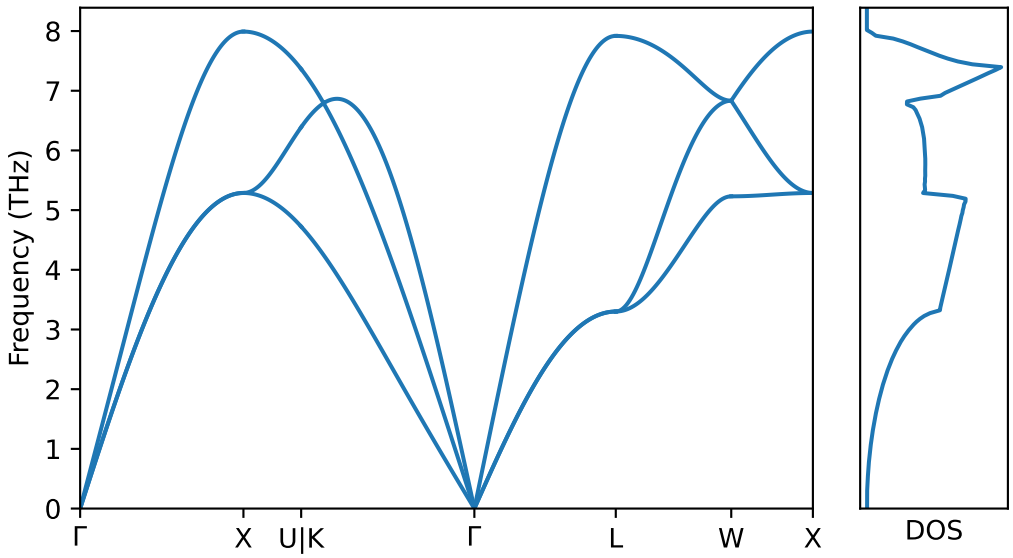

Figure 2.5: Phonon dispersion and density of states in aluminum calculated using an effective medium theory potential.

In practice the density of states is commonly calculated on some k-space grid and the delta-function is approximated using some nascent delta-function with a smearing parameter. Other methods include integration schemes using, e.g., the tetrahedron method [53]. Because of the linear dispersion near the Γ-point where the lowest energy modes live the density of states goes like $\rho(\omega) \propto \omega^2$ for a 3D system. A plot of the phonon dispersion and density of states in aluminum can be seen in Fig. 2.5.

The density of states is related to the free energy via the partition function

$$Z = \int_0^\infty \mathrm{d}\omega \rho(\omega) \mathrm{e}^{-\hbar\omega/k_\mathrm{B}T}. \tag{2.28}$$

This is an important relationship and in Chapter 3 we shall also see the connection to the velocity-velocity autocorrelation.

As a last example we shall look at the dynamical structure factor. The dynamical structure factor can be evaluated in the harmonic approximation

$$S_s(Q,\omega) \propto \sum_k \left|F_s(Q,-k)\right|^2 (n_s(k)+1)\delta(\omega-\omega_s(k))\Delta(Q-k), \tag{2.29}$$

where Q is the scattering vector, ω the energy, n is the Bose-Einstein distribution and Δ is 1 whenever the argument is a reciprocal lattice vector G and zero otherwise. F_s is

given by

$$F_s(Q,k) = \sum_i \sqrt{\frac{\hbar}{2m_i\omega_s(k)}} b_i \mathrm{e}^{-W_i/2} \mathrm{e}^{i(Q+k)\cdot r_i} Q \cdot e_{js}(k), \tag{2.30}$$

where b is the neutron scattering length which needs to be replaced by a Q-dependent form factor in the x-ray case and W is the Debye-Waller factor. The Debye-Waller factor is given by $W_i = \langle q \cdot u_i \rangle^2$ and is a thermal average that smears out the structure factor.

2.3 Lifetimes and spectral functions

The harmonic model of vibrations in crystals works very well in many cases, especially at low temperatures. However, with increasing temperature, the displacements increase and anharmonic effects become important. Most notably, the harmonic model has infinite lifetimes and lacks thermal expansion. The phonons will thus move through the lattice without scattering. A first attempt to fix this is via the quasi-harmonic approximation where FCs are calculated at different volumes. From this information about the volume dependence of the frequencies, the Gibbs free energy can be calculated and related properties extracted such as Grüneisen and thermal expansion parameters.

While this approach is often sufficient for calculating equilibrium properties for many materials, the modes are still independent and no scattering can take place. We thus introduce the first-order perturbation in the form of the third-order FCs.

$$H' = \frac{1}{3!} \sum \Phi_{ijk} u_i u_j u_k. \tag{2.31}$$

By considering the third-order FCs as a perturbation to the harmonic phonons we can start to explore how anharmonicity affects the previously independent modes of vibrations.

The introduction of a perturbation will make our previous independent modes start to interact. This can be thought of as if the phonons will now oscillate in a slightly different way with a slightly different frequency. Furthermore, if we excite a phonon mode at time t_0 and ask the question how many phonons are in the mode at a later time t_1 we will observe a change. This is captured by the lifetime of the mode which can be thought of to represent how long time it takes for a phonon to decay. These effects are captured by the line shift Δ and the line width Γ of the mode. How to relate and calculate these quantities to observables is typically done in the framework of many-body perturbation theory using Green's functions methods and diagrammatic techniques [54–56]. What it boils down to is a way to translate the real space perturbation H_3 to second and higher-order correlation functions (or moments) of the phonons. The

hope is to rewrite the correlation functions into a series which either converges fast or is easy to sum to infinity. Typically the correlation functions (or propagators/Green's functions) can be more easily related to macroscopic observables such as cross sections or thermodynamic quantities. Independent of the technique used (Feynman diagrams, renormalized operators or decoupled Green's functions) we start from something we know and, using a recipe, calculate something we do not know but which looks similar to what we do know.

The building blocks for all three methods are quadratic form of creation and destruction operators. Examples include the correlation function

$$G(t) = \langle a(t)a^{\dagger}(0)\rangle, \tag{2.32}$$

which is the overlap of the state of an additional particle created at time 0 with itself at a later time t. In the harmonic case the time evolution is simple and we get

$$G_0(t) = \mathrm{e}^{-i\omega_0 t}, \tag{2.33}$$

i.e., just a phase factor with the frequency given by the frequency of the mode. The Fourier transform of the free propagator is given by

$$G_0(\omega) = \frac{1}{\omega - \omega_0}. \tag{2.34}$$

Notice that this is not a delta-function. The departure from the free propagator is given by the spectral function A which can be used to calculate different types of propagators. In the harmonic case this is a delta-function, while in the interacting case the archetypical form of the spectral function is the Lorentzian

$$A(\omega) = \frac{1}{(\omega - \omega')^2 + \Gamma^2}, \tag{2.35}$$

which results in the quasi-particle propagator

$$G(\omega) = \frac{1}{\omega - \omega' + i\Gamma}. \tag{2.36}$$

The representation of the propagators using the spectral function is called the Lehmann representation

$$G(\omega) = \int d\omega' \frac{A(\omega')}{\omega - \omega'}. \tag{2.37}$$

From this we can also see that the spectral function is intimately related to the imaginary part of the propagator. In practice the spectral function is obtained by calculating the self-energy Σ, which is related to the free G_0 and interacting G propagators via

$$\Sigma = \Delta + i\Gamma = G_0^{-1} - G^{-1} \tag{2.38}$$

and is in some sense an equivalent way of quantifying the departure from the free theory.

In reality the self-energy is frequency dependent which makes life hard but interesting. The next step is to apply second-order perturbation theory with the third-order FCs as a perturbation. In this way the corrections to the energy levels of the phonons can be determined. To first order they are generally found to be imaginary with no shift in the frequencies. The lifetime is related to the imaginary part of the self energy and can be calculated using many-body perturbation theory to give

$$\Gamma_\lambda(\omega) = \frac{36\pi}{\hbar^2} \sum_{\lambda' \lambda''} \left|\Phi_{-\lambda\lambda'\lambda''}\right|^2 [\,(n_{\lambda'} + n_{\lambda''} + 1)\delta(\omega - \omega_{\lambda'} - \omega_{\lambda''}) + \\ (n_{\lambda'} - n_{\lambda''})(\delta(\omega + \omega_{\lambda'} - \omega_{\lambda''}) - \delta(\omega - \omega_{\lambda'} - \omega_{\lambda''}))\,],$$

where λ is a compound index over the momentum coordinate k and band index s. The self-energy (and thus the lifetime) depends on the Fourier transformed third-order interactions and the temperature-dependent occupations n. Important to note is that the self-energy of a mode depends on the frequency ω. The energy shift is given by similar expressions and can be found in, e.g., the book by Wallace [34].

With the self-energy at hand any single particle property can be calculated. One such property is the 1-phonon neutron scattering cross section which turns out to be proportional to the spectral function function. Using the above self energy we get [38, 57].

$$\sigma(\omega) \propto \frac{\omega_\lambda \Gamma_\lambda(\omega)}{(\omega^2 - \omega_\lambda^2 - 2\omega_\lambda \Delta_\lambda(\omega))^2 + 4\omega_\lambda^2 \Gamma_\lambda^2(\omega)} \tag{2.39}$$

for the spectral function which can be compared to neutron scattering experiments.

Similarly other properties such as free energies or Raman spectra can be calculated using Green's function methods. However, due to the computational cost of extracting higher-order FCs and the complexity of the subsequent computations typically some kind of renormalization scheme is used, which will be described in the next section.

The above expressions can be derived in a couple of ways see, e.g., [35, 42, 43, 58]. Since the interaction element contains crystal-momentum conserving delta-functions the lifetimes depend not only on the strength of the interaction (anharmonicity) but also on the geometry of the dispersion relation. For example in BAs, which has a large phonon band gap, higher-order processes must be included to correctly describe the dynamics in the crystal [59] as the higher-energy states (bands) cannot be reached from the low energy states via three-phonon processes due to energy (and momentum) conservation laws. To overcome this limitation requires including fourth-order interactions in the thermal conductivity calculations as we shall see in Chapter 4, providing further motivation for methods for efficient extraction of higher-order FCs. The need for higher-order FCs can also show up when the harmonic phonons have negative en-

ergies (imaginary frequencies) as can happen in dynamically stabilized materials such as body-centered cubic (BCC)-Ti.

If the harmonic phonons are still well behaved quasi-particles, it is sometimes sufficient to calculate second-order corrections to the energies and lifetimes with ordinary perturbation theory. In second-order perturbation theory there is a contribution from both third and fourth-order FCs to both frequencies and lifetimes. Typically Green's function or variational methods are used to construct effective harmonic FCs corresponding to the renormalized propagators. For more information see, e.g., [60–62] and references therein.

2.4 Renormalized phonons

When the anharmonicity of the material is strong it is not enough to consider the departure from the harmonic case as a perturbation. In this case higher-order terms in the PES must be included and there are a few approaches for incorporating these. One way is to extract the higher-order FCs and continue to use, e.g., many-body perturbation theory. By including the higher-order processes it is possible to further correct the lifetimes and frequencies of the phonons. This is for example implemented in ALAMODE [43]. There are, however, methods to include the renormalization by choosing the displacements used to create the FCs as we will now see.

2.4.1 Variational principles

The choice of fitting the forces has an interesting relation to a variational principle via the Bogoliubov inequality. By applying Jensen's inequality ($\psi(\langle X \rangle) \leq \langle \psi(X) \rangle$ for ψ convex) to the Zwanzig free energy perturbation formula [63] for the free energy difference ΔF between two systems with Hamiltonians H and $\widetilde{H}$

$$\Delta F = \widetilde{F} - F = -\beta^{-1} \log \left\langle e^{-\beta \Delta E} \right\rangle_H = \langle \Delta E \rangle_H - \frac{\beta}{2} \left\langle \Delta E^2 \right\rangle_H \leq \langle \Delta E \rangle_H \,, \tag{2.40}$$

it is possible to establish a variational principle for the model (H) free energy F. In other words, the model free energy is minimized under the constraint that the first cumulant is zero. By applying this idea it is possible to show that using the OLS loss function for the forces f of a harmonic model

$$\min \left\langle \left(f - \tilde{f} \right)^2 \right\rangle_H \quad \text{subject to} \quad \langle \Delta E \rangle_H = 0 \tag{2.41}$$

is equivalent to

$$\min F \quad \text{subject to} \quad \langle \Delta E \rangle_H = 0. \tag{2.42}$$

where the minimization is with respect to the free parameters of the model, i.e., the FCs. If the true ensemble described by the exact Hamiltonian is used as the sampling

ensemble the same idea holds but the model free energy must be maximized instead. In other words the idea is symmetric in H and $\tilde{H}$. Notice that in practice the constraint is trivially enforced by the constant term in the model Hamiltonian.

This establishes a rationale for these methods and the above relations can also be obtained in the quantum case. Two common methods to be described below are based on this idea and differ in whether the sampling is in the true exact ensemble (accessible by, e.g., ab initio MD) or in the model ensemble.

2.4.2 Self-consistent harmonic phonons

If the procedure is based on sampling using the same model we want to construct, it is called a self-consistent method [62]. In lattice dynamics it is often called the self-consistent harmonic approximation (SCHA) or just the self consistent phonons (SCP) method and it is described in, e.g., [34]. These methods have firm roots in theoretical techniques such as Green's function methods and diagrammatic perturbation theory or the statistical perturbation method based on operator renormalization [64]. In practice on a computer we can generate displaced configurations and fit a harmonic model to the forces iteratively until the procedure has converged. The initial guess of the FCs is often in the form of an Einstein crystal and then as the model improves new configurations are generated using, e.g., the phonon rattle method where the modes are randomly populated according to the known statistics of the harmonic oscillator. A variation of this method is the stochastic self-consistent harmonic approximation (SSCHA) where the free energy is minimized using a stochastic gradient descent method [64–68]. In practice this makes it easy to minimize also the Gibbs free energy by varying the cell metric.

One of the main problems with any harmonic method is that it is only possible to effectively capture anharmonic effects in the harmonic FCs up to a certain degree. This can be partly remedied by including anharmonic effects in the sampling and in the model. The second large problem is deterioration of the ensemble average as the model improves. The old configurations are based on a different model than the present and thus all ensemble averages will be short-term biased. Clever methods exist, however, to discard configurations deemed to be of no use for the current model and thus the convergence can be sped up by including less data, a kind of bias-variance trade-off. In other words we can include fewer samples from the more correct distribution and remove bias terms but obtain a larger random error due to the finite samples size Or we can include more data and remove errors due to small sample size but be penalized by a small systematic error because of sampling from the (slightly wrong) distribution.

2.4.3 Effective harmonic models

An alternative is to sample configurations from ab initio molecular dynamics (AIMD) simulations. This ensures physical configurations but can be expensive depending on the underlying ab initio method, code, system and so on. This approach is also called the temperature-dependent effective potential (TDEP) method after the eponymous program [69–71]. With this method effective harmonic models (EHMs) can be generated where higher-order FCs have been captured (or renormalized) into the second-order FCs. This allows for the calculation of temperature-dependent phonons and related quantities. Naturally also higher-order models can be constructed in this way to access, e.g., lifetimes and by extension the thermal conductivity [72]. The main downside of this method is the expensive sampling, especially if quantum effects must be taken into account which would require, e.g., path integral MD. This can be partly overcome by stochastic initialization and up-sampling techniques [73]. Effective harmonic models can also be used to access otherwise hard to get properties via lattice dynamics even when a cheap analytical potential is used where properties are (in principle) accessible using other methods. In this fashion it is, for example, possible to calculate free energies via an EHM instead of via thermodynamic integration. How well this works in practice is, however, system dependent and can differ between systems [74].

2.4.4 Anharmonic higher order models

Lastly there is the possibility to construct effective or self-consistent anharmonic FC models. With this method anharmonic expansions are fitted to either AIMD or the model itself is sampled using Monte Carlo (MC) or MD simulations. While MD has been performed using FCs [75], to the best of my knowledge self-consistent anharmonic models were not done before Brorsson *et al.* [45]. In the limit of infinite order and cutoff this method should produce the same true expansion of the PES independent of whether the sampling is in the true or the model Hamiltonian.

In practice this method using anharmonic FCs and MD allows for non-perturbative treatment of high-order perturbations, e.g., up to fourth order in the energy expansion. This can be useful where normal perturbation theory struggles. In addition the self-consistent procedure ensures that the PES is stable for reasonable configurations. Typically an anharmonic force constant potential (FCP) will be somewhat unstable when running MD if the training data is not diverse enough. This can often be fixed by including configurations from an MD run close to where the system misbehaves. Unfortunately many systems exhibit "thermodynamically necessary" defects which can even be created spontaneously in MD simulation when the PES is soft or close to melting [76]. In theses situations FCPs are ill-suited although there have been attempts to artificially stabilize/constrain the expansion. The problem with anharmonic FCPs in general is that even if a good model is found it is not necessarily easier to find accurate proper-

ties of interest from this model compared to a lower-order model. For example, the free energy via perturbation theory from a self-consistent fourth-order model might not be more accurate than the exact free energy from a self-consistent harmonic model due to the extra level of approximations when dealing with fourth-order FCs.

3

Full anharmonicity

Molecular dynamics (MD) is a computational technique where the equations of motion for a system of atoms are (numerically) integrated in time [77]. The forces acting on the atoms are computed from some (conservative) force field as the gradient of the interatomic potential with respect to the positions. Since the force is the gradient of the energy with respect to positions the force field is a gradient of a scalar potential, hence the name interatomic potential.

For small systems and short time scales it is in principle possible to perform so-called AIMD simulations in order to analyze the motion of atoms. In that case the atomic forces (and other observables) are calculated by solving the (electronic) Schrödinger equation and integrating the equations of motion. For large systems this becomes, however, exceedingly expensive due to the poor scaling of DFT calculations (especially with respect to system size, as the cost scales approximately with the cube of the number of electrons). Thus we need to approximate the Born-Oppenheimer PES with a simple analytical form involving only the positions of the ions in order to study large systems on long time scales. Such an approximation of the PES is captured by an interatomic potential and can be roughly divided into two classes: traditional analytical (or empirical) potentials with comparably few parameters and simple functional forms, and modern heavily parameterized potentials often incorporating machine learning (ML) techniques in the construction of the potential and/or in the functional form itself.

We will start this chapter with a brief overview of interatomic potentials and the need for ML potentials and end with an overview of the MD technique. The final section will be dedicated to correlation functions. There we will show how all the properties we could calculate using perturbation theory can in principle be extracted from MD simulations.

3.1 Interatomic potentials

Interatomic potentials are roughly divided into analytical potentials and ML potentials. Analytical potentials have functional forms which are handcrafted, often based on some electronic structure theory. ML potentials have general functional forms with numerous tunable parameters. It is nice to understand the former in order to work with the latter.

3.1.1 Analytical potentials

The first serious use of an interatomic potential was perhaps the work of Fermi, Pasta, Ulam and Tsingou in the 1950s [78, 79]. They used the newly constructed MANIAC computer system to study the interactions between particles in a linear chain, a standard textbook problem in solid state physics (see Sect. 1.3). The particles were connected by simple harmonic springs with a small anharmonic perturbation and what they found was a surprising recurrence of the phase space path breaking the ergodic hypothesis, a cornerstone of MD.

After the linear chain and other simple systems such as interacting hard spheres, the Lennard-Jones (LJ) [1] liquid was analyzed by computational means in the 1960s. The LJ potential is one of the simplest analytical interatomic interactions and still widely used today. The term analytical potential comes from the possibility to write down an analytical expression for the interaction. The LJ potential consists of a weak attractive part modeling the vdW interactions and a strong repulsive core modeling the Pauli exclusion principle. The functional form is

$$V(r) = 4\epsilon \left[\left(\frac{\sigma}{r} \right)^{12} - \left(\frac{\sigma}{r} \right)^{6} \right] \tag{3.1}$$

and the potential is plotted in Fig. 3.1. The free parameters σ and ϵ determine the length and the strength of the interaction and are specific for a given system, say Argon or Helium. Despite its simplicity the LJ potential exhibits interesting behavior such as phase transitions.

The LJ potential is a simple example of a pair potential that works well for gases and some liquids, and pair potentials in general are heavily used in generalized vdW theory [80] (also known as classical DFT). Often the functional form consists of just a few parameters. Due to the simplicity they can be made to obey certain limiting properties for, e.g., low and high densities which makes them more well behaved in MD simulations. For gases (low density) and liquids (high disorder) two-body potentials work well or when the Coulomb pair-interaction dominates in ionic materials.

During the 1970s many systems were investigated using pair potentials such as water, molecules, and even proteins [81]. But in order to describe more complex materials

[1] Named after Sir John Lennard-Jones

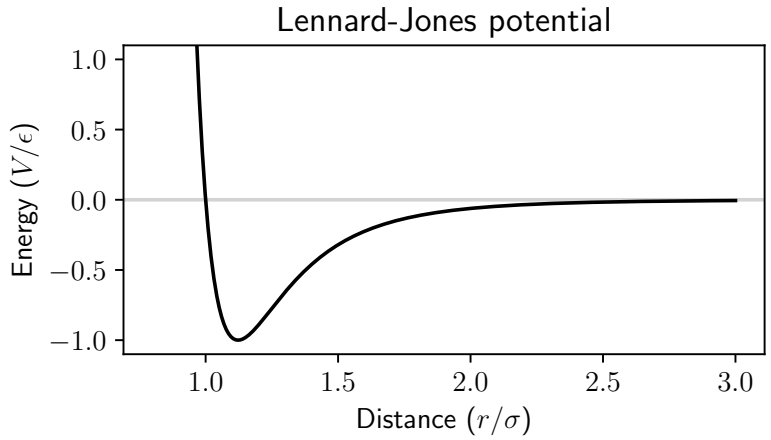

Figure 3.1: The Lennard-Jones potential. To the left of the minimum the strong repulsive part modeling the Pauli exclusion force dominates, while on the right the weak attractive part due to vdW interactions dominates. The minimum is located at a distance of $\sqrt[6]{2}\sigma$ where the potential energy is $-\epsilon$. Notice how the potential is nearly zero beyond approximately 3σ.

many-body affects must be taken into account. Such models emerged during the 1980s and include, e.g., embedded atom method (EAM) potentials [82], which can be cast in the form

$$V = \sum_{ij} V_2(r_{ij}) + \sum_i F\Big[\sum_j \rho(r_{ij})\Big]. \tag{3.2}$$

Here V_2 is a pair potential and F is called the embedding function. The form is well suited to model metals where the atoms move in a sea of electrons and the many-body effects enter as a density dependent two-body interaction ρ. Potentials of this type are sometimes called (pair) functionals as they are parameterized via functions instead of real parameters. This idea can be seen as a precursor to the modern types of heavily parameterized potentials.

For more complex molecules or covalently bonded materials such as silicon we need also angular dependence which enters as a "true" three-body effect (e.g., via angles) instead of an aggregated effect such as the density, see Fig. 3.2. One such approach is the bond-order potential formalism developed in the late 1980s by Abell [83] and Tersoff [84]

$$V = \sum_{ij} V_2^R(r_{ij}) + b_{ij} V_2^A(r_{ij}), \tag{3.3}$$

where b_{ij} depends on all angles θ_{ikj}. For more information on analytical potentials see [85].

During the 1990s and 2000s these types of potentials were successfully used for many systems including multi-component systems and also combinations of several types of

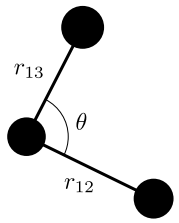

Figure 3.2: A cluster of three atoms described by three parameters, two bond distances and one bond angle. The potential energy $V(r_{12}, r_{13}, \theta)$ is an explicit function of the angle and can in general not be described/decomposed into pure two-body interactions. This model would be suitable for e.g. the internal forces in a water molecule.

potentials. However, they are hard to develop and systematically improve. Thus in tandem with faster hardware and development of the ML field new types of potentials emerged during the 2010s which were heavily parameterized. For more information about the historical development of analytical potentials see [86, 87].

3.1.2 Machine learning potentials

With the growth of the field of ML and the increasing performance of computers another class of potentials has emerged called ML potentials. For an overview of ML potentials see [88]. The aim is to bridge the gap between pure ab-initio methods and analytical potentials. The main problem with analytical potentials is that for complex systems it becomes difficult to construct a functional form suitable for describing all the interactions. The idea behind ML potentials is that a very flexible functional (e.g., neural networks (NNs) [89–91] or Gaussian process (GP) [92, 93]) can be trained given enough data. The drawback with these types of potentials is that the functional form is not easily (if at all) interpretable by a human and thus gives little insight into the underlying physics. Furthermore the parameter landscape is typically vast and care must be taken during the optimization to mitigate both overfitting and underfitting. Finally, these potentials have essentially no extrapolation capacity but should be considered as pure interpolations of the configuration space seen during training. It is thus very important to choose training structures spanning the phase space of interest.

The first part of a ML potential are the descriptors which capture the local environment around an atom and serve as inputs to the functional form instead of the raw atomic coordinates. There are a huge number of atomic descriptors and the challenge is to create descriptors such that the resulting PES obeys relevant global symmetries such as translational and rotational invariance. The construction of (good) descriptors is difficult. They must be simple enough to be fast to calculate but span a complex enough space so that different atomic configurations are discernible. They should also be robust so that similar descriptors represent similar structures. Some examples of atomic de-

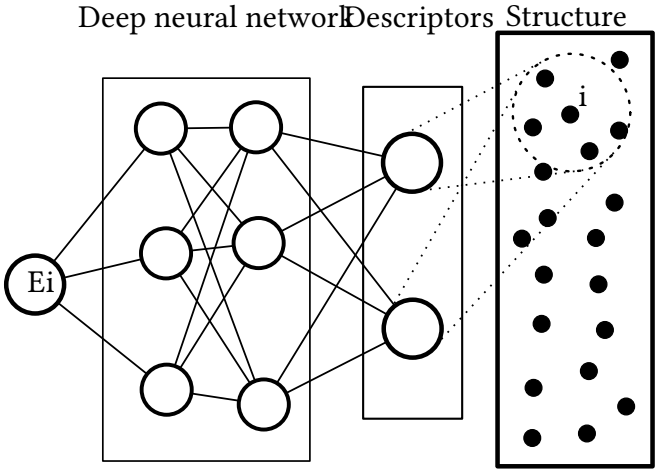

Figure 3.3: Illustration of a neural network based machine learning potential. To the right is a configuration of atoms. Two descriptor functions transform the Cartesian coordinates of the neighboring atoms around the atom in the center to suitable input to a (in this case deep) neural network. The network outputs the energy of the center atom.

scriptors commonly used in materials physics are distances, angles, Coulomb-matrices, smooth overlap of atomic potentials, atom-centered symmetry functions, many-body tensor representations and the atomic cluster expansion, see, e.g., [94]. Typically the number of descriptors (i.e., the complexity or size of the basis) should be systematically expandable until it is, in principle, possible to reconstruct the original configuration.

The functional form takes the output from the descriptors and calculates the energy (or other properties) of the system, see Fig. 3.3. To be useful for MD purposes derivatives of the descriptors with respect to the Cartesian atomic positions and the derivative of the functional form with respect to the descriptors must be available in order to calculate forces and virials. The functional form can for example be based on GPs [92], NNs [89, 95] or linear models [96, 97], but any regression model can in principle be used.

The training method for ML potentials follows the general procedure as outlined in the section about regularized regression (Appendix A) except that non-linear optimization is needed. Typically the functional forms are comparably well understood and the techniques to train them well tested for various applications. Typical methods include stochastic gradient descent, evolutionary algorithms and maximum likelihood estimation [98].

ML potentials are typically described as interpolation techniques and as such sometimes behave unexpectedly when posed with unseen structures or local environments. Analytical potentials on the other hand are often constructed based on physical insight and only contain a handful of parameters (highly regularized). As a result, they can yield at least somewhat sensible results beyond the training regime. While the choice

of descriptors and functional forms as well as optimization techniques are fairly well understood, the selection of training structures is still a rather delicate aspect. Here, physical intuition and experience play a large role as well as prior understanding of the material at hand. There are various techniques to systematically choose good training data based on active learning and entropy maximization but this is ongoing research [99]. For an instructive comparison and discussion of ML potentials see [100].

3.2 Molecular dynamics

Once a suitable potential is chosen we need some general procedure in order to sample the phase space. The sampling of an interacting many body system is typically done using either MC or MD techniques, see, e.g., Frenkel and Smit [77]. MD is the key technique used to model atomic motion in materials as it gives access to time-dependent quantities.

3.2.1 Sampling phase space

The idea is to integrate the equations of motions $\boldsymbol{f} = m\ddot{\boldsymbol{x}}$ (a second order non-linear differential equation) where the force is given as the gradient of the interatomic potential $\boldsymbol{f}_i = -\nabla_{\boldsymbol{x}_i} V(\boldsymbol{x})$ with respect to the atomic positions $\boldsymbol{x}_i$. Many advanced integrators are available that can take multiple steps which can sometimes be useful in AIMD but for practical purposes when dealing with empirical potentials almost always a variant of the Verlet algorithm [101] is used such as velocity Verlet. One of the most important properties of an integrator is to be able to conserve the energy of the system in order to properly represent the microcanonical (NVE) ensemble. These types of integrators are called symplectic integrators. The ergodic hypothesis can then be used to calculate thermodynamic properties via time averages instead of ensemble averages

$$\langle A \rangle = \frac{1}{T} \int_0^T A(t)\, \mathrm{d}t, \tag{3.4}$$

where the angle bracket denotes an ensemble average corresponding to the macroscopic observable A. The ergodic hypothesis states that all microstates are equally likely to be observed. This is often not the case in computer simulations due to limited time. Other limitations of MD typically include lack of nuclear quantum effects and computational cost, MD being somewhat of a brute force approach. The quantum mechanical aspect can to some degree be remedied by using path integral MD [102]. Fortunately, at low temperatures where quantum effects start to become important other techniques can be used due to the harmonic nature of the potential at low temperatures. Furthermore for certain properties there are corrections which can be applied in a post process but fully quantum MD simulations is still an area of active research [103].

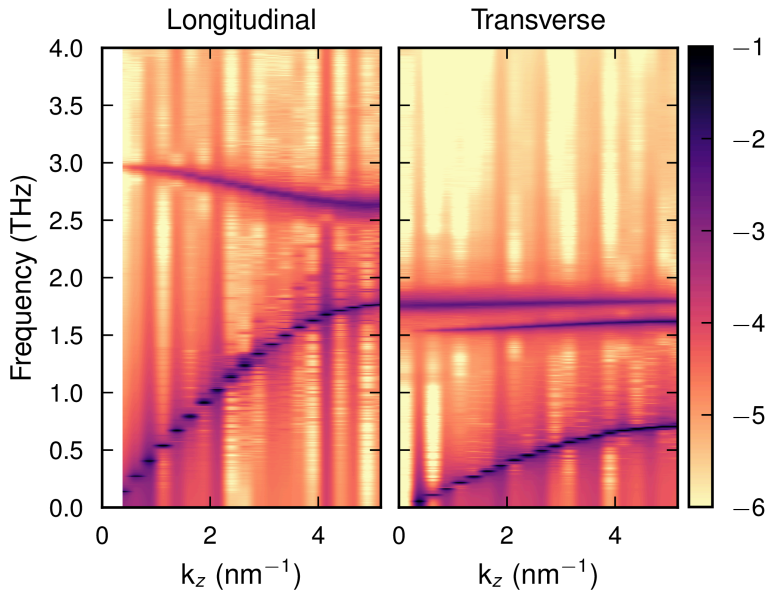

Figure 3.4: Typical dispersion relation calculated using velocity auto-correlation functions (ACFs). To the left is longitudinal modes where the vibrations are in the direction of the momentum (such as sound waves). To the right are transverse mode with motion perpendicular to the momentum (such as electromagnetic waves). The acoustic modes originate from the Γ-point while the optical modes appear as horizontal bands. This example is bulk MoS_2 in the through-plane direction taken from Paper III. The line width of the dispersion is very thin indicating a harmonic system with long lifetimes. The striped appearance appears since a supercell can only represent a finite number of momentum transfer vectors.

In order to sample other ensembles such as the canonical (NVT) or isothermal-isobaric (NPT) ensembles a thermostat and/or a barostat is needed. These can be based on instantaneous expressions for the thermodynamic properties they try to regulate or on time-averaged properties. In general the temperature is comparably easy to control via, e.g., the equipartition theorem. Typically the integrator is modified in order to incorporate and additional term in the Hamiltonian modeling heat exchange with an external bath system. Care must be taken to have a sufficiently large system so that the effect of the thermostat is comparably weak when sampling dynamical properties. This is motivated by the fact that in the infinite system size limit the NVE and NVT ensembles are equivalent. Thermostats will appear again later in Chapter 4 during the discussion of thermal conductivity as they can be used to transport heat or to probe the response function of a system. Commonly used thermostats include the Nosé-Hoover family [77], the Bussi–Donadio–Parrinello [104] thermostat and the Langevin thermostat [77].

Barostats typically require more detailed information about the interatomic poten-

tial in question. In principle the instantaneous stress tensor must be calculated which requires the virials, which can be challenging for many-body potentials and when periodic boundary conditions are present [105]. The impact of many-body effects on state variables is in general well understood in terms of hydrodynamic variables but in practice challenging to implement explicitly.

3.2.2 Equilibrium properties

Now let us look at some properties of interest similar to the ones in Chapter 2. Using a symplectic integrator we can simulate the microcanonical ensemble where the energy is kept fixed and no external force acts on the system. Provided we can simulate a large enough system to avoid finite size effects the dynamics in this simulation should correspond to the physical one. In practice however we often want to simulate from a correct canonical ensemble without going to very large systems. The partition function corresponding to the canonical ensemble reads

$$Z = \int \mathrm{e}^{-\beta H(x,p)} \,\mathrm{d}x \,\mathrm{d}p. \tag{3.5}$$

Thus, any thermodynamic equilibrium observable can be calculated as an ensemble average sampling from this distribution. For example the heat capacity can be calculated as the change of the expectation value of the energy with respect to a temperature change

$$C = \frac{\partial \langle H \rangle}{\partial T} = \frac{\partial}{\partial T} Z^{-1} \int H(x,p) \mathrm{e}^{-\beta H(x,p)} \,\mathrm{d}x \,\mathrm{d}p = \frac{1}{k_\mathrm{B} T^2} \left\langle (H - \langle H \rangle)^2 \right\rangle. \tag{3.6}$$

and is found to be equal to the variance of the total energy.

There are also some very general results from statistical mechanics which can be useful such as the equipartition theorem

$$\left\langle A \frac{\partial H}{\partial (q \text{ or } p)} \right\rangle = k_\mathrm{B} T \left\langle \frac{\partial A}{\partial (q \text{ or } p)} \right\rangle \tag{3.7}$$

for any operator A[86]. This can for example be used to relate the temperature T to the average kinetic energy. For a purely harmonic system we can also see that

$$\left\langle u^2 \right\rangle = \frac{k_\mathrm{B} T}{m\omega^2}. \tag{3.8}$$

The problem with simulating in the canonical ensemble is that the coupling to an external heat bath introduces a perturbation which can affect the dynamics of interest in the system. For example the Langevin thermostat introduces an artificial damping and lifetime via a stochastic force which effectively limits system lifetimes.

Before proceeding to time dependent properties let us take a look at the free energy which is a notoriously hard property to calculate and one of the reasons why the effective harmonic methods described in Chapter 2 are so popular. The free energy can be calculated in a few different ways. For instance one can use free energy perturbation which is the basis of the effective harmonic methods of Chapter 2. There the free energy difference between a system A of known free energy and the target system B was computed as

$$\Delta F = -k_{\mathrm{B}} T \log \left\langle \mathrm{e}^{-\beta(H_B - H_A)} \right\rangle_{H_A}. \tag{3.9}$$

The expressions are, however, totally symmetric in A and B, such that in principle any ensemble can be used. This expression, however, deals with very non-linear operators and is in general hard to converge. In practice thermodynamic (or λ) integration is used instead where the interatomic potential is continuously varied between the potential of a system of known free energy and the system for which the free energy is sought. The potential is typically given by a linear mixing $V(\lambda) = H_A + \lambda(H_B - H_A)$ such that as λ goes from 0 to 1 the interaction switches from, say, the know system A to the system B of unknown free energy. The free energy change is then given by

$$\Delta F = \int_0^1 \langle H_B - H_A \rangle_{H(\lambda)} \, \mathrm{d}\lambda. \tag{3.10}$$

For this method to work in practice the model potential A and the target potential B must be relatively similar such that the difference varies smoothly so that the integral converges numerically. With this we conclude the equilibrium part of the discussion about MD and turn to dynamic properties.

3.3 Correlation functions

Many interesting properties are directly accessible from trajectories obtained from MD simulations such as microscopic mechanisms for diffusion of defects [76]. One of the main advantages of the MD technique over MC is that it also gives us the possibility to sample time-dependent properties such as time-correlation functions. In the near-equilibrium limit the fluctuation-dissipation theorem and linear response theory give us direct access to non-equilibrium properties such as thermal conductivities (see Chapter 4) given that suitable observables can be defined.

One important property is the spectral function which can be calculated from the ACFs of the atomic motion [106, 107]. The spectral function is the dispersion relation of a material and relates the wavelength of lattice waves/phonons to the frequency of the same waves, see Fig. 3.4. This provides us with a method to non-perturbatively sample the dispersion relation and lifetimes/line widths of the system that can be compared to results obtained from theoretical methods using lattice dynamics or to experiments via, e.g., inelastic scattering with neutrons [108] or x-rays.

The dynamic structure factor is often used to capture the dynamics of the system partitioned into different wavelength and frequencies. It can be shown that the dynamical structure factor is related to the ACF of density fluctuations as

$$S(k,\omega) = \int \mathrm{e}^{-i\omega t} \langle \rho(k,t)\rho(k,0)\rangle = \int e^{-i\omega t} \sum_{ij} \left\langle \mathrm{e}^{-ikx_i(t)} \mathrm{e}^{ikx_j(0)} \right\rangle . \tag{3.11}$$

This quantity we can recognize from the Green's function in Chapter 2.

3.3.1 Dynamic structure factor from neutrons

To motivate the use of the dynamic structure factor we can study the scattering of neutrons (Sect. 1.2.3). There are many techniques used to study materials involving neutron scattering, with the two archetypes being elastic neutron diffraction and inelastic neutron scattering. Both can be described in the framework of time-dependent perturbation theory.

The incident and scattered neutron can be described by plane wave (free) states described by

$$\Psi_k(x) = e^{-ikx} \tag{3.12}$$

with energy E_k for the momentum quantum number k. From time-dependent perturbation theory we can show that the amplitude of a final state $\Psi_{k'}(x)$ can be written to first order as

$$c_{k'}(t \to \infty) = \frac{-i}{\hbar} \int_0^{t\to\infty} dt' \int dx \overline{\Psi}_{k'}(x) V(x,t') \Psi_k(x) e^{-i(E_k - E_{k'})t'/\hbar}. \tag{3.13}$$

Inserting the plane-wave basis we can rewrite the expression as

$$c_{k'}(t \to \infty) = \frac{-i}{\hbar} \int_0^{t\to\infty} dt' \int dx e^{ik'x} V(x,t') e^{-ikx} e^{-i(E_k - E_{k'})t'/\hbar} = \frac{-i}{\hbar} \tilde{V}(Q,\omega) \tag{3.14}$$

with $Q = k - k'$ and $\omega = (E_k - E_{k'})/\hbar$. The scattering amplitude is thus related to the spatial and temporal Fourier transform of the scattering potential, which is a quite general result.

For systems made up of particles the scattering can be written as a sum over all point scatterers.

$$V(x,t) = \sum_i V_i(x - x_i(t)) \tag{3.15}$$

and the transform is given by

$$\tilde{V}(Q,\omega) = \int e^{-i\omega t} \sum_i e^{-iQx_i(t)} \underbrace{\int V_i(x) e^{-iQx}}_{f(Q)}, \tag{3.16}$$

where f is called the form factor of the scatterer. For thermal neutrons the wavelength is much larger than the nuclei and the interaction can be modeled as a point scatterer using the Dirac delta-function as potential. The form factor for neutrons is thus reported as a single number b for different isotopes. Using this we can calculate the scattering probability S using the convolution theorem

$$S \propto \left|\tilde{V}(Q,\omega)\right|^2 = \left| \int e^{-i\omega t} \sum_i b_i e^{-iQx_i(t)} \right|^2 = \int e^{-i\omega t} \sum_{ij} b_i \bar{b}_j \left\langle e^{-iQx_i(t)} e^{iQx_j(0)} \right\rangle \tag{3.17}$$

where on the right hand side we recognize the dynamic structure factor

$$S(Q,\omega) = \int e^{-i\omega t} \sum_{ij} b_i \bar{b}_j \left\langle e^{-iQ(x_i(t)-x_j(0))} \right\rangle . \tag{3.18}$$

Note that while Eq. (3.17) is valid even in the quantum case this last equation is not.

3.3.2 Auto-correlation functions and mode projections

By measuring ACFs of observables many properties can be computed. For example using a model for the polarizability the Raman spectrum can be computed from a polarizability-polarizability ACF. Similarly diffusion coefficients and thermal conductivities can also be computed by fluctuations of their respective susceptibilities. For the dynamical structure factor we do a position ACF but it is also possible to perform a similar analysis on the velocities. In this case it is called a current-current or velocity-velocity ACF and is closely connected to the vibrational density of states. In fact it can be shown that the velocity-velocity ACF is related to the density of states. For instance by using the equipartition theorem applied to the kinetic energy it can be shown that the density of states is given by

$$\rho(\omega) = \frac{1}{3Nk_{\mathrm{B}}T} \sum_i m_i \int \mathrm{e}^{-i\omega t} \left\langle v_i(t) \cdot v_i(0) \right\rangle \, \mathrm{d}t. \tag{3.19}$$

If a set of polarization vectors were given it is possible to project the atomic motion onto the normal modes instead. This is known as mode projection. By inserting

$$v_i^{\alpha}(n) = \frac{1}{\sqrt{m_i}} \sum_{ks} \dot{q}_s(k) W_{is}^{\alpha} \mathrm{e}^{ikR(n)} \tag{3.20}$$

into the density of states we get the density of states for each mode

$$\rho(\omega) = \sum_{ks} \rho_s(k,\omega) = \sum_{ks} \frac{1}{3Nk_{\mathrm{B}}T} \int \mathrm{e}^{-i\omega t} \left\langle \dot{q}_s(k,t) \dot{q}_s(-k,0) \right\rangle \, \mathrm{d}t. \tag{3.21}$$

This way the spectrum can be defined for each mode as the contribution to the total density of states. Notice, however, that since neither the polarization vectors nor the frequencies enter explicitly we could as well choose the dynamical matrix to be diagonal. Therefore by summing over the band indices we get

$$\rho_i(k,\omega) = \frac{1}{3Nk_{\mathrm{B}}T}\sum_n \mathrm{e}^{-ikR(n)} \int \mathrm{e}^{-i\omega t}\,\langle v_i(n,t)\cdot v_i(n,0)\rangle\ \mathrm{d}t, \tag{3.22}$$

which is sometimes called the spectral energy density for basis atom i.

As we can see there are many ways in which the vibrations can be analyzed, both in the phonon and the atom basis. Analyzing MD trajectories by projecting the motion onto normal modes is one of the most powerful tools available for understanding material dynamics.

A simple approximation to the observed dynamics of nearly independent harmonic oscillators which works extremely well is the damped harmonic oscillator model. In the damped harmonic oscillator model the normal mode oscillates under the influence of a stochastic background which dampens and kicks the mode in a way consistent with the canonical ensemble. This is sometimes called Langevin dynamics and by using a suitable set of polarization vectors the frequency shifts and lifetimes can be extracted from the spectral functions by fitting the observed spectra to that of a damped harmonic oscillator for which there are analytical expression.

3.3.3 Damped harmonic oscillator model

Consider the phonon mode coordinate $q_s(k)$ as an oscillator in a stochastic background. A classical driven and damped harmonic oscillator can be modeled using the following equations of motion

$$\ddot{x}(t) = -\Gamma\dot{x}(t) - \omega_0^2 x(t) + f(t) \tag{3.23}$$

for some driving force f. If we take the Fourier transform of this equation we get

$$\tilde{x}(\omega) = \frac{1}{\omega_0^2 - \omega^2 + i\Gamma\omega}\tilde{f}(\omega) = \tilde{\chi}(\omega)\tilde{f}(\omega), \tag{3.24}$$

where we can identify the Green's function as the susceptibility of the system. The susceptibility can be decomposed into its real and imaginary parts

$$\tilde{\chi}(\omega) = \tilde{\chi}'(\omega) + i\tilde{\chi}''(\omega) = \frac{\omega_0^2 - \omega^2}{\left(\omega^2 - \omega_0^2\right)^2 + \Gamma^2\omega^2} + i\frac{-\Gamma\omega}{\left(\omega^2 - \omega_0^2\right)^2 + \Gamma^2\omega^2}. \tag{3.25}$$

The imaginary part of the susceptibility, sometimes called the spectral function, can in turn be related to the fluctuations in the system via the fluctuation-dissipation theorem

$$S(\omega) = -\frac{2k_{\mathrm{B}}T}{\omega}\frac{-\Gamma\omega}{\left(\omega^2 - \omega_0^2\right)^2 + \Gamma^2\omega^2} = \frac{2k_{\mathrm{B}}T\Gamma}{\left(\omega^2 - \omega_0^2\right)^2 + \Gamma^2\omega^2}. \tag{3.26}$$

Assuming the driving force $\tilde{f}(\omega) = \sigma$ is a white noise process with intensity σ^2 we can calculate the power spectrum for the process directly from Eq. (3.24) and identify the noise as $\sigma^2 = 2k_\mathrm{B}T\Gamma$ consistent with what we know from Langevin dynamics.

From the power spectrum we can calculate the ACF of this process using the Wiener-Khinchin theorem as

$$C(t) = \mathscr{F}^{-1}[S(\omega)](t) = \frac{k_\mathrm{B}T}{\omega_0^2} e^{-t/\tau} \left(\cos \omega_e t + \frac{1}{\tau\omega_e} \sin \omega_e t \right) \quad \text{for} \quad t \geq 0, \tag{3.27}$$

where $\omega_e^2 = \omega_0^2 - \tau^{-2}$ and $\tau = 2/\Gamma$. Notice how the zero-time limit recovers the result from the equipartition theorem.

The driven damped classical harmonic oscillator illustrates a few concepts. The inclusion of the damping term Γ introduces a lifetime to the oscillator. This shows up as an exponential decay in the ACF. In the frequency domain the pole of the susceptibility tells us about the broadening and we find that it is proportional to the inverse lifetime. With this it is possible to analyze and predict phonon spectra and even individual lifetimes for certain modes. This was utilized in Paper V where this kind of analysis was performed even for strongly overdamped modes as the system underwent phase transitions.

With this we conclude the discussion of MD and the connection to lattice dynamics. Both techniques are extremely useful, especially when combined. Going further it is possible to define higher-order correlation functions and with different types of energy partitioning schemes it is possible to track many-body correlations and energy flows among phonons [109]. While this can give great insight it is computational expensive and sometimes requires explicit calculation of higher-order force constants.

In the following chapter we will take a look at the thermal conductivity and how it can be calculated using using both the methods from lattice dynamics and the MD technique.

4

Thermal transport

The macroscopic equation describing thermal conductivity is Fourier's law

$$\boldsymbol{J} = -\kappa \nabla \boldsymbol{T}, \tag{4.1}$$

where $\boldsymbol{J}$ is the heat current, κ is the coefficient of thermal conductivity and $\nabla \boldsymbol{T}$ is the temperature gradient. κ is typically measured in units of W/m/K. There are many approaches for calculating the thermal conductivity in condensed matter systems. Loosely they belong to three classes based on thermostats, fluctuations via the Green-Kubo (GK) relations and PBTE [110], respectively.

The most straightforward approach is non-equilibrium molecular dynamics (NEMD) where two separated regions in an MD simulation are held at different temperatures using thermostats. The heat will flow from the hot to the cold end via an intermediate region, which evolves under NVE conditions [111]. The thermal conductivity can simply be calculated from the temperature gradient and the amount of heat that is pumped between two thermostated regions per unit time. This is a conceptually simple method and very useful for measuring interface conductivities. For bulk conductivities, however, the method has some drawbacks. First, the temperature gradient is typically very large as the temperature difference needs to be larger than typical fluctuations while the length scales are typically quite short. Second, the spatial limitation, or boundary conditions, in the simulation may impose an artificial wavelength/mean-free-path cutoff similar to a boundary scattering term in PBTE [42, 112]. Since the low lying acoustic modes, which have typically long mean free paths, carry much of the heat this can lead to an underestimation of the lattice thermal conductivity (LTC). The mean free path is the typical distance a phonon can travel (and thus conduct heat) before it scatters. It is calculated as the group velocity of the mode $v = \partial_k \omega(k)$ times the lifetime τ. Fortunately, as the temperature increases the mean free path decreases so this is typically

more problematic for low temperatures where other approaches (PBTE) can be used instead.

The two other methods (PBTE and equilibrium molecular dynamics (EMD)) will now be discussed in some detail starting with the PBTE.

4.1 Peierls-Boltzmann transport theory

When the motion of atoms in a solid is highly correlated it is often useful to make a Fourier transform and instead describe the motion in terms of the resulting collective excitations (phonons) as described earlier in Chapter 2. The resulting phase space is now given by the phonon coordinates and momenta, and the quasi-particles are effectively assumed to behave similarly to the particles in a dilute gas. This system is called a weakly interacting Bose gas as the phonons follows the Bose-Einstein statistic. Here, the heat carriers are the phonon quasi-particles and the corresponding PBTE is solved by constructing a scattering integral based on the phonon-phonon interactions calculated from anharmonic FCs using, e.g., Green's function methods as described in Chapter 2. The method thus relies on an accurate description of the PES in terms of FCs. The method is in some sense semi-classical but does include quantum effects. For many materials 0 K or effective third-order FCs are enough but for some materials four-phonon interactions are important and thus the corresponding scattering rates (the rate at which phonons decay into other phonons) must be included [59, 113]. The main issue with PBTE is the computational cost of constructing FCs and solving the PBTE for systems with large primitive cells, e.g., systems with complex crystal structures or disordered systems.

In order to relate the phonon dynamics to macroscopic transport we need to introduce a notion of localization. While formally the phonons are only exact excitations for an infinite (periodic) crystal and thus spread out over a large region they can be localized in space by considering wave packets. The physical picture is thus that phonons are created at a certain macroscopic point in space and travel for a time as a wave packet and are annihilated at another point in space later, resulting in the transfer of energy and heat. Theses wave packets thus have a frequency ω, a speed of propagation $v = \partial_q \omega$ and a lifetime τ. In addition we can think of each wave packet carrying some energy $\hbar\omega$ and thus a wave packet that is created (excited) at a point x in the system will carry an energy $\hbar\omega$ with speed v for a time τ before being annihilated at a point $x' = x + v\tau = x + \Lambda$ where Λ is the mean free path. The reason why there is a flow of heat is because of the difference in phonon populations at different points in space due to the thermal gradient. It is this difference in populations we calculate using the PBTE. In the following this formalism will be briefly described. For a more extensive account of PBTE see, e.g., [32, 114] and for ab-initio thermal transport in general see [115].

The Peierls-Boltzmann theory of thermal transport begins with the assumption of a well defined local equilibrium distribution function,

$$n_\lambda^0(T(x)) = \frac{1}{\mathrm{e}^{\hbar\omega_\lambda/k_\mathrm{B}T(x)} - 1}, \tag{4.2}$$

for the mode λ, which is defined by the lattice momentum and band index. The spatial variation enters through the spatial variation of the temperature. The phonon transport equation is now equivalent to the transport equation in the kinetic theory of gases. First the Liouville equation is integrated down to a single particle distribution function to yield the Boltzmann equation,

$$\frac{\mathrm{d}\rho}{\mathrm{d}t} = 0 \quad \Longrightarrow \quad \frac{\mathrm{d}n_\lambda}{\mathrm{d}t} = S_\lambda[n], \tag{4.3}$$

with the assumption that the scattering integral S depends only on the single particle distribution itself. In more detail we have

$$\frac{\partial n_\lambda}{\partial t} + \frac{\partial n_\lambda}{\partial x} v_\lambda = S_\lambda[n], \tag{4.4}$$

for a phonon of type λ at position x moving with velocity v_λ as given by the dispersion relation. Now we assume that the change in occupation due to the thermal gradient is a small perturbation to the equilibrium distribution $n = n^0 + n'$ and that the spatial variation of the population is solely due to the spatial variation of the temperature in the equilibrium ensemble. In equilibrium ($\partial_t = 0$ and $S[n^0] = 0$) we get the typical linearized PBTE

$$\frac{C_\lambda v_\lambda}{\hbar\omega_\lambda}\nabla T = \frac{\partial S_\lambda[n^0]}{\partial n_{\lambda'}} n'_{\lambda'} = \Gamma_{\lambda\lambda'} n'_{\lambda'} \tag{4.5}$$

with the scattering matrix $\Gamma_{\lambda\lambda'}$. The heat current is defined as

$$J = \sum_\lambda \hbar\omega\, v_\lambda\, n'_\lambda, \tag{4.6}$$

which is simply the energy of a phonon λ times the velocity times the number (difference) of phonons in that state. Plugging in our expression for the populations we then find

$$J = \sum_\lambda \hbar\omega_\lambda v_\lambda \frac{C_{\lambda'} v_{\lambda'}}{\hbar\omega_{\lambda'}} \Gamma^{-1}_{\lambda\lambda'}. \tag{4.7}$$

In deriving the above expression we have postulated that the out-of-equilibrium distribution returns to equilibrium via linear relaxation. This is called the relaxation time approximation (RTA) which states that the backward transition is proportional to the perturbation. The lifetime can be taken to be the inverse of the self-energy (at the

harmonic frequency) of each phonon as described earlier and will depend on the occupations via the scattering rates. In the single-mode relaxation time approximation (SMRTA) we furthermore simply use only the diagonal part of the scattering matrix $\Gamma^{-1}_{\lambda\lambda} = \tau_\lambda$ and the expression for the thermal conductivity reduces to the typical

$$\kappa = \sum_\lambda C_\lambda v_\lambda^2 \tau. \tag{4.8}$$

The main drawback of the SMRTA is that it underestimates the repopulation of modes which is important for some materials [116]. To improve this result the full scattering matrix can be inverted either via a direct approach or iteratively [58].

The main problem with the PBTE is that it is hard to calculate the scattering rates which appear in the scattering matrix. Typically Fermi's golden rule can be used to calculate single rates but in principle the scattering process should be time-dependent and the complete spectral function should be used [116].

It is also possible to include higher-order processes when calculating the relaxation times as described in Chapter 2 and as implemented in [113]. Recent insights into the PBTE include the Wigner formulation described in [13, 117] where glass-like transport is more readily handled and spectral based methods like [118]. The Wigner method is implemented in both PHONO3PY and KALDO [119].

4.2 Green-Kubo relations

For an excellent overview of the GK formalism see [120] which is the basis for this short introduction. In the 1950s Green and Kubo developed a theory of linear transport based on the work of Callen and Welton on the fluctuation-dissipation theorem. The theory relates equilibrium fluctuations expressed as time correlation functions with the corresponding transport coefficients,

$$\kappa \propto \int_0^\infty \langle \boldsymbol{J}(t)\boldsymbol{J}(0)\rangle \, \mathrm{d}t. \tag{4.9}$$

Thus an MD simulation can be performed in the NVE ensemble and the auto-correlation of the heat flux $\boldsymbol{J}$ is measured to provide the thermal conductivity coefficient κ. This EMD approach is a very general method and in principle free from bias as the system evolves without any external perturbation.

Compared to the NEMD method the effect of boundary conditions is not as severe. Although the allowed wave vectors are limited (since not all wavelengths can be supported by a finite supercell) their mean free paths are not as the modes are free to propagate through the periodic boundary conditions. The main problem lies in the challenge to adequately sample the correlation function, especially for harmonic materials with long life times (i.e., materials with a large LTC). This can be overcome by the

use of clever methods from signal analysis allowing even the direct use of AIMD, see again [120] and also [121].

For a macroscopic system we stipulate that there exists a energy density function $e(x, \Gamma)$ that measures the local energy at a point x in the system in state Γ. This density is related to the total energy of the system via

$$\int e(x, \Gamma) \mathrm{d}x = H(\Gamma), \tag{4.10}$$

where Γ is a point in the phase space of the system and $\mathrm{d}x$ is large compared to the range of the interatomic interactions. The energy is furthermore a (locally) conserved quantity and thus the energy density obeys the continuity equation

$$-i\omega\, e(q, \omega) = -iq\, j(q, \omega) \tag{4.11}$$

for some heat current density j. The long-wavelength parts of conserved densities are called hydrodynamic variables and our goal now is to find their equations of motion.

In the small field limit the equation of motion for the energy density can be linearized in Fourier space

$$-i\omega\, e(q, \omega) = \Lambda(q, \omega)\, e(q, \omega) \tag{4.12}$$

and we can thus identify the heat current density as

$$j(q, \omega) = -\frac{1}{iq} \Lambda(q, \omega) e(q, \omega). \tag{4.13}$$

From general considerations the constant and linear term must vanish in Λ due to causality and parity considerations. As a result, the macroscopic flux $\boldsymbol{J} = \int j \,\mathrm{d}x$ and the macroscopic density gradient $\boldsymbol{D} = \int \nabla e \,\mathrm{d}x$ are linearly related via $\boldsymbol{J} = \lambda \boldsymbol{D}$. Because of assumptions of local equilibrium of the state variables we can also write the relation in terms of the thermodynamic force $\boldsymbol{F} = \int \nabla \beta \,\mathrm{d}x$ where $\beta = 1/T$ is the intensive conjugate variable to the internal energy and we arrive at

$$\boldsymbol{J} = L\boldsymbol{F} \tag{4.14}$$

for some parameter L and force $\boldsymbol{F}$ to be determined. Note here that the natural cause of a heat current is actually the gradient of the inverse temperature. Nevertheless, in the linear regime any equivalent measure can be used and the corresponding transport coefficient will only differ by a function of the equilibrium state variables.

The GK relations allow us to calculate the parameter L by studying the equilibrium fluctuations of the flux $\boldsymbol{J}$. Specifically for a perturbation $V = \int v(x) e(x) \,\mathrm{d}x$ with some coupling constant v (the driving field) to the original Hamiltonian the corresponding thermodynamic force is given by

$$\boldsymbol{F} = \beta_0 \int \nabla v \,\mathrm{d}x \tag{4.15}$$

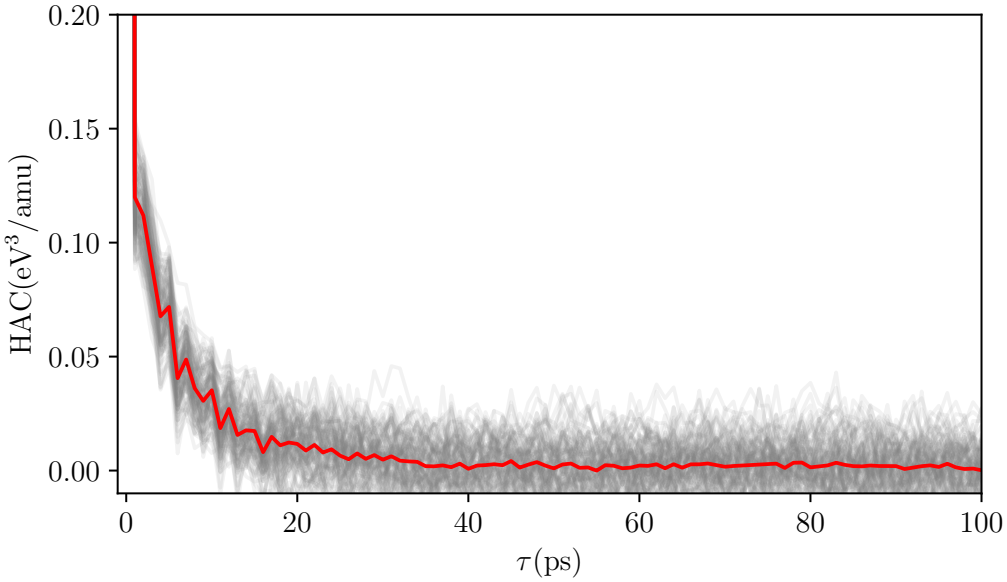

Figure 4.1: Heat current auto correlation (HAC) in the through plane direction of Graphite at 600 K. The gray curves are 100 individual simulations overlayed and the red curve is the unfiltered mean. At around 40 ps the correlation is almost zero and should be enough to get a converged value of the thermal conductivity.

and the corresponding transport coefficient is

$$L = \int_0^\infty \langle \boldsymbol{J}(t)\boldsymbol{J}(0)\rangle_0 \, \mathrm{d}t. \tag{4.16}$$

For a coupling field $v = -\Delta T/T_0$ the (mechanical) perturbation mimics the effect of a temperature field. This will be important later for the homogeneous non-equilibrium molecular dynamics (HNEMD) method where this observation allows us to study the heat current response to a perturbation. Continuing, the corresponding force for the above perturbation just becomes the temperature (T) gradient and finally the thermal conductivity is given by

$$\kappa = \frac{1}{V k_B T^2} \int_0^\infty \langle \boldsymbol{J}(t)\boldsymbol{J}(0)\rangle_0 \, \mathrm{d}t. \tag{4.17}$$

An exampled of a heat current auto-correlation function can be seen in Fig. 4.1 while the corresponding integrated thermal conductivity can be seen in Fig. 4.2.

Now the only thing left is a local definition of heat or internal energy that is consistent and compatible with both our microscopic and macroscopic understanding. This can be conceptually challenging due to the ambiguity in the localization of the internal

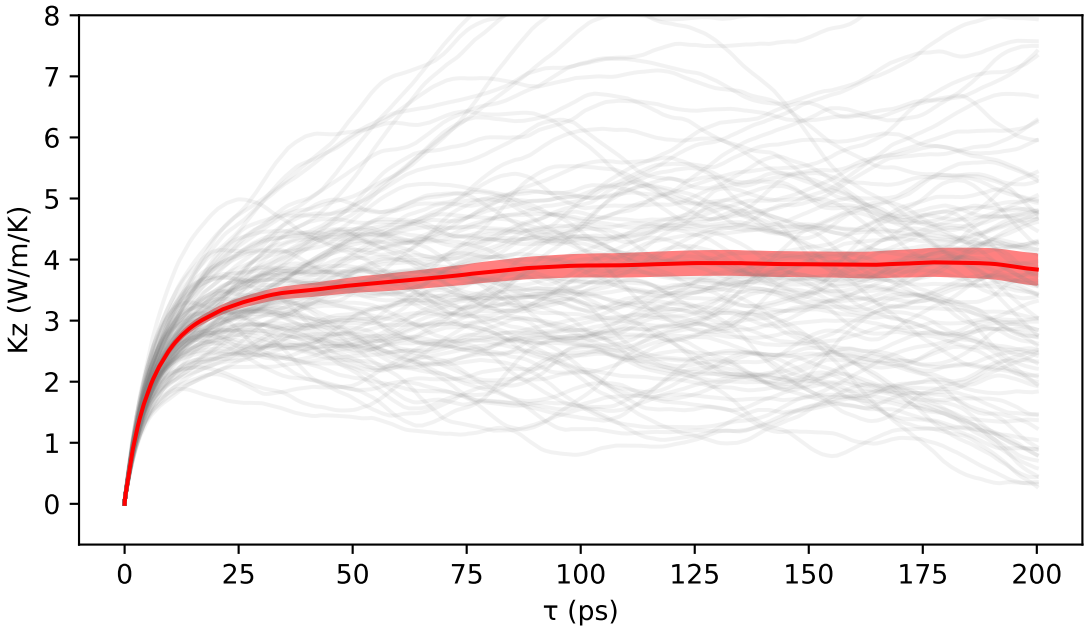

Figure 4.2: Running thermal conductivity corresponding to Fig. 4.1. The gray lines show the results from 100 individual simulations while the red curve shows the mean and standard deviation. After around 40 ps the thermal conductivity is converged.

energy. Recent research has, however, shown that the exact definition of the energy density on the atomic level is not important [120]. As long as general principles are obeyed all definitions should give equivalent results. Thus from the conservation of energy and from the local character of the interatomic potential we stipulate that in the thermodynamic limit of coarse graining there must exist a local measure of the internal energy obeying the continuity equation for a suitable definition of the heat flux. In practice the energy is divided up into atomic energies

$$E = \sum_i E_i = \sum_i \frac{p_i^2}{2m_i} + V_i(x) \tag{4.18}$$

and each atom is considered a heat carrier and the corresponding current is analogous to, e.g., a mass or charge current.

The EMD method can also be combined with a perturbing thermostat in order to artificially increase the fluctuations and thus provide a stronger signal to noise ratio, leading to faster computational convergence. Evans *et al.* have shown that a time-dependent field $F(t)$ can be used to drive the system out of equilibrium, enhancing the fluctuations [122]. By studying the correlation between the driving force and the response of the heat current the thermal transport coefficient can be calculated using

a simple formula relating the force to the induced heat current

$$\frac{\langle \boldsymbol{J}(t) \rangle}{TV} = \kappa F(t). \tag{4.19}$$

Fan *et al.* generalized this method to many-body potentials [123] and implemented it specifically for HNEMD [124] in the GPUMD software package used in Paper III.

5

Outlook

> No! The quote was "Yes, we could look it up but it is much more fun to speculate."
>
> Esmée Berger

To first order, the future looks bright, at least for computational materials dynamics.

Hardware. From a computational materials science perspective we can still rely to some degree on the increase in computer performance. If this will continue forever is not certain but progress seem steady, although at a slower pace. The recent years have also seen an increase in use of GPUs as a compute resource. This is to a large degree motivated by the interest in ML and artificial intelligence. Future challenges might be to adapt traditional methods to this new type of hardware which is arguably more suitable for many numerical computations than traditional CPUs. This might be accomplished by writing directly in frameworks such as CUDA, using, e.g., just-in-time compilation to write in a high-level language and target GPUs, or use frameworks such as JAX and PyTorch. A solid understanding of how to use modern ML frameworks might be as important as cache localization was 20 years ago.

Software. Speaking about software, nothing in this thesis would be possible without open source (or at least open access) software. The maturity of the present array of software and methods made available during the last decades is impressive. Implementing new methods by using existing software packages from different countries, authors and funding agencies gives hope for the future. On the flip side the sustainability of the open source software development has been questioned in society in general (see

for example the heartbleed bug). For us physicists this manifests in the funding of software projects, issues relating to citations and attributions and software maintenance. Towards the end of my PhD the last point stands out to me. A software is only as alive as the documentation and community around it. Maybe something in the way we fund and work needs to change in order to not loose the work we put into development.

Machine learning. A more engaging development in society is that of ML and artificial intelligence. These old concepts have now started to become very popular and will probably permeate into every part of science even more. One very nice aspect is that since the concepts and problems are so general the piggybacking factor is large. This means that development in one field should in principle be directly applicable in many others. Challenges still remain though which do not only affect physics. Interpretability of models and uncertainty estimation are two challenges that stand out to me. A somewhat under-explored field is using ML to find patterns in vibrational motion. While the static case, e.g., structure analysis, has been explored for a long time I have not seen similar applications to dynamics.

Electronic structure methods. Electronic structure theory and especially DFT will probably continue to improve and become both comparably less expensive and more accurate. This implies that perhaps ab-initio MD, possibly coupled with ML potentials, will be the dominant method to study vibrations. However, even though there are many exchange-correlation functionals which work very well for many materials, the disagreement between different functionals is often a concern. So maybe there will be a transition over to other more accurate but more expensive methods and we are back to training cheap potentials again. Other approaches that are starting to be used is to transfer learn DFT ML potentials using the expensive but accurate alternative methods. Or, someone (probably a machine) might learn the true exchange-correlation functional. Regardless if we can construct fast and correct potentials for the ionic potential there is still a problem with large scale simulations, quantum effects and interactions with other excitations in matter.

Lattice dynamics. As accurate and computationally efficient ML potentials become increasingly more common place the usefulness of lattice dynamics based methods compared to MD methods might be questioned. While the relatively low cost of harmonic FCs for simple systems and direct access to quantum effects have made lattice dynamics the workhorse of vibrational dynamics, one can suspect that higher-order FCs will become less widely used. The possibility to connect such relations to theory might, however, makes them useful for benchmarking other potentials with respect to, e.g., quantum dynamics, and to provide physical interpretability. Another use case is to

compare Boltzmann transport methods with GK based using the same underlying representation of the PES.

Even though we have access to interatomic potentials the PES is still quite conveniently studied using harmonic and potentially lower-order FCs. The main drawback is the problem of describing the PES for unstable phases. Therefore it would be useful to have an automatic procedure which makes it possible to partially include third and fourth-order FCs that are important for the unstable modes. Ideally this should be as simple and automatic as the standard zero Kelvin calculations and provide a solid basis for further studies. So some work could still be done to make such analysis readily accessible to non-experts.

In terms of future development of HIPHIVE there is still missing the ability to handle cell deformations. This can also naturally be related to FC expansions in internal coordinates similar to classical intramolecular force fields used in chemistry. This would also be a natural framework to start studying disordered systems. There is always a point for any basis when its efficacy breaks down, and with the increased popularity of ML potentials many properties could perhaps be more easily obtained by constructing a suitable ML potential instead. However, in the end we wish to learn something about the underlying physics and thus there will perhaps remain a need for simpler potentials. Just as ML potentials bridge analytical potentials and ab-initio methods, one might require a bridge between a deep NN and an analytical potential.

High-throughput. From a practical perspective we want accurate methods that can predict properties with low computational cost and limited human input. This is the goal of so-called high-throughput studies [125] but unfortunately this is hard to pull off in practice as there are as many details as there are materials. Another angle is to make certain types of standard procedures semi-automatic for the end user. One such attempt is active learning of ML potentials which has been successfully applied to a range of systems, see, e.g., [126, 127]. A third approach is to sacrifice computational cost for human effort and go directly from ab-initio calculations to properties of interest via exact methods such as GK [128, 129]. One could argue that is akin tp "kicking the can down the road" as there are approximations made even in DFT, nevertheless this type of methods will probably grow in popularity. Thus here it could be interesting to further develop methods to quickly calculate properties of anharmonic and unstable energy landscapes as in [130].

Accuracy and sources of error. For the construction of FCs some questions remain open (at least from my perspective) concerning the relationship between different methods. For example, when should EHMs be preferred over SCP? What is actually being optimized in the different self-consistent procedures? How are the derived properties related to the observed properties? One potentially insightful approach here would

be to compare PBTE and GK directly by using the same FCP as input. This would allow one to explore the details of recent progress of relating PBTE and GK on the same footing.

As methods become increasingly precise the question of accuracy becomes more important. At one point the errors made in certain approximations such as, e.g., the PBTE will be smaller than the errors in input data obtained from ab-initio techniques. In addition many properties of condensed matter systems are ignored such as interactions of phonons with other excitations and degrees of freedom such as electrons and spins as well as structural properties such as defects and boundaries.

Path integral MD. During the last decade, interatomic ML potentials have started to dominate how we model the PES acquired from DFT calculations. More recently path integral MD has gained increased interest where some quantum mechanical effects can be incorporated into MD simulations. Quantum effects are one of the last limitations of MD and thus it is valuable to fully understand the limitations of this approach when studying dynamics. Maybe there is the need to develop equivalent methods for ions as for electrons to propagate the ionic wave functions?

Vibrational analysis and moiré structures. Many of the above points culminate in the study of thermal conductivity in disordered vdW structures that continues beyond the third paper in this thesis. In spite there being accurate potentials and many experimental studies, the nature of thermal transport in these types of materials is still not completely understood. This might be the lack of physical intuition on the side of the researcher but it might also be due to a lack of tools. For simple systems a lot of questions might be answerable in the language of lattice dynamics. For complicated systems such as glassy materials with disorder or systems with grain boundaries the picture is not as clear. I thus think there are prospects to develop tools to understand vibrational dynamics from MD trajectories, perhaps using ML approaches.

6

Summary of papers

Paper I

The Hiphive Package for the Extraction of High-Order Force Constants by Machine Learning.

Paper I is the first of a set of two papers related to the extraction and application of FC expansions. In this paper we present methods and workflows as well as some demonstrations of the HIPHIVE package that we developed. The focus is on the advantages of an accessible framework to work with FCs and how to use auxiliary software such as SCIKIT-LEARN to accelerate the regression extraction. The main features of HIPHIVE are presented as well as the concepts necessary to work with FCs in practice. This includes proper handling of both local crystal symmetries as well as global symmetries such as translational and rotational invariance. The translational symmetries are exactly fulfilled by using integer numerics to find the kernel of the translational sum rule constraint matrix. HIPHIVE handles FC expansions up to arbitrary order allowing for accurate descriptions of complex PESs. This allows, for example, for exact non-perturbative treatments of properties of interest.

Demonstrations include proper handling of rotational invariance and phonon dispersions of the two-dimensional material MoS_2 as well as the thermal conductivity. Furthermore we demonstrate how to use higher-order FCPs to run MD via the ASE library.

Paper II

Efficient construction of linear models in materials modeling and applications to force constant expansions.

In paper II we used HIPHIVE in conjunction with the SCIKIT-LEARN package to benchmark and test the use of compressive sensing and related techniques to the FC extraction problem in the setting of the regression approach. The regression method can vastly cut down the number of DFT calculations needed and we tested several different methods including least absolute shrinkage and selection operator (LASSO), adaptive LASSO, recursive feature elimination (RFE) and automatic relevance determination regression (ARDR) on different systems. In terms of methods RFE with OLS works well in many cases while ARDR tends to suffer from bad scaling as the training size increase.

The single most important thing when fitting FCs is to tune the cutoffs properly. The regularized regression methods should in principle be able to find the correct parameters and discard clusters that are beyond the interaction length of the potential. However, the size of the training set needed for such approaches might be too large to handle for some of these algorithms.

The second important observation is that for some physical properties the accuracy does not correlate with the root mean squared error (RMSE) measure. This highlights the pitfalls of blindly optimizing for this measure and led us to conjecture that using estimators from information theory such as Bayesian information criterion (BIC) and Akaike information criterion (AIC) should provide more sensible models. Furthermore the highly popular LASSO method does not perform as well as some other methods and suffers from over-selection. Therefore post-LASSO methods are preferable such as adaptive-LASSO. Finally, we demonstrated that temperature-dependent thermal conductivities including fourth-order effective renormalization and beyond is computationally feasible and necessary in complex clathrates with 54 atoms in the unit cell.

In conclusion, despite compressive sensing (CS) being somewhat useful for configurational cluster expansions [131, 132], we did not find the methods very useful for our systems compared to Zhou *et al.* [133]. For FC expansions it is much easier to generate new data as each configuration contributes $3N$ new data points for systems where the cutoffs are comparable or longer than the size of the system. We also found that a naive use of advanced regularized regression methods can sometimes add a significant computational cost so care must be taken.

Paper III

Extremely anisotropic van der Waals thermal conductors.

In paper III we employed MD to explain the extremely low through-plane conductivity of rotationally disordered MoS_2 vdW structures. The work was a collaboration with the groups of David Muller, David Cahill, and Jiwoong Park who performed the synthesis and experimental measurements. The main challenge was the complexity of the unit cell for these kind of materials. Molybdenum disulfide MoS_2 consists of stacked layers of single sheets much like graphite is build from stacked layers of graphene. These types of materials have been studied before [134] in the bulk configuration with small unit cells using PBTE and the transport mechanism is rather well understood. For rotational disorder, however, things become complicated as the size of the cell grows rapidly as the inter-planar angles decrease. Many studies have been carried out on so-called bi-layer moiré structures, where two free standing layers are rotated relative to each other with some magic angles in order to ensure that both layers can fit in the same supercell. However, generating a large supercell with rotationally disordered (many different rotational angles between layers) is not trivial. To approach this challenge, we implemented an algorithm to stack many layers on top of each other with random interlayer rotations while allowing for some strain in each layer. To calculate the thermal conductivity we used the HNEMD method [122] together with an analytical potential [135] implemented in GPUMD [136] instead of PBTE as the latter would be computationally to demanding for this kind of setup. Using this approach we could replicate nearly quantitatively the experimental measurements, most crucially the drop in the through-plane conductivity confirming the claim of an extremely high anisotropy in the thermal conductivity. Based on our simulations We posited that the microscopic mechanism can be related to the extreme softening of the through-plane transverse modes. However, it might also be due to general disorder arguments as the coupling between longitudinal through-plane and in-plane modes decreases.

Paper IV

Tuning the through-plane lattice thermal conductivity
in van der Waals structures through rotational (dis)ordering.

In the fourth paper the rotationally disordered vdW structures are investigated further. Motivated by the results in the previous paper the goal is to understand if the observed effects generalize to other, similar materials. Thus we used the neuroevolution potential method (a ML approach) and constructed models for hexagonal boron nitride and graphene/graphite in addition to molybdenum disulphide. Our results showed that the same drop in through-plane thermal conductivity can be observed in the other materials. In particular the results stayed more or less the same for the original material MoS_2 despite using a new potential and employing GK equilibrium MD instead of the HNEMD method. The choice of using the standard GK method was largely motivated

by not having to converge the extra hyperparameter associated with the external driving force in the HNEMD approach.

Furthermore we expanded on the analysis of the microscopic mechanism responsible for the conduction by studying how the conductivity changed as a function of twist angle in the moiré structures. We found the conductivity to correlate with the entropy associated with a simple interplane order parameter which agrees with the common notion that the conductivity decreases with disorder. The difference between the materials and aspects of the reconstruction of the moiré structures was linked to the slip surfaces of the materials.

The work, however, left some questions still open concerning the exact mechanism dictating conduction in these materials. For example, the through-plane transverse acoustic modes become extremely soft and naive PBTE calculations show that this effect can also push down the conductivity without any need for structural disorder. There is thus still work to be done related to thermal conduction in these structures in particular and in semi-disordered materials in general.

Paper V

Limits of the phonon quasi-particle picture at the cubic-to-tetragonal phase transition in halide perovskites.

In the final paper we studied the dynamics of the tilt-modes in the prototypical halide perovskite $CsPbBr_3$ using a neuroevolution potential and MD simulations. In particular the dynamics close to phase transitions were analyzed. This is important as they relate to the shape of spectral functions observed in experiments when studying these phase transitions. The frequencies of the soft tilting modes were analyzed using several different renormalized methods and compared to the fully anharmonic methods based on MD and mode projection. We found that the simple model of the damped harmonic oscillator worked well using the MD approach for the dynamics of the modes even when the modes were overdamped. Most interestingly we found that the overdamped dynamics extend by as much as 200 K above the transition temperature.

A

Regularized linear regression

Once structures are generated the FC expansion can be constructed using linear regression as long as the corresponding properties are linear functions of the free parameters (e.g., forces and energies). When there is plenty of training data, and the data is homogeneous there is often no reason not to use OLS. In Fig. A.1 a typical learning curve is shown. For low amount of data the training error is very different from the validation error indicating overfitting. However, even when the resulting fit matrix is larger than the number of parameters, the matrix rank can still be lower and thus the regression problem can still be ill-conditioned. This can, for example, happen in systems with a large primitive cell. Regularized regression is a technique used to combat over-fitting and used together with cross-validation to assess the performance of the resulting model, see [137–139] for applications to FCs where it is sometimes called CS.

During regularized linear regression in addition to the (typically) squared error imposed on the difference in forces an extra term is introduced to penalize large parameter vectors. Thus not only must we find an accurate model but we must find it using few or small parameters. Two common approaches are LASSO (L_1) and ridge regression (L_2) which are typically defined as

$$\min_x \|Ax - b\|_2 + \lambda \|p\|_n \tag{A.1}$$

where the choice $n = 1$ is called LASSO and $n = 2$ is called ridge regression. The parameter λ is called the regularization parameter and controls the trade-off between bias and variance errors. A high bias error means that the model is unable to predict patterns in the data and is thus under-fitted. If the variance error is high the model is sensitive to noise in the training data and is over-fitted.

Many regularization techniques can also be formulated in a Bayesian framework. The LASSO method is for example equivalent to a Laplace prior distribution together

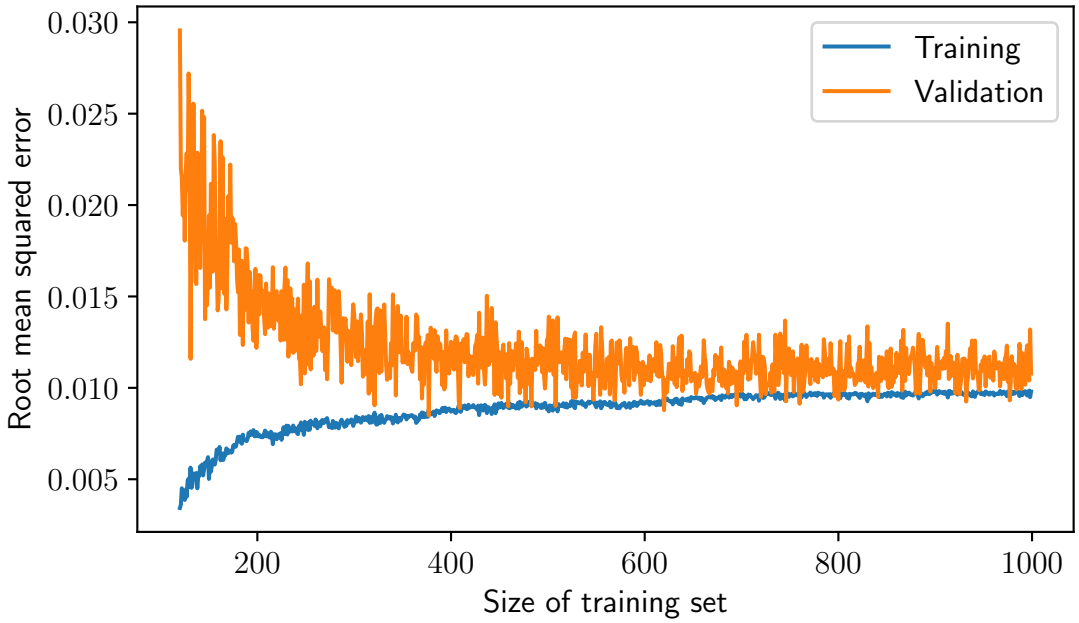

Figure A.1: Typical learning curve. As the training set increases the training error goes up (less overfitting) while the validation error goes down until they meet at the noise level.

with an assumption of Gaussian noise. The reformulation of the regularization problem in terms of Bayesian inference provides powerful tools to quantify uncertainties in the models. It is, for example, possible to assess the effect of uncertainties in the PES on the dispersion relation and use such error estimation to steer model construction.

A.1 Feature selection

A natural consequence of the regularization is that we get information about what features in our model matter and which do not. Feature selection (and regularization in general) has different names in different fields. In signal processing it is called compressed sensing and is typically based on l_1 regularization, i.e., LASSO. By assuming sparse solutions of the problem the set of possible solutions can be reduced and consequently signals can be recovered even when the amount of data is seemingly not enough. From a Bayesian point of view we can regard it as a prior knowledge about the correlation between the solution coefficients where we encode that not all coefficients can be large at the same time.

Popular methods include RFE and orthogonal matching pursuit (OMP) which can be added on top of any standard training method. In RFE the least important features are dropped iteratively starting from a full solution. In OMP features are instead itera-

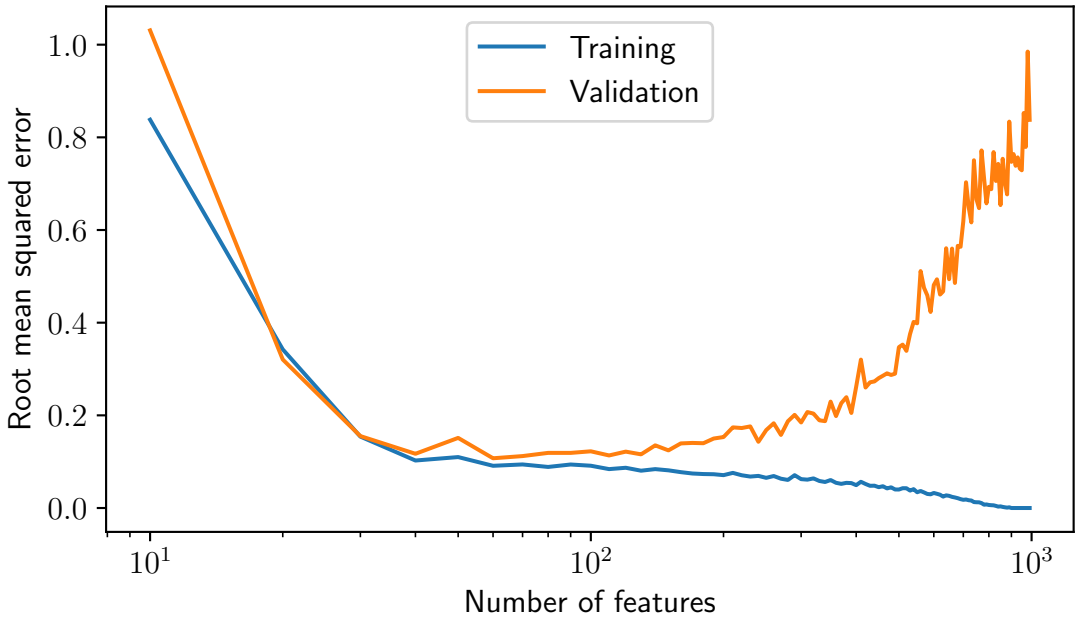

Figure A.2: Typical hyper-parameter scan with RFE. The training error decreases monotonically as the model increases in complexity. At a certain point the validation error goes up indicating overfitting. The minimum of the validation curve should in principle correspond to the best generalization but in practice less complex models (less features) may be preferred.

tively added from a zero solution. Bayesian methods include ARDR which puts individual Gaussian priors on the coefficients and eliminates coefficients if their magnitude relative to the posterior falls below a pre-defined threshold.[1]

All methods discussed have one or more hyper-parameters that must be tuned. They can either be the number of features or some continuous parameter(s). In either case cross-validation can be used to determine optimal hyper-parameter to use.

A.2 Cross validation

In order to assess the performance of the model and to mitigate both over and under-fitting cross-validation should be performed. The generated data is divided in three sets: training, validation, and testing. Typically the training set is large compare to the two other sets. The training set is used to fit the model and the validation set is used to optimize the regularization parameter. If a large amount of data is available the training error and the validation errors are the same, see Fig. A.1. This is equivalent to

[1]The threshold value is a hyper-parameter of this method.

saying that the learning curve has converged. If the validation error is at a minimum with respect to the regularization parameter but much larger than the training error we are in principle over-fitted but the error stems from lack of data, see Fig. A.2 for an illustration. Once the optimal hyper-parameters have been selected the final model can be evaluated again against the test set. If the scores on the validation and test sets are similar the optimal choice of hyper-parameters should be independent of the choice of validation set.

In addition to the RMSE information criteria can be used, such as AIC and BIC. For Gaussian errors the BIC is given by (lower is better)

$$\mathrm{BIC}(k|n) = n\log(\mathrm{MSE}) + k\log(n), \tag{A.2}$$

where n is the number of samples and k the number of parameters. Here, we can see that the BIC balances low error (low mean squared error (MSE)) against a complex model (large k). Such criteria can aid in automatic determination of optimal models.

A.3 The Bayesian perspective

As mentioned, regularized regression and many other aspects of machine learning can be analyzed in a Bayesian framework. This is especially useful when analyzing model uncertainties or to encode general physical intuition. For linear models this analysis is especially simple under some simplifying assumptions of the character of the noise.

Consider the linear model

$$y = X\beta + \epsilon \tag{A.3}$$

where y is the observations, X are the regressors, β are the sought parameters and ϵ models the noise in the data. In the Bayesian framework we have some prior knowledge about the true parameters encoded as a probability distribution. This is simply called "the prior distribution" $P_{\mathrm{prior}}(\beta;\theta_\beta)$ which can depend on some auxiliary parameter θ. This auxiliary parameter is called a hyper parameter. Our model above defines a likelihood function under some suitable choice of the noise function. The noise is typically assumed to be normally distributed $\epsilon \sim N(\sigma^2)$ with some unknown variance. The variance is also controlled by some hyper parameter θ_σ. This fully defines the prior knowledge and the likelihood function L of making the observation (y, X) given the parameters (β, σ). For our simple model we get

$$L(X, y; \beta, \sigma) \propto \exp(-(X\beta - y)^2/\sigma^2). \tag{A.4}$$

Bayes theorem then states that the posterior distribution on the parameters is given by

$$P_{\mathrm{posterior}}(\beta, \sigma) \propto L(y, X; \beta, \sigma)P(\beta, \sigma; \theta). \tag{A.5}$$

For certain combinations of distributions and likelihood functions it is possible to directly relate $\theta_{\text{posterior}}$ with θ_{prior} given the observations. Certain regularizations directly corresponds to the choice of the prior distribution. For example the ridge regression corresponds to the normal distribution and the solution is given by a closed form. LASSO on the other hand corresponds to a Laplace prior and must be solved using numerical methods.

B

Derivation of the Green-Kubo expression

As a bonus section I'll try to motivate the Green-Kubo formula in a language which might be more familiar. Consider the macroscopic energy density $E(x,t)$ of the material where we assume that the energy has been shifted so that $\langle E(x,t)\rangle = 0$ in equilibrium. The energy density obeys the continuity equation

$$\dot{E} = -\nabla j \tag{B.1}$$

for some energy current $j(x,t)$. In the weak field limit the current can be assumed to vary linearly with the gradient of the energy density (Fourier's law)

$$j = -\alpha \nabla E \tag{B.2}$$

where α is the thermal diffusivity (area per time). Putting these two together we get the heat equation

$$\dot{E} = \alpha \nabla^2 E. \tag{B.3}$$

This is the macroscopic equations of motion for the thermal conduction in the material. We shall now see what the corresponding equations look like for the microscopic picture.

The microscopic energy density can be written as

$$E(x,t) = \sum_i E_i(t)\delta(x - x_i(t)) \tag{B.4}$$

for some atomic partition of the energies. In principle any proxy for the temperature for which the macroscopic continuity equation holds should be sufficient. The spatial

Fourier transform of the energy density looks like

$$E(k,t) = \sum_i E_i(t) e^{-ikx_i(t)}. \tag{B.5}$$

By inserting this into the heat equation we get

$$\dot{E}(k,t) = -\alpha k^2 E(k,t). \tag{B.6}$$

Now let's multiply both sides with $\dot{\bar{E}}(k,0)$ (a bar signifies complex conjugation) and Taylor expand the L.H.S. to second order in k to match the R.H.S.

$$\frac{1}{2}\frac{\partial^2}{\partial k^2}\left(\dot{E}(k,t)\dot{\bar{E}}(k,0)\right)_{k=0} = -\alpha E(0,t)\dot{\bar{E}}(0,0). \tag{B.7}$$

Notice the similarity with the other correlation we've seen. We now define the Fourier transformed current density as

$$j(k,t) = \frac{\partial}{\partial t}\sum_i E_i(t)x_i(t)e^{-ikx_i(t)} \tag{B.8}$$

and notice that $\partial_k \dot{E} = -ij$ leading to (suppressing $k = 0$)

$$j(t)\bar{j}(0) - \frac{1}{2}\left(j'(t)\dot{\bar{E}}(0) + \dot{E}(t)\bar{j}'(0)\right) = -\alpha E(t)\dot{\bar{E}}(0). \tag{B.9}$$

where $j'(t) = \partial_t \sum_i E_i(t)x_i^2(t)$. We can now in the long wavelength limit drop the complex conjugation since all variables are real. Now let's embrace the equation with an ensemble average and tidy up

$$C_{jj}(t) - \frac{1}{2}\left(C_{j'\dot{E}}(t) + C_{\dot{E}j'}(t)\right) = -\alpha C_{E\dot{E}}(t). \tag{B.10}$$

where we have defined the correlation function as $C_{AB}(t) = \langle A(t)B(0)\rangle$. We now make use of some properties of correlation functions. First we know that $C_{AB}(t) = C_{BA}(-t)$ and second that $\dot{C}_{AB} = C_{\dot{A}B}$. We get

$$C_{jj}(t) - \frac{1}{2}\frac{\partial}{\partial t}\left(-C_{Ej'}(-t) + C_{Ej'}(t)\right) = \alpha \dot{C}_{EE}(-t). \tag{B.11}$$

Finally after we perform a Laplace transform and take the $s = 0$ limit the second term at the L.H.S. will vanish (or by invoking detailed balance already in the step above)

$$\int_0^\infty C_{jj}(t)dt = \alpha\int_0^\infty \dot{C}_{EE}(-t)dt = -\alpha\left[C_{EE}(\tau)\right]_0^{-\infty} = \alpha\left\langle E^2\right\rangle \tag{B.12}$$

where we recognize (remember $E = H - \langle H \rangle$) the R.H.S. as $\left\langle E^2 \right\rangle = V C_V k_B T^2$. We can thus conclude that since the thermal diffusivity is given by the thermal conductivity as $\alpha = \kappa / C_V$ we get

$$\kappa = \frac{1}{V k_B T^2} \int_0^\infty C_{jj}(\tau) d\tau \tag{B.13}$$

which is the Green-Kubo expression from before. The steps needed was (1) a continuity equation for the energy density, (2) the linear response step where the current was proportional to the gradient, and (3) a long wavelength limit followed by a low frequency limit.

Acknowledgments

First I'd like to thank my supervisor Paul Erhart for your infinite support.

Thank you Erik for for being a great friend and colleague.

I'd also like to thank all colleagues at the division over the years for making the office a great place to come to. Especially thanks to Petter, Esmée, Florian and Prakriti for great discussions about phonons, and Göran for the same and for your support as my examiner.

This would not have been possible without friends (and other nice persons), past and present, both at and outside of Chalmers, you know who you are.

Finally I'd like to thank my family. I love you very much.

Bibliography

[1] T. Lanigan-Atkins, S. Yang, J. L. Niedziela, D. Bansal, A. F. May, A. A. Puretzky, J. Y. Y. Lin, D. M. Pajerowski, T. Hong, S. Chi, G. Ehlers, and O. Delaire, *Extended anharmonic collapse of phonon dispersions in SnS and SnSe,* Nature Communications **11**, (2020). doi:10.1038/s41467-020-18121-4.

[2] L.-D. Zhao, S.-H. Lo, Y. Zhang, H. Sun, G. Tan, C. Uher, C. Wolverton, V. P. Dravid, and M. G. Kanatzidis, *Ultralow thermal conductivity and high thermoelectric figure of merit in SnSe crystals,* Nature **508**, 373–377 (2014). doi:10.1038/nature13184.

[3] O. Delaire, J. Ma, K. Marty, A. F. May, M. A. McGuire, M.-H. Du, D. J. Singh, A. Podlesnyak, G. Ehlers, M. D. Lumsden, and B. C. Sales, *Giant anharmonic phonon scattering in PbTe,* Nature Materials **10**, 614–619 (2011). doi:10.1038/nmat3035.

[4] Q. Ren, M. K. Gupta, M. Jin, J. Ding, J. Wu, Z. Chen, S. Lin, O. Fabelo, J. A. Rodríguez-Velamazán, M. Kofu, K. Nakajima, M. Wolf, F. Zhu, J. Wang, Z. Cheng, G. Wang, X. Tong, Y. Pei, O. Delaire, and J. Ma, *Extreme phonon anharmonicity underpins superionic diffusion and ultralow thermal conductivity in argyrodite Ag_8SnSe_6,* Nature Materials **22**, 999–1006 (2023). doi:10.1038/s41563-023-01560-x.

[5] C. W. Li, J. Hong, A. F. May, D. Bansal, S. Chi, T. Hong, G. Ehlers, and O. Delaire, *Orbitally driven giant phonon anharmonicity in SnSe,* Nature Physics **11**, 1063–1069 (2015). doi:10.1038/nphys3492.

[6] M. K. Gupta, J. Ding, N. C. Osti, D. L. Abernathy, W. Arnold, H. Wang, Z. Hood, and O. Delaire, *Fast Na diffusion and anharmonic phonon dynamics in superionic Na_3PS_4,* Energy & Environmental Science **14**, 6554–6563 (2021). doi:10.1039/d1ee01509e.

[7] V. Kapil, C. Schran, A. Zen, J. Chen, C. J. Pickard, and A. Michaelides, *The first-principles phase diagram of monolayer nanoconfined water,* Nature **609**, 512–516 (2022). doi:10.1038/s41586-022-05036-x.

[8] K. Esfarjani, G. Chen, and H. T. Stokes, *Heat transport in silicon from first-principles calculations,* Physical Review B **84**, 085204 (2011). doi:10.1103/physrevb.84.085204.

[9] K. Biswas, J. He, I. D. Blum, C.-I. Wu, T. P. Hogan, D. N. Seidman, V. P. Dravid, and M. G. Kanatzidis, *High-performance bulk thermoelectrics with all-scale hierarchical architectures,* Nature **489**, 414–418 (2012). doi:10.1038/nature11439.

[10] D. G. Cahill, *Thermal conductivity measurement from 30 to 750 K: the 3ω method,* Review of Scientific Instruments **61**, 802–808 (1990). doi:10.1063/1.1141498.

[11] D. G. Cahill, *Analysis of heat flow in layered structures for time-domain thermoreflectance,* Review of Scientific Instruments **75**, 5119–5122 (2004). doi:10.1063/1.1819431.

[12] A. J. Minnich, J. A. Johnson, A. J. Schmidt, K. Esfarjani, M. S. Dresselhaus, K. A. Nelson, and G. Chen, *Thermal Conductivity Spectroscopy Technique to Measure Phonon Mean Free Paths,* Physical Review Letters **107**, 095901 (2011). doi:10.1103/physrevlett.107.095901.

[13] M. Simoncelli, N. Marzari, and F. Mauri, *Unified theory of thermal transport in crystals and glasses,* Nature Physics **15**, 809 (2019). doi:/10.1038/s41567-019-0520-x.

[14] E. Drigo, M. G. Izzo, and S. Baroni, *Heat conductivity from energy-density fluctuations,* The Journal of Chemical Physics **159**, 184107 (2023). doi:10.1063/5.0168732.

[15] J.-J. Max and C. Chapados, *Isotope effects in liquid water by infrared spectroscopy. III. H_2O and D_2O spectra from 6000 to 0 cm^{-1},* The Journal of Chemical Physics **131**, 184505 (2009). doi:10.1063/1.3258646.

[16] M. Karlsson, M. E. Björketun, P. G. Sundell, A. Matic, G. Wahnström, D. Engberg, L. Börjesson, I. Ahmed, S. Eriksson, and P. Berastegui, *Vibrational properties of protons in hydrated $Ba\,In_x\,Zr_{1-x}\,O_{3-x/2}$,* Physical Review B **72**, 094303 (2005). doi:10.1103/physrevb.72.094303.

[17] N. Xu, P. Rosander, C. Schäfer, E. Lindgren, N. Österbacka, M. Fang, W. Chen, Y. He, Z. Fan, and P. Erhart, *Tensorial properties via the neuroevolution potential framework: Fast simulation of infrared and Raman spectra,* 2023. doi:10.48550/arxiv.2312.05233.

[18] M. Karlsson, *Proton dynamics in oxides: insight into the mechanics of proton conduction from quasielastic neutron scattering,* Physical Chemistry Chemical Physics **17**, 26–38 (2015). doi:10.1039/c4cp04112g.

[19] A. Perrichon, E. Jedvik Granhed, G. Romanelli, A. Piovano, A. Lindman, P. Hyldgaard, G. Wahnström, and M. Karlsson, *Unraveling the Ground-State Structure of $BaZrO_3$ by Neutron Scattering Experiments and First-Principles Calculations,* Chemistry of Materials **32**, 2824–2835 (2020). doi:10.1021/acs.chemmater.9b04437.

[20] P. Rosander, E. Fransson, C. Milesi-Brault, C. Toulouse, F. Bourdarot, A. Piovano, A. Bossak, M. Guennou, and G. Wahnström, *Anharmonicity of the antiferrodistortive soft mode in barium zirconate ($BaZrO_3$),* Physical Review B **108**, 014309 (2023). doi:10.1103/physrevb.108.014309.

[21] Y. K. Koh, M.-H. Bae, D. G. Cahill, and E. Pop, *Heat Conduction across Monolayer and Few-Layer Graphenes,* Nano Letters **10**, 4363–4368 (2010). doi:10.1021/nl101790k.

[22] A. Sood, E. Pop, M. Asheghi, and K. E. Goodson, *The Heat Conduction Renaissance,* in *2018 17th IEEE Intersociety Conference on Thermal and Thermomechanical Phenomena in Electronic Systems (ITherm)*, IEEE, 2018. doi:10.1109/itherm.2018.8419484.

[23] A. Sood, F. Xiong, S. Chen, R. Cheaito, F. Lian, M. Asheghi, Y. Cui, D. Donadio, K. E. Goodson, and E. Pop, *Quasi-Ballistic Thermal Transport Across MoS_2 Thin Films,* Nano Letters **19**, 2434–2442 (2019). doi:10.1021/acs.nanolett.8b05174.

[24] E. Pop, V. Varshney, and A. K. Roy, *Thermal properties of graphene: Fundamentals and applications,* MRS Bulletin **37**, 1273–1281 (2012). doi:10.1557/mrs.2012.203.

[25] S. Lee, D. Broido, K. Esfarjani, and G. Chen, *Hydrodynamic phonon transport in suspended graphene,* Nature Communications **6**, (2015). doi:10.1038/ncomms7290.

[26] D. G. Cahill and R. O. Pohl, *Lattice Vibrations and Heat Transport in Crystals and Glasses,* Annual Review of Physical Chemistry **39**, 93–121 (1988). doi:10.1146/annurev.pc.39.100188.000521.

[27] D. G. Cahill, S. K. Watson, and R. O. Pohl, *Lower limit to the thermal conductivity of disordered crystals,* Physical Review B **46**, 6131–6140 (1992). doi:10.1103/physrevb.46.6131.

[28] C. Chiritescu, D. G. Cahill, N. Nguyen, D. Johnson, A. Bodapati, P. Keblinski, and P. Zschack, *Ultralow Thermal Conductivity in Disordered, Layered WSe_2 Crystals,* Science **315**, 351–353 (2007). doi:10.1126/science.1136494.

[29] F. Brivio, J. M. Frost, J. M. Skelton, A. J. Jackson, O. J. Weber, M. T. Weller, A. R. Goñi, A. M. A. Leguy, P. R. F. Barnes, and A. Walsh, *Lattice dynamics and vibrational spectra of the orthorhombic, tetragonal, and cubic phases of methylammonium lead iodide,* Physical Review B **92**, 144308 (2015). doi:10.1103/physrevb.92.144308.

[30] X. He, D. Bansal, B. Winn, S. Chi, L. Boatner, and O. Delaire, *Anharmonic Eigenvectors and Acoustic Phonon Disappearance in Quantum Paraelectric $SrTiO_3$,* Physical Review Letters **124**, 145901 (2020). doi:10.1103/physrevlett.124.145901.

[31] M. Born and K. Huang, *Dynamical Theory of Crystal Lattices* (Oxford University Press, 1998). ISBN 0198503695.

[32] J. M. Ziman, *Electrons and Phonons* (Oxford University Press, London, 1960).

[33] P. Choquard, *The anharmonic crystal* (New York: W. A. Benjamin, Inc., 1967).

[34] D. C. Wallace, *Thermodynamics of Crystals* (Dover Publications, 1998). ISBN 0-486-40212-6.

[35] G. P. Srivastava, *The physics of phonons* (New York: Taylor and Francis Group, 1990).

[36] R. A. Cowley, *Anharmonic crystals,* Reports on Progress in Physics **31**, 123–166 (1968). doi:10.1088/0034-4885/31/1/303.

[37] J. Callaway, *Quantum Theory of the Solid State* (Elsevier Science, 2012). ISBN 9780323142250.

[38] M. T. Dove, *Introduction to Lattice Dynamics* (Cambridge University Press, 1993). ISBN 9780511619885. doi:10.1017/cbo9780511619885.

[39] K. Parlinski, Z. Q. Li, and Y. Kawazoe, *First-Principles Determination of the Soft Mode in Cubic ZrO_2,* Physical Review Letters **78**, 4063 (1997). doi:10.1103/PhysRevLett.78.4063.

[40] A. Togo and I. Tanaka, *First principles phonon calculations in materials science,* Scripta Materialia **108**, 1 (2015). doi:10.1016/j.scriptamat.2015.07.021.

[41] W. Li, L. Lindsay, D. A. Broido, D. A. Stewart, and N. Mingo, *Thermal conductivity of bulk and nanowire $Mg_2Si_xSn_{1-x}$ alloys from first principles,* Physical Review B **86**, 174307 (2012).

[42] A. Togo, L. Chaput, and I. Tanaka, *Distributions of phonon lifetimes in Brillouin zones,* Physical Review B **91**, 094306 (2015). doi:10.1103/PhysRevB.91.094306.

[43] T. Tadano, Y. Gohda, and S. Tsuneyuki, *Anharmonic force constants extracted from first-principles molecular dynamics: applications to heat transfer simulations,* Journal of Physics: Condensed Matter **26**, 225402 (2014). doi:10.1088/0953-8984/26/22/225402.

[44] K. Esfarjani and H. T. Stokes, *Method to extract anharmonic force constants from first principles calculations,* Physical Review B **77**, 144112 (2008). doi:10.1103/PhysRevB.77.144112.

[45] J. Brorsson, A. Hashemi, Z. Fan, E. Fransson, F. Eriksson, T. Ala-Nissila, A. V. Krasheninnikov, H.-P. Komsa, and P. Erhart, *Efficient Calculation of the Lattice Thermal Conductivity by Atomistic Simulations with Ab Initio Accuracy,* Advanced Theory and Simulations **5**, 2100217 (2022). doi:10.1002/adts.202100217.

[46] A. Togo and I. Tanaka, *Spglib: a software library for crystal symmetry search,* 2018. doi:10.48550/arxiv.1808.01590.

[47] J. Carrete, W. Li, L. Lindsay, D. A. Broido, L. J. Gallego, and N. Mingo, *Physically founded phonon dispersions of few-layer materials and the case of borophene,* Materials Research Letters **4**, 204 (2016). doi:10.1080/21663831.2016.1174163.

[48] X. Gonze and C. Lee, *Dynamical matrices, Born effective charges, dielectric permittivity tensors, and interatomic force constants from density-functional perturbation theory,* Physical Review B **55**, 10355 (1997). doi:10.1103/PhysRevB.55.10355.

[49] P. Giannozzi, S. de Gironcoli, P. Pavone, and S. Baroni, *Ab initio calculation of phonon dispersions in semiconductors,* Physical Review B **43**, 7231 (1991). doi:10.1103/PhysRevB.43.7231.

[50] R. M. Pick, M. H. Cohen, and R. M. Martin, *Microscopic Theory of Force Constants in the Adiabatic Approximation,* Physical Review B **1**, 910 (1970). doi:10.1103/PhysRevB.1.910.

[51] X. Gonze and C. Lee, *Dynamical matrices, Born effective charges, dielectric permittivity tensors, and interatomic force constants from density-functional perturbation theory,* Physical Review B **55**, 10355 (1997). doi:10.1103/PhysRevB.55.10355.

[52] S. Tanaka and Y. Komeiji, *Thermal and quantum fluctuations of harmonic oscillator,* 2022. doi:10.48550/arxiv.2210.03531.

[53] P. E. Blöchl, O. Jepsen, and O. K. Andersen, *Improved tetrahedron method for Brillouin-zone integrations,* Physical Review B **49**, 16223 (1994). doi:10.1103/PhysRevB.49.16223.

[54] R. Mattuck, *A Guide to Feynman Diagrams in the Many-body Problem* (Dover Publications, 1992). ISBN 9780486670478.

[55] A. A. Abrikosov, L. P. Gorkow, and I. E. Dzyaloshinski, *Methods of quantum field theory in statistical physics* (Prentice-Hall, 1963).

[56] S. Doniach and E. Sondheimer, *Green's Functions for Solid State Physicists* (W. A. Benjamin, Inc., 1982).

[57] A. A. Maradudin and A. E. Fein, *Scattering of Neutrons by an Anharmonic Crystal,* Physical Review **128**, 2589 (1962). doi:10.1103/PhysRev.128.2589.

[58] W. Li, J. Carrete, N. A. Katcho, and N. Mingo, *ShengBTE: A solver of the Boltzmann transport equation for phonons,* Computer Physics Communications **185**, 1747–1758 (2014). doi:10.1016/j.cpc.2014.02.015.

[59] T. Feng, L. Lindsay, and X. Ruan, *Four-phonon scattering significantly reduces intrinsic thermal conductivity of solids,* Physical Review B **96**, 161201 (2017). doi:10.1103/PhysRevB.96.161201.

[60] T. Tadano and S. Tsuneyuki, *Self-consistent phonon calculations of lattice dynamical properties in cubic* $SrTiO_3$ *with first-principles anharmonic force constants,* Physical Review B **92**, 054301 (2015). doi:10.1103/PhysRevB.92.054301.

[61] Y. Oba, T. Tadano, R. Akashi, and S. Tsuneyuki, *First-principles study of phonon anharmonicity and negative thermal expansion in* ScF_3*,* Physical Review Materials **3**, 033601 (2019). doi:10.1103/PhysRevMaterials.3.033601.

[62] K. Esfarjani and Y. Liang, *Thermodynamics of anharmonic lattices from first principles,* in *Nanoscale Energy Transport* (IOP Publishing, 2020), p. 1. doi:10.1088/978-0-7503-1738-2ch7.

[63] R. W. Zwanzig, *High-Temperature Equation of State by a Perturbation Method. I. Nonpolar Gases,* The Journal of Chemical Physics **22**, 1420–1426 (1954). doi:10.1063/1.1740409.

[64] R. Bianco, I. Errea, L. Paulatto, M. Calandra, and F. Mauri, *Second-order structural phase transitions, free energy curvature, and temperature-dependent anharmonic phonons in the self-consistent harmonic approximation: Theory and stochastic implementation,* Physical Review B **96**, 014111 (2017). doi:10.1103/PhysRevB.96.014111.

[65] I. Errea, M. Calandra, and F. Mauri, *Anharmonic free energies and phonon dispersions from the stochastic self-consistent harmonic approximation: Application to platinum and palladium hydrides,* Physical Review B **89**, 064302 (2014). doi:10.1103/PhysRevB.89.064302.

[66] L. Monacelli, I. Errea, M. Calandra, and F. Mauri, *Pressure and stress tensor of complex anharmonic crystals within the stochastic self-consistent harmonic approximation,* Physical Review B **98**, 024106 (2018). doi:10.1103/PhysRevB.98.024106.

[67] L. Monacelli, R. Bianco, M. Cherubini, M. Calandra, I. Errea, and F. Mauri, *The stochastic self-consistent harmonic approximation: calculating vibrational properties of materials with full quantum and anharmonic effects,* Journal of Physics: Condensed Matter **33**, 363001 (2021). doi:10.1088/1361-648x/ac066b.

[68] I. Errea, M. Calandra, and F. Mauri, *First-Principles Theory of Anharmonicity and the Inverse Isotope Effect in Superconducting Palladium-Hydride Compounds,* Physical Review Letters **111**, 177002 (2013). doi:10.1103/PhysRevLett.111.177002.

[69] O. Hellman, I. A. Abrikosov, and S. I. Simak, *Lattice dynamics of anharmonic solids from first principles,* Physical Review B **84**, 180301 (2011). doi:10.1103/PhysRevB.84.180301.

[70] O. Hellman and I. A. Abrikosov, *Temperature-dependent effective third-order interatomic force constants from first principles,* Physical Review B **88**, 144301 (2013). doi:10.1103/PhysRevB.88.144301.

[71] O. Hellman, P. Steneteg, I. A. Abrikosov, and S. I. Simak, *Temperature dependent effective potential method for accurate free energy calculations of solids,* Physical Review B **87**, 104111 (2013). doi:10.1103/PhysRevB.87.104111.

[72] D. O. Lindroth, J. Brorsson, E. Fransson, F. Eriksson, A. Palmqvist, and P. Erhart, *Thermal conductivity in intermetallic clathrates: A first-principles perspective,* Physical Review B **100**, 045206 (2019). doi:10.1103/PhysRevB.100.045206.

[73] N. Shulumba, O. Hellman, and A. J. Minnich, *Intrinsic localized mode and low thermal conductivity of PbSe,* Physical Review B **95**, 014302 (2017). doi:10.1103/physrevb.95.014302.

[74] V. Kapil, E. Engel, M. Rossi, and M. Ceriotti, *Assessment of Approximate Methods for Anharmonic Free Energies,* Journal of Chemical Theory and Computation **15**, 5845–5857 (2019). doi:10.1021/acs.jctc.9b00596.

[75] F. Zhou, W. Nielson, Y. Xia, and V. Ozoliņš, *Lattice Anharmonicity and Thermal Conductivity from Compressive Sensing of First-Principles Calculations,* Physical Review Letters **113**, 185501 (2014). doi:10.1103/PhysRevLett.113.185501.

[76] E. Fransson and P. Erhart, *Defects from phonons: Atomic transport by concerted motion in simple crystalline metals,* Acta Materialia **196**, 770 (2020). doi:10.1016/j.actamat.2020.06.040.

[77] D. Frenkel and B. Smit, *Understanding Molecular Simulation: From Algorithms to Applications* (Academic Press, 1996).

[78] E. Fermi, J. Pasta, and S. Ulam, *Studies of nonlinear problems. I.,* Tech. Rep. LA-1940, Los Alamos, 1955.

[79] T. Dauxois, *Fermi, Pasta, Ulam, and a mysterious lady,* Physics Today **61**, 55 (2008). doi:10.1063/1.2835154.

[80] S. Nordholm, J. Forsman, C. Woodward, B. Freasier, and Z. Abbas, *Generalized van der Waals Theory of Molecular Fluids in Bulk and at Surfaces* (Elsevier, 2018). doi:10.1016/C2015-0-06831-9.

[81] J. A. McCammon, B. R. Gelin, and M. Karplus, *Dynamics of folded proteins,* Nature **267**, 585–590 (1977). doi:10.1038/267585a0.

[82] M. S. Daw and M. I. Baskes, *Embedded-atom method: Derivation and application to impurities, surfaces, and other defects in metals,* Physical Review B **29**, 6443 (1984). doi:10.1103/PhysRevB.29.6443.

[83] G. C. Abell, *Empirical chemical pseudopotential theory of molecular and metallic bonding,* Physical Review B **31**, 6184 (1985). doi:10.1103/PhysRevB.31.6184.

[84] J. Tersoff, *New empirical approach for the structure and energy of covalent systems,* Physical Review B **37**, 6991 (1988). doi:10.1103/PhysRevB.37.6991.

[85] A. Stukowski, E. Fransson, M. Mock, and P. Erhart, *Atomicrex–a general purpose tool for the construction of atomic interaction models,* Modelling and Simulation in Materials Science and Engineering **25**, 055003 (2017). doi:10.1088/1361-651x/aa6ecf.

[86] M. P. Allen and D. J. Tildesley, *Computer Simulation of Liquids* (Oxford: Oxford University Press, 1987).

[87] M. Petisme, *Atomistic modeling of interfaces in WC-Co cemented carbides.* PhD thesis, Chalmers university of technology, 2015.

[88] J. Behler, *Perspective: Machine learning potentials for atomistic simulations,* The Journal of Chemical Physics **145**, 170901 (2016). doi:10.1063/1.4966192.

[89] J. Behler and M. Parrinello, *Generalized Neural-Network Representation of High-Dimensional Potential-Energy Surfaces,* Physical Review Letters **98**, 146401 (2007). doi:10.1103/PhysRevLett.98.146401.

[90] J. Behler, *Four Generations of High-Dimensional Neural Network Potentials,* Chemical Reviews **121**, 10037 (2021). doi:10.1021/acs.chemrev.0c00868.

[91] E. Kocer, T. W. Ko, and J. Behler, *Neural Network Potentials: A Concise Overview of Methods,* Annual Review of Physical Chemistry **73**, 163 (2022). doi:10.1146/annurev-physchem-082720-034254.

[92] A. P. Bartók, M. C. Payne, R. Kondor, and G. Csányi, *Gaussian Approximation Potentials: The Accuracy of Quantum Mechanics, without the Electrons,* Physical Review Letters **104**, (2010). doi:10.1103/physrevlett.104.136403.

[93] S. Chmiela, H. E. Sauceda, K.-R. Müller, and A. Tkatchenko, *Towards exact molecular dynamics simulations with machine-learned force fields,* Nature Communications **9**, 3887 (2018). doi:10.1038/s41467-018-06169-2.

[94] L. Himanen, M. O. Jäger, E. V. Morooka, F. Federici Canova, Y. S. Ranawat, D. Z. Gao, P. Rinke, and A. S. Foster, *DScribe: Library of descriptors for machine learning in materials science,* Computer Physics Communications **247**, 106949 (2020). doi:10.1016/j.cpc.2019.106949.

[95] Z. Fan, Z. Zeng, C. Zhang, Y. Wang, K. Song, H. Dong, Y. Chen, and T. Ala-Nissila, *Neuroevolution machine learning potentials: Combining high accuracy and low cost in atomistic simulations and application to heat transport,* Physical Review B **104**, 104309 (2021). doi:10.1103/PhysRevB.104.104309.

[96] A. V. Shapeev, *Moment Tensor Potentials: A Class of Systematically Improvable Interatomic Potentials,* Multiscale Modeling & Simulation **14**, 1153 (2016). doi:10.1137/15m1054183.

[97] R. Drautz, *Atomic cluster expansion for accurate and transferable interatomic potentials,* Physical Review B **99**, 014104 (2019). doi:10.1103/physrevb.99.014104.

[98] F. Pedregosa, G. Varoquaux, A. Gramfort, V. Michel, B. Thirion, O. Grisel, M. Blondel, P. Prettenhofer, R. Weiss, V. Dubourg, J. Vanderplas, A. Passos, D. Cournapeau, M. Brucher, M. Perrot, and E. Duchesnay, *Scikit-learn: Machine Learning in Python,* Journal of Machine Learning Research **12**, 2825 (2011).

[99] M. Karabin and D. Perez, *An entropy-maximization approach to automated training set generation for interatomic potentials,* The Journal of Chemical Physics **153**, 094110 (2020). doi:10.1063/5.0013059.

[100] Y. Zuo, C. Chen, X. Li, Z. Deng, Y. Chen, J. Behler, G. Csányi, A. V. Shapeev, A. P. Thompson, M. A. Wood, and S. P. Ong, *Performance and Cost Assessment of Machine Learning Interatomic Potentials,* The Journal of Physical Chemistry A **124**, 731 (2020). doi:10.1021/acs.jpca.9b08723.

[101] L. Verlet, *Computer "Experiments" on Classical Fluids. I. Thermodynamical Properties of Lennard-Jones Molecules,* Physical Review **159**, 98 (1967). doi:10.1103/PhysRev.159.98.

[102] M. Ceriotti, J. More, and D. E. Manolopoulos, *i-PI: A Python interface for ab initio path integral molecular dynamics simulations,* Computer Physics Communications **185**, 1019 (2014). doi:10.1016/j.cpc.2013.10.027.

[103] S. C. Althorpe, *Path-integral approximations to quantum dynamics,* The European Physical Journal B **94**, (2021). doi:10.1140/epjb/s10051-021-00155-2.

[104] G. Bussi, D. Donadio, and M. Parrinello, *Canonical sampling through velocity rescaling,* The Journal of Chemical Physics **126**, 014101 (2007). doi:10.1063/1.2408420.

[105] A. P. Thompson, S. J. Plimpton, and W. Mattson, *General formulation of pressure and stress tensor for arbitrary many-body interaction potentials under periodic boundary conditions,* The Journal of Chemical Physics **131**, 154107 (2009). doi:10.1063/1.3245303.

[106] E. Fransson, M. Slabanja, P. Erhart, and G. Wahnström, *dynasor—A Tool for Extracting Dynamical Structure Factors and Current Correlation Functions from Molecular Dynamics Simulations,* Advanced Theory and Simulations **4**, 2000240 (2021). doi:10.1002/adts.202000240.

[107] A. Carreras, A. Togo, and I. Tanaka, *DynaPhoPy: A code for extracting phonon quasiparticles from molecular dynamics simulations,* Computer Physics Communications **221**, 221 (2017). doi:10.1016/j.cpc.2017.08.017.

[108] R. Fair, A. Jackson, D. Voneshen, D. Jochym, D. Le, K. Refson, and T. Perring, *Euphonic: inelastic neutron scattering simulations from force constants and visualisation tools for phonon properties,* 2022. doi:10.48550/arxiv.2206.15289.

[109] A. Rohskopf, R. Li, T. Luo, and A. Henry, *A computational framework for modeling and simulating vibrational mode dynamics,* Modelling and Simulation in Materials Science and Engineering **30**, 045010 (2022). doi:10.1088/1361-651x/ac5ebb.

[110] R. Peierls, *Zur kinetischen Theorie der Wärmeleitung in Kristallen,* Annalen der Physik **395**, 1055 (1929). doi:10.1002/andp.19293950803.

[111] F. Müller-Plathe, *A simple nonequilibrium molecular dynamics method for calculating the thermal conductivity,* The Journal of Chemical Physics **106**, 6082–6085 (1997). doi:10.1063/1.473271.

[112] W. Li, N. Mingo, L. Lindsay, D. A. Broido, D. A. Stewart, and N. A. Katcho, *Thermal conductivity of diamond nanowires from first principles,* Physical Review B **85**, 195436 (2012). doi:10.1103/PhysRevB.85.195436.

[113] Z. Han, X. Yang, W. Li, T. Feng, and X. Ruan, *FourPhonon: An extension module to ShengBTE for computing four-phonon scattering rates and thermal conductivity,* Computer Physics Communications **270**, 108179 (2022). doi:10.1016/j.cpc.2021.108179.

[114] D. Lindroth, *Thermal transport in van der Waals Solids and Inorganic Clathrates from first-principles calculations.* PhD thesis, Chalmers university of technology, 2018.

[115] L. Lindsay, A. Katre, A. Cepellotti, and N. Mingo, *Perspective on ab initio phonon thermal transport,* Journal of Applied Physics **126**, 050902 (2019). doi:10.1063/1.5108651.

[116] L. Chaput, *Direct Solution to the Linearized Phonon Boltzmann Equation,* Physical Review Letters **110**, 265506 (2013). doi:10.1103/PhysRevLett.110.265506.

[117] M. Simoncelli, N. Marzari, and F. Mauri, *Wigner Formulation of Thermal Transport in Solids,* Physical Review X **12**, 041011 (2022). doi:10.1103/PhysRevX.12.041011.

[118] D. Dangic, O. Hellman, S. Fahy, and I. Savić, *The origin of the lattice thermal conductivity enhancement at the ferroelectric phase transition in GeTe,* npj Computational Materials 7, (2021). doi:10.1038/s41524-021-00523-7.

[119] G. Barbalinardo, Z. Chen, N. W. Lundgren, and D. Donadio, *Efficient anharmonic lattice dynamics calculations of thermal transport in crystalline and disordered solids,* Journal of Applied Physics **128**, (2020). doi:10.1063/5.0020443.

[120] S. Baroni, R. Bertossa, L. Ercole, F. Grasselli, and A. Marcolongo, *Heat Transport in Insulators from Ab Initio Green-Kubo Theory.* In W. Andreoni and S. Yip, eds., *Handbook of Materials Modeling: Applications: Current and Emerging Materials* (Cham: Springer International Publishing, 2020). doi:10.1007/978-3-319-44680-6_12.

[121] P. Pegolo, *Charge and heat transport in ionic conductors.* PhD thesis, Scuola Internazionale Superiore di Studi Avanzati, 2023.

[122] D. J. Evans, *Homogeneous NEMD algorithm for thermal conductivity—Application of noncanonical linear response theory,* Physics Letters A **91**, 457 (1982). doi:10.1016/0375-9601(82)90748-4.

[123] Z. Fan, L. F. C. Pereira, H.-Q. Wang, J.-C. Zheng, D. Donadio, and A. Harju, *Force and heat current formulas for many-body potentials in molecular dynamics simulations with applications to thermal conductivity calculations,* Physical Review B **92**, 094301 (2015). doi:10.1103/PhysRevB.92.094301.

[124] Z. Fan, H. Dong, A. Harju, and T. Ala-Nissila, *Homogeneous nonequilibrium molecular dynamics method for heat transport and spectral decomposition with many-body potentials,* Physical Review B **99**, 064308 (2019). doi:10.1103/PhysRevB.99.064308.

[125] S. Curtarolo, G. L. W. Hart, M. B. Nardelli, N. Mingo, S. Sanvito, and O. Levy, *The high-throughput highway to computational materials design.,* Nature Materials **12**, 191–201 (2013). doi:10.1038/nmat3568.

[126] R. Jinnouchi, K. Miwa, F. Karsai, G. Kresse, and R. Asahi, *On-the-Fly Active Learning of Interatomic Potentials for Large-Scale Atomistic Simulations,* The Journal of Physical Chemistry Letters **11**, 6946 (2020). doi:10.1021/acs.jpclett.0c01061.

[127] Z. Fan, Y. Wang, P. Ying, K. Song, J. Wang, Y. Wang, Z. Zeng, K. Xu, E. Lindgren, J. M. Rahm, A. J. Gabourie, J. Liu, H. Dong, J. Wu, Y. Chen, Z. Zhong, J. Sun, P. Erhart, Y. Su, and T. Ala-Nissila, *GPUMD: A package for constructing accurate machine-learned potentials and performing highly efficient atomistic simulations,* 2022. doi:10.48550/arxiv.2205.10046.

[128] C. Carbogno, R. Ramprasad, and M. Scheffler, *Ab Initio Green-Kubo Approach for the Thermal Conductivity of Solids,* Physical Review Letters **118**, 175901 (2017). doi:10.1103/PhysRevLett.118.175901.

[129] F. Knoop, *Heat transport in strongly anharmonic solids from first principles.* PhD thesis, Humboldt-Universität zu Berlin, Mathematisch-Naturwissenschaftliche Fakultät, 2022. doi:http://dx.doi.org/10.18452/24244.

[130] I. Pallikara, P. Kayastha, J. M. Skelton, and L. D. Whalley, *The physical significance of imaginary phonon modes in crystals,* Electronic Structure **4**, 033002 (2022). doi:10.1088/2516-1075/ac78b3.

[131] M. Ångqvist, W. A. Muñoz, J. M. Rahm, E. Fransson, C. Durniak, P. Rozyczko, T. H. Rod, and P. Erhart, *ICET – A Python Library for Constructing and Sampling Alloy Cluster*

Expansions, Advanced Theory and Simulations **2**, 1900015 (2019). doi:10.1002/adts.201900015.

[132] L. J. Nelson, V. Ozoliņš, C. S. Reese, F. Zhou, and G. L. W. Hart, *Cluster expansion made easy with Bayesian compressive sensing,* Physical Review B **88**, 155105 (2013). doi:10.1103/PhysRevB.88.155105.

[133] F. Zhou, W. Nielson, Y. Xia, and V. Ozolins, *Lattice anharmonicity and thermal conductivity from compressive sensing of first-principles calculations,* Physical Review Letters **113**, 185501 (2014). doi:10.1103/PhysRevLett.113.185501.

[134] D. O. Lindroth and P. Erhart, *Thermal transport in van der Waals solids from first-principles calculations,* Physical Review B **94**, 115205 (2016). doi:10.1103/PhysRevB.94.115205.

[135] T. Liang, S. R. Phillpot, and S. B. Sinnott, *Parametrization of a reactive many-body potential for Mo–S systems,* Physical Review B **79**, 245110 (2009). doi:10.1103/PhysRevB.79.245110.

[136] Z. Fan, T. Siro, and A. Harju, *Accelerated molecular dynamics force evaluation on graphics processing units for thermal conductivity calculations,* Computer Physics Communications **184**, 1414 (2013). doi:10.1016/j.cpc.2013.01.008.

[137] F. Zhou, W. Nielson, Y. Xia, and V. Ozoliņš, *Compressive sensing lattice dynamics. I. General formalism,* Physical Review B **100**, 184308 (2019). doi:10.1103/PhysRevB.100.184308.

[138] F. Zhou, B. Sadigh, D. Åberg, Y. Xia, and V. Ozoliņš, *Compressive sensing lattice dynamics. II. Efficient phonon calculations and long-range interactions,* Physical Review B **100**, 184309 (2019). doi:10.1103/PhysRevB.100.184309.

[139] E. Fransson, *Atomic-scale investigation of interfacial structures in WC-Co at finite temperatures.* PhD thesis, Chalmers University of Technology, 2021.